

NANOPATTERNED TUBULAR COLLAGEN SCAFFOLDS
FOR VASCULAR TISSUE ENGINEERING

A THESIS SUBMITTED TO
THE GRADUATE SCHOOL OF NATURAL AND APPLIED SCIENCES
OF
MIDDLE EAST TECHNICAL UNIVERSITY

BY

PINAR ZORLUTUNA

IN PARTIAL FULFILLMENT OF THE REQUIREMENTS
FOR
THE DEGREE OF DOCTOR OF PHILOSOPHY
IN
BIOTECHNOLOGY

JULY 2009

Approval of the thesis:

**NANOPATTERNED TUBULAR COLLAGEN SCAFFOLDS
FOR VASCULAR TISSUE ENGINEERING**

submitted by **PINAR ZORLUTUNA** in partial fulfillment of the requirements for the degree of **Doctor of Philosophy in Department of Biotechnology, Middle East Technical University** by,

Prof. Dr. Canan Özgen _____
Dean, Graduate School of **Natural and Applied Sciences**

Prof. Dr. Gülay Özcengiz _____
Head of Department, **Biotechnology**

Prof. Dr. Vasif Hasırcı _____
Supervisor, **Biological Sciences Dept., METU**

Prof. Dr. Pankaj Vadgama _____
Co-Supervisor, **School of Eng. And Materials Science, IRC in Biomaterials, QM, University of London**

Examining Committee Members:

Prof. Dr. Atilla Aydın _____
Dept. of Physics, Bilkent Uni.

Prof. Dr. Vasif Hasırcı _____
Biological Sciences Dept., METU

Prof. Dr. Gülay Özcengiz _____
Biological Sciences Dept., METU

Assoc. Prof. Dr. Gamze Torun Köse _____
Genetics and Bioengineering Dept.,
Yeditepe Uni.

Assist. Prof. Dr. Ayşe Elif Erson _____
Biological Sciences Dept., METU

Date: 10.07.2009

I hereby declare that all information in this document has been obtained and presented in accordance with academic rules and ethical conduct. I also declare that, as required by these rules and conduct, I have fully cited and referenced all material and results that are not original to this work.

Name, Last name: Pınar Zorlutuna

Signature:

ABSTRACT

NANOPATTERNED TUBULAR COLLAGEN SCAFFOLDS FOR VASCULAR TISSUE ENGINEERING

Zorlutuna, Pinar

Ph.D., Department of Biotechnology

Supervisor : Prof. Dr. Vasıf Hasırcı

Co-Supervisor: Prof. Dr. Pankaj Vadgama

July 2009, 123 pages

One of the major causes of death in developed countries is cardiovascular disease that affects small and medium sized blood vessels. In most cases autologous grafts have to be used which have limited availability. A functional tissue engineered vessel can be the ultimate solution for vascular reconstruction. Tissue engineered constructs with cells growing in an organized manner have been shown to have improved mechanical properties. In the present study collagen scaffolds with 650 nm, 500 nm and 332.5 nm wide channels and ridges were seeded with human vascular smooth muscle cells (VSMC) and human endothelial cells separately and then co-cultured on tubular scaffolds. When the films were seeded with endothelial cells it was observed that nanopatterns do not affect cell proliferation or initial cell alignment; however, they significantly influenced cell retention under shear (fluid flow). While 35 ± 10 % of the cells were retained on unpatterned films, 75 ± 4 % was retained on 332.5 nm patterned films

and even higher, $91 \pm 5 \%$ was retained on 650 nm patterned films. It was shown that nanopatterns as small as 332.5 nm could align the vascular smooth muscle cells (VSMC) and that alignment significantly improved mechanical properties. Presence of nanopatterns increased the ultimate tensile strength (UTS) from 0.55 ± 0.11 on Day 0 to as much as 1.63 ± 0.46 MPa on Day 75, a value within the range of natural arteries and veins. Similarly, Young's Modulus values were ca. 4 MPa, again in the range of the natural vessels. Since the films would be ultimately rolled into tubes of collagen, nutrient transfer through the films is quite crucial. Diffusion coefficient for 4-acetaminophenol and oxygen through the collagen films were found to be $1.86 \pm 0.39 \times 10^{-7} \text{ cm}^2 \cdot \text{s}^{-1}$ and $5.41 \pm 2.14 \times 10^{-7} \text{ cm}^2 \cdot \text{s}^{-1}$, respectively in the unseeded form, and increased by 4 fold after cell seeding, which is comparable to that in natural tissues. When both cell types were co-cultured on the nanopatterned tubes (a both-side nanopatterned collagen tube), it was shown that on the outside of the tube VSMCs proliferated in an oriented manner and on the inside endothelial cells proliferated as a monolayer.

Therefore, this study showed that cell guidance enhances the mechanical properties of engineered vessels, and help overcome the two most important challenges in vascular tissue engineering; the need for adequate mechanical properties and continuous lining of endothelial cells even under physiological shear stress.

Keywords: Tissue Engineering, Blood Vessel, Vascular Smooth Muscle Cells, Endothelial Cells, Nanopatterning, Collagen.

ÖZ

DAMAR DOKU MÜHENDİSLİĞİ AMAÇLI NANODESENİLİ TÜBÜLER KOLLAJEN HÜCRE TAŞIYICILARI

Zorlutuna, Pınar

Doktora, Biyoteknoloji Bölümü

Tez Yöneticisi : Prof. Dr. Vasıf Hasırcı

Ortak Tez Yöneticisi: Prof. Dr. Pankaj Vadgama

Temmuz 2009, 123 sayfa

Gelişmiş ülkelerde başta gelen ölüm sebeplerinden biri, küçük ve orta çaplı damarları etkileyen kalp damar hastalıklarıdır. Bu gibi durumlarda genellikle sınırlı miktarda olan otolog damarlar kullanılmaktadır. Doku mühendisliği ile üretilmiş bir yapay damar bu soruna nihai çözüm olabilir. Hücrelerin, hücre taşıyıcıları üzerinde, doğal dokuda oldu gibi organize bir şekilde büyütülmesi geliştirilmiş mekanik özelliklere sahip yapay dokuların elde edilmesi için araştırılmaktadır. Bu çalışmada 650 nm, 500 nm ve 332.5 nm eninde kanallara sahip kolajen hücre taşıyıcılarına insan damar düz kas ve insan endotel hücreleri önce ayrı ayrı ekilmiş sonra da tübüler formdaki taşıyıcılarda ko-kültüre edilmişlerdir. Film şeklindeki taşıyıcılar endotel hücreleri ile ekildiklerinde nanodesenlerin hücreleri yönlendirmediği, yüzeye ilk tutunmalarını ve yüzeyde çoğalmalarını

etkilemedikleri, buna karşın sıvı akışı altında hücrelerin yüzeyde kalmalarını belirgin ölçüde arttırdıkları gözlenmiştir. Desensiz yüzeylerde sıvı akışı uygulandıktan sonraki hücre miktarı ilk ekilenin % 35 ± 10 'i iken 332.5 nm desenli yüzeyde % 75 ± 4 ve 650 nm desenli yüzeyde % 91 ± 5 olarak bulunmuştur. Düz kas hücreleri ile ekildiklerinde 332.5 nm olan en küçük boyutlu desenin bile hücre yönlenmesini sağladığı ve bu yönlenmenin mekanik özellikleri arttırdığı görülmüştür. Nanodesenlerin varlığı mutlak kopma mukavemetini (UTS) sıfırıncı gündeki değer olan 0.55 ± 0.11 'den 75. günde 1.63 ± 0.46 MPa'a kadar çıkarmıştır ki bu değer doğal damarların UTS değer aralığı içindedir. 4 MPa civarında bulunan Elastik Modül de bu aralık içerisinde. Bu filmler son kademedede sarılarak tüp şekline çevrildikleri için hücrelerin beslenmesinde rol oynayacak olan moleküler difüzyon, oksijen and 4-asetaminofenol molekülleri için incelenmiş ve hücresiz formda sırasıyla $1.86 \pm 0.39 \times 10^{-7} \text{ cm}^2 \cdot \text{s}^{-1}$ ve $5.41 \pm 2.14 \times 10^{-7} \text{ cm}^2 \cdot \text{s}^{-1}$ olarak bulunan bu değerler hücre ekildiğinde 4 katına çıkmıştır ki, bu değerler doğal dokuların değer aralığındadır. Tüp şeklindeki taşıyıcı (iki tarafında da nanodesen bulunan kolajen tüp) üzerinde her iki tip hücre ko-kültüre edildiklerinde düz kas hücrelerinin tüpün dış tarafında büyüdüğü ve yönlendikleri, ve endotellerin tüpün iç yüzeyinde tek katman halinde büyüdüğü gözlemlenmiştir.

Sonuç olarak bu çalışma hücre yönlendirmesinin doku mühendisliği yöntemleri ile elde edilmiş damarların mekanik özelliklerinin artırılmasında kullanılabileceğini ve damar doku mühendisliğinin en önemli iki sorunu olan yetersiz mekanik özellikler ve sıvı akışı koşullarında tek katman halinde bir endotel tabakası elde edilmesinin başarılmasında kullanılabileceğini göstermiştir.

Anahtar Kelimeler: Doku Mühendisliği, Damar, Damar Düz Kas Hücresi, Endotel Hücresi, Nanodesen, Kolajen.

Dedicated to my family...

ACKNOWLEDGEMENTS

I would like to express my most sincere gratitude to my supervisor Prof. Dr. Vasıf HASIRCI for his continuous guidance, support, encouragement and patience throughout my studies. I also appreciate deeply his useful advice, comments and valuable suggestions, and the time and effort he has spent to improve my experience during my graduate years.

I am also deeply indebted to my co-advisor Prof. Dr. Pankaj VADGAMA for his guidance, valuable suggestions and for giving me a wonderful opportunity to study in his labs which indeed helped improve this thesis.

I wish to express my deeply felt gratefulness to my father, Assoc. Prof. Dr. Yaman ZORLUTUNA (Bayındır Hastanesi), for his continuous support during my thesis, for his valuable advices and also for providing materials for this study.

I also gratefully acknowledge Dr. Ahmed ELSHEIKH (University of Dundee) for his useful suggestions, for teaching me mechanical testing and calculations, and for providing me the opportunity to work in his lab.

I would like to extend my thanks to Prof. Dr. Atilla AYDINLI and Aşkın KOCABAŞ (both of Bilkent University) for providing the nanopatterned templates, an indispensable component of this study.

I wish to express my sincere gratitude to Prof. Dr. Nesrin HASIRCI for her helpful suggestions and guidance.

My sincere acknowledgements go to my thesis progress committee members, Assoc. Prof. Dr. Gamze TORUN KÖSE and Assist. Prof. Dr. Ayşe Elif ERSON for their useful comments and suggestions throughout this thesis.

I would like to thank Nural KORKUT for providing the Teflon madrels; an inevitable component of this study, which without him would be very hard to reach.

I am grateful to Dr. Zimei RONG (IRC in Biomedical Materials, QM, Uni. of London) for his help in diffusivity measurements and for his valuable friendship.

I would like to thank to my special friends and lab partners Pınar YILGÖR and Buket BAŞMANAV for their friendship and support during the long hours we spent working hard together.

I wish to thank to all my friends, the members of METU-BIOMAT group, Halime KENAR, Deniz YÜCEL, Albana NDREU, Aysel KIZILTAY, Tuğba ENDOĞAN, Arda BÜYÜKSUNGUR, Erkin AYDIN, Hayriye ÖZÇELİK, Birsen DEMİRBAĞ, Özge KARADAŞ, Gizem ALTAY, Beste KINIKOĞLU, Gökhan BAHÇECİOĞLU, Sinem KARDEŞLER and our technician Zeynel AKIN for their support in this study.

This study was supported by METU-BAP-01-08-2009-01, DPT 2006K 120920-20, TUBITAK TBAG-105T508 and TUBITAK TBAG-108T576. I gratefully acknowledge all for making this study possible and especially TUBITAK for giving me scholarships through projects 105T508 and 108T576.

Finally, I would like to express my deepest gratitude to my family, for their understanding, patience and continuous support and trust in me, without which it would not be possible to succeed.

TABLE OF CONTENTS

ABSTRACT	iv
ÖZ.....	vi
ACKNOWLEDGEMENTS.....	ix
TABLE OF CONTENTS.....	xi
LIST OF TABLES.....	xv
LIST OF FIGURES.....	xvi
LIST OF ABBREVIATIONS.....	xxiii
CHAPTERS	
1. INTRODUCTION.....	1
1.1. Structure and Function of Blood Vessels	1
1.2. Vascular Disease.....	2
1.3. Approaches for Vascular Reconstruction.....	4
1.3.1. Autogenous Grafts.....	4
1.3.2. Synthetic Prosthetic Grafts.....	4
1.3.3. Biological Prosthetic Grafts.....	8
1.3.4. Tissue Engineered Grafts.....	9
1.4. Tissue Engineering.....	9
1.4.1. Cell Types and Sources Used in Tissue Engineering.....	10
1.4.2. Scaffolds Used in Tissue Engineering.....	11
1.4.2.1. Sythetic Polymers.....	11
1.4.2.2. Natural Polymers.....	11
1.4.2.2.1. Collagen.....	12
1.4.2.3. Processing, Modification and Characterization of Scaffolds.....	13
1.4.2.3.1. Surface Modifications.....	15
1.4.2.3.2. Nano-scale Modification of Scaffold Surfaces.....	16
1.5. Vascular Tissue Engineering.....	18

1.6. Approach and Novelty of the Study.....	24
2. MATERIALS AND METHODS.....	26
2.1. Materials.....	26
2.2. Methods.....	27
2.2.1. Scaffold Preparation.....	27
2.2.1.1. Collagen.....	27
2.2.1.1.1. Isolation.....	27
2.2.1.1.2. SDS-PAGE Analysis of Isolated Collagen Type I.....	28
2.2.1.2. Template Preparation.....	28
2.2.1.3. Film Preparation	29
2.2.1.3.1. Single-side Nanopatterned Films.....	29
2.2.1.3.2. Double-side Nanopatterned Films.....	29
2.2.1.4. Preparation of Tubular Scaffolds.....	29
2.2.2. Characterization.....	30
2.2.2.1. Atomic Force Microscopy.....	30
2.2.2.2. Scanning Electron Microscopy.....	30
2.2.2.3. Stereomicroscopy.....	30
2.2.2.4. Diffusivity.....	30
2.2.3. <i>In Vitro</i> Studies.....	32
2.2.3.1. Human Microvascular Endothelial Cells (HMEC).....	32
2.2.3.1.1. HMEC cell culture.....	32
2.2.3.1.2. Studies with HMECs on Collagen Films.....	32
2.2.3.1.2.1. Cell proliferation.....	33
2.2.3.1.2.2. Microscopy (SEM, Fluorescence).....	33
2.2.3.1.2.3. Flow-Shear Studies.....	33
2.2.3.2. Human Vascular Smooth Muscle Cells (VSMC).....	34
2.2.3.2.1. Cell Isolation.....	34
2.2.3.2.2. Culturing.....	35
2.2.3.2.3. Characterization.....	35
2.2.3.2.4. Studies with VSMCs on Collagen Films.....	36
2.2.3.2.4.1. Cell proliferation.....	37

2.2.3.2.4.2. Microscopy (SEM, Fluorescence).....	37
2.2.3.2.4.3. Mechanical Tests.....	37
2.2.3.2.5. Studies with VSMCs on Tubular Scaffolds.....	38
2.2.3.3. Human Internal Thoracic Artery Endothelial Cells (HITAEC)	39
2.2.4. Co-Culture of VSMCs and HITAECs on Collagen Tubes.....	39
2.2.4.1. Microscopy (SEM, Fluorescence).....	40
2.2.4.2. Histology.....	40
2.2.5. Statistical Analysis.....	40
3. RESULTS AND DISCUSSION.....	41
3.1. Characterization of Templates.....	41
3.2. Characterization of Collagen films.....	45
3.2.1. SDS-PAGE of Isolated Collagen Type I.....	45
3.2.2. Microscopic Characterization.....	45
3.2.3. Diffusivity of Cell-free Collagen films.....	52
3.2.3.1. Acetaminophenol Diffusivity.....	52
3.2.3.2. Oxygen Diffusivity.....	54
3.3. Characterization of Cell-free Tubular Scaffolds.....	55
3.4. Studies with HMECs.....	58
3.4.1. HMEC viability on Collagen Films.....	58
3.4.2. Diffusivity of HMEC Seeded Films.....	59
3.4.3. Cell Proliferation.....	61
3.4.4. HMEC Orientation.....	62
3.4.5. Flow-Shear Test.....	65
3.5. Studies with VSMCs.....	66
3.5.1. Isolation and Characterization of VSMCs.....	66
3.5.2. VSMCs on Collagen Films.....	69
3.5.2.1. Cell Proliferation.....	69
3.5.2.2. Cell Morphology, Orientation and Phenotype.....	70
3.5.2.3. Mechanical Tests.....	80
3.5.3. VSMCs on Collagen Tubes.....	85
3.5.3.1. Optimization of VSMC Seeding on Tubular Scaffolds.....	85

3.5.3.1.1. Cell Attachment and Proliferation.....	86
3.5.3.1.2. Microscopy (SEM, Fluorescence).....	87
3.6. Tubular Scaffolds with 2 cell types: Co-culture of VSMCs and HITAECs on Tubular Scaffolds.....	91
3.6.1. Characterization of HITACs	91
3.6.2. Cell Proliferation.....	91
3.6.3. Microscopy (SEM, Fluorescence).....	93
3.6.4. Histology.....	97
4. CONCLUSIONS.....	100
REFERENCES.....	101
APPENDICES	
A. ETHICAL COMMITTEE APPROVAL.....	119
B. FORMULA FOR ALAMAR BLUE CALCULATIONS.....	120
C. CALIBRATION CURVES FOR CELL NUMBER DETERMINATION.....	121
CURRICULUM VITAE.....	122

LIST OF TABLES

TABLES

Table 3.1. Diffusion of unseeded and unseeded and fixed collagen films to 4 acetaminophen and oxygen.....	54
Table 3.2. Diffusivity of cell seeded, unseeded, fixed or unfixed collagen films to 4-acetaminophen and oxygen.....	61
Table 3.3. UTS and Young's Moduli of the seeded and unseeded collagen films (n=6).....	83

LIST OF FIGURES

FIGURES

Figure 1.1. General organization of a blood vessel.....	2
Figure 1.2. Comparison of healthy (a) and atherosclerotic (b) artery.....	3
Figure 1.3. a) Dacron vascular graft, b) Woven (left) and knitted (center and right) fabrics used for Dacron vascular grafts.....	6
Figure 1.4. ePTFE vascular graft.....	7
Figure 1.5. Polyurethane vascular graft.....	8
Figure 1.6. Structure of collagen. (a) Ball and stick model of two turns of one polypeptide chain, (b) model of a single collagen chain, (c) collagen superhelix.....	13
Figure 1.7. SEM micrograph of silicon wafers created by e-beam lithography. a) 14 nm wide lines, b) 30-40 nm dots and c) ~20 nm lines (Robinson et al., 1999).....	18
Figure 1.8. Development of (a) collagen gel-based, (b) rolled sheet and (c) degradable scaffold vascular grafts.....	19
Figure 2.1. Rank cells.....	31
Figure 2.2. Schematic representation of tubular collagen construct in 24 well tissue culture plate.....	38
Figure 3.1. Silicon template with 332.5 nm channel width. a) top view, b) 3D view, c) view and dimensions.....	42
Figure 3.2. Silicon template with 500 nm channel width. a) top view, b) 3D view, c) top view and dimensions.....	43
Figure 3.3. Silicon template with 650 nm channel width. a) top view, b) 3D view, c) top view, hard zoomed, d) 3D view, hard zoomed, e) top view and dimensions.....	44

Figure 3.4. SDS-PAGE of type I collagen isolated from rat tail. Column 1 is the protein marker (ladder), Columns 2 and 4 are isolated collagen (I) (same sample applied as duplicate), 3 and 5 are commercial pure type I collagen (C) (duplicate).....	45
Figure 3.5. SEM images of the nanopatterned collagen films before crosslinking. a) 650 nm channel width (x 5000), b) 650 nm channel width (x 10000), c) 332.5 nm channel width (x 15753), d) 332.5 nm channel width (x 115500).....	46
Figure 3.6. SEM images of collagen films crosslinked while on silicon templates. a) 332.5 nm channel width (x17934), b) 332.5 nm channel width (x110629), c) 500 nm channel width (x9500), d) 500 nm channel width (x45504), e) 650 nm channel width (x4753), f) 650 nm channel width (x40623).....	47
Figure 3.7. SEM images of crosslinked collagen films prepared on PDMS replicas. a) unpatterned (x5000), b) unpatterned (x10000), c) 332.5 nm channel width (x5000), d) 332.5 nm channel width (x10000), e) 500 nm channel width (x5000), f) 500 nm channel width (x10000), g) 650 nm channel width (x5000), h) 650 nm channel width (x10000).....	48
Figure 3.8. Collagen film with 650 nm channel width. Uncrosslinked film a) top view, b) 3D view. Crosslinked film c) top view, d) 3D view e) top view showing the dimensions.....	50
Figure 3.9. SEM images of two sides of the both side patterned collagen films (before crosslinking).....	51
Figure 3.10. SEM images of two sides of the both side patterned collagen films after crosslinking.....	52
Figure 3.11. Control measurement for 4-acetaminophenol diffusion (without the collagen film in place).....	53
Figure 3.12. 4-acetaminophenol diffusivity of collagen films. a) unseeded, b) unseeded and fixed.....	53

Figure 3.13. Control measurement for oxygen diffusivity (without the collagen film in place).....	54
Figure 3.14. Oxygen diffusivity of unseeded collagen film. a) unseeded, b) unseeded and fixed film.....	55
Figure 3.15. SEM images of tubular collagen scaffold. a) outside, b) inside, c) cross section.....	56
Figure 3.16. SEM images of tubular collagen scaffolds. a) drawing of the tubular scaffold, b) inside of the double side patterned tubular scaffold, c) outside of the double side patterned tubular scaffold, d) inside of the unpatterned tubular scaffold, e) outside of the unpatterned tubular scaffold.....	57
Figure 3.17. Stereomicrographs of tubular collagen scaffold after 28 days of incubation under cell culture conditions. a) cross-section, b) outside view.....	58
Figure 3.18. Calcein AM - ethidium homodimer-2 double staining. a) cells on the TCPS at the excitation wavelength for Calcein (488 nm), b) cells on the collagen film at the excitation wavelength for Calcein, c) cells on the collagen film at the excitation wavelength for ethidium homodimer-2 (590 nm).....	59
Figure 3.19. Diffusivity of cell seeded collagen films. a) 4-acetaminophenol diffusivity of cell seeded, unfixed film and b) 4-acetaminophenol diffusivity of cell seeded and fixed film, c) oxygen diffusivity of cell seeded and fixed collagen film.....	60
Figure 3.20. Alamar Blue test results showing the effect of seeding with HMEC with different initial seeding densities on cell proliferation on nanopatterned and unpatterned collagen films. (Incubation time: 48 h, $n=3$).....	62
Figure 3.21. Fluorescence micrographs of HMECs on collagen films at 24 h (DAPI staining). a) unpatterned, b) 332.5 nm patterned, c) 500 nm patterned, d) 650 nm patterned (x 200).....	63

Figure 3.22. SEM images of HMECs seeded on 500 nm nanopatterned collagen films at 48 h. a) a single aligned cell, b) a single unaligned cell, c) initial seeding density of 2×10^4 , d) initial seeding density of 5×10^4 , e) initial seeding density of 1×10^5	64
Figure 3.23. Cell numbers on flow-shear applied HMECs on nanopatterned and unpatterned films compared to cell numbers on films that were not subjected to shear. * indicates the significantly different values ($p < 0.05$).....	66
Figure 3.24. VSMC isolation from saphenous vein. a) intact saphenous vein after dissecting longitudinally, b) saphenous vein after removal of intima layer, c) fragments of the media layer of the saphenous vein (ready for explant culture).....	67
Figure 3.25. Light micrographs of VSMCs in explant culture. a) cells in the vicinity of the explant tissue (x 400) and b) cells in the medium (x 100).....	67
Figure 3.26. Confocal images of VSMCs with anti- α -smooth muscle actin staining (x 200).....	68
Figure 3.27. Fluorescence micrographs of VSMCs double stained with anti- α -smooth muscle actin and DAPI. Passages a) 4, b) 5 and c) 6 (x 100).....	69
Figure 3.28. VSMC proliferation on collagen films. Alamar Blue assay ($n=3$).....	70
Figure 3.29. VSMC on collagen films. a) unpatterned, b) 332.5 nm, c) 500 nm, d) 650 nm (x 100). Day 1 anti- α -smooth muscle actin stain	71
Figure 3.30. VSMC on collagen films. a) unpatterned, b) 332.5 nm, c) 500 nm, d) 650 nm (x 100). Day 7 anti- α -smooth muscle actin stain	72
Figure 3.31. VSMC on collagen films. a) unpatterned, b) 332.5 nm, c) 500 nm, d) 650 nm (x 100). Day 14 anti- α -smooth muscle actin stain.....	73

Figure 3.32. VSMC on collagen films. a) unpatterned, b) 332.5 nm, c) 500 nm, d) 650 nm (x 100). Day 21 anti- α -smooth muscle actin stain.....	74
Figure 3.33. SEM micrographs of VSMCs on collagen films on Day 1. a) unpatterned film (x 700), b) 332.5 nm patterned film (x 261), b') 332.5 nm patterned film (region of the sample not occupied by the cells, x 10,000), c) 500 nm patterned film (x 200), c') 500 nm patterned film (region of the sample not occupied by the cells, x 10,000), d) 650 nm patterned film (x 600), d') 500 nm patterned film (region of the sample not occupied by the cells, x 12,000). White arrow indicates the direction of the patterns.....	76
Figure 3.34. SEM micrographs of VSMCs on collagen films on Day 7. a) unpatterned film (x 265), b) 332.5 nm patterned film (x 100), c) 500 nm patterned film (x 500), d) 650 nm patterned film (x 900). White arrow indicates the direction of the patterns.....	77
Figure 3.35. SEM micrographs of VSMCs on collagen films on Day 14. a) unpatterned film (x 200), b) 332.5 nm patterned film (x 200), c) 500 nm patterned film (x 600), d) 650 nm patterned film (x 200). White arrow indicates the direction of the patterns.....	78
Figure 3.36. SEM micrographs of VSMCs on collagen films on Day 21. a) unpatterned film (x 200), b) unpatterned film (x 600), c) 332.5 nm patterned film (x 200), d) 332.5 nm patterned film (x 600), e) 500 nm patterned film (x 200), f) 500 nm patterned film (x 600), g) 650 nm patterned film (rolled by contraction by the cells, x 200), h) 650 nm patterned film (x 600). White arrow indicates the direction of the patterns.....	79
Figure 3.37. Stress-Strain plot of unseeded collagen films. Dashed curves are individual tests and the smooth curve is the average.....	81

Figure 3.38. Stress-Strain graph of average curves of unseeded and VSMC seeded nanopatterned and unpatterned collagen films after 45 or 75 days of incubation (n=6).....	82
Figure 3.39. UTS values of VSMC seeded nanopatterned collagen films after 45 and 75 days of incubation.....	82
Figure 3.40. Young's Modulus values of VSMC seeded nanopatterned collagen films after 45 and 75 days of incubation.....	83
Figure 3.41. VSMC proliferation seeded at different densities on tubular scaffolds as determined with Alamar Blue assay.....	86
Figure 3.42. VSMC proliferation on nanopatterned (650 nm) and unpatterned tubular scaffolds as determined with Alamar Blue assay. (2×10^5 cells/tube seeding density).....	87
Figure 3.43. Fluorescence micrographs of VSMCs on collagen tubes stained with DAPI for the cell nuclei and with anti- α -smooth muscle actin. a) 5×10^4 cells/tube initial seeding density, DAPI staining, b) 5×10^4 cells/tube initial seeding density, stained for α -smooth muscle actin, c) 1×10^5 cells/tube initial seeding density, DAPI staining, d) 1×10^5 cells/tube initial seeding density, stained for α -smooth muscle actin e) 2×10^5 cells/tube initial seeding density, DAPI staining, f) 2×10^5 cells/tube initial seeding density, stained for α -smoothmuscle actin (x 200).....	88
Figure 3.44. SEM of the inside (unseeded side) of the VSMC seeded tubular scaffold. Day 21 (x 12,000).....	89
Figure 3.45. SEM images of the outside of the VSMC seeded tubular scaffold. a to c) VSMC sheets on different regions, d) region labeled with white rectangle in part c showing the cell sheet-film interface, e) magnification of white rectangle in part d, f) magnification of white rectangle in part e.....	90
Figure 3.46. Fluorescence micrographs of anti-PECAM and DAPI staining of HITAECS at x 100 (left) and x 200 (right) magnifications.....	91

Figure 3.47. VSMC growth on nanopatterned tubular scaffold before endothelial cell seeding on Day 14.....	92
Figure 3.48. Cell proliferation in VSMC and HITAEC co-culture for 21 Days.....	93
Figure 3.49. Fluorescence micrographs of immunostained VSMCs and HITAECs on nanopatterned tubular scaffolds. Anti- α -smooth muscle actin staining on a) Day 1 (x 200), b) Day 7 (x 200), c) Day 14 (x 200) and d) Day 21. Anti-CD31 staining on e) Day 21 (x 100) and f) Day 21 (x 200).....	94
Figure 3.50. SEM images of the outside of the nanopatterned tubular scaffold, seeded with VSMCs. a) Day 1 (x 500), b) nanopatterns on the surface near the VSMCs on Day 1 (x 1000), c) Day 7 (x 500), d) Day 7 (x 1000), e) Day 14 (x 500), f) Day 14 (x 1000), g) on Day 21 (x 500), h) Day 21 (x 1000).....	95
Figure 3.51. SEM images of the inside of the nanopatterned tubular scaffolds seeded HITAECs. Day 21. a) x 500, b) x 1000, c) another region x 1000, d) another region x 1000.....	97
Figure 3. 52. Histological examination of unseeded tubular scaffolds on Day 21. a) x100 and b) x 400.....	98
Figure 3. 53. Histological examination of VSMC and HITAEC seeded tubular scaffolds on Day 21. a) x100, b and c) x200, d) x 400...	99
Figure A.1. Ethical committee approval.....	120
Figure C.1. Calibration curve of VSMCs for Alamar Blue Assay.....	122
Figure C.2. Calibration curve of VSMCs for Alamar Blue Assay.....	122

LIST OF ABBREVIATIONS

2D	2 dimensional
3D	3 dimensional
AFM	Atomic Force Microscope
BSA	Bovine Serum Albumin
DAPI	4',6-diamidino-2-phenylindole
DMEM	Dulbecco's Modified Eagle Medium
DMSO	Dimethyl Sulfoxide
DPN	Dip-Pen Nanolithography
ECGS	Endothelial Cell Growth Supplement
ECM	Extracellular Matrix
EDC	Ethyl(dimethylamino)propyl Carbodiimide
ePTFE	Expanded Poly(tetrafluoroethylene)
FCS	Fetal Calf Serum
Gly	Glycine
HITAEC	Human Internal Thoracic Artery Endothelial Cells
HMEC	Human Microvascular Endothelial Cell
Hydroxy-Pro	Hydroxyproline
Mw	Molecular Weight
NHS	N-hydroxysuccinimide
OD	Optical Density
PBS	Phosphate Buffer Saline
PCL	Poly(ϵ -caprolactone)
PDMS	Polydimethyl Siloxane
PHA	polyhydroxyalkanoates
PHBV	Poly(3-hydroxybutyrate-co-3-hydroxyvalerate)
PGA	Poly(glycolic acid)

PLA	Poly(lactic acid)
PLGA	Poly(lactide- <i>co</i> -glycolic acid)
Pro	Proline
RP	Rapid Prototyping
SEM	Scanning Electron Microscopy
TCPS	Tissue Culture Polystyrene
UTS	Ultimate Tensile Strength
VSMC	Vascular Smooth Muscle Cells

CHAPTER 1

INTRODUCTION

In this study the goal was to prepare small diameter tissue engineered vascular grafts in order to satisfy the need for replacement necessitated by disease and age. In order to achieve this, nanopatterned collagen scaffolds were designed and tested *in vitro*.

1.1. Structure and Function of Blood Vessels

The function of blood vessels is to carry blood in the body. Arteries and veins form a branched system that varies in size, biochemical and cellular content, mechanical properties and structural organization depending on its location in the body, volume of blood to be carried, flow rate and vasoactivity. The aorta is the largest artery and it transports the blood leaving the heart. Large arteries become narrower to form smaller diameter muscular arteries which deliver the blood from large arteries to tissue and the organs. These small diameter arteries then branch into arterioles and further narrow to capillaries. Capillaries are the part of the vascular system where the exchange of nutrients, wastes and gases between blood and interstitial fluid takes place. After that, blood is returned to the heart through venules, which combine to form veins and eventually the vena cava. Large and medium sized vessels are constituted of an intima, media and adventitia (Figure 1.1). The intima is the inner layer that faces the lumen of the vessel and consists of a single layer of endothelial cells. Around that, there is the media which consists of smooth muscle cells and elastin fibers that are oriented circumferentially. The outer

layer is adventitia, which is actually a connective tissue and consists of collagen fibers. Capillaries, on the other hand, consist of only a single layer of endothelial cells (Ratcliffe et al., 2000).

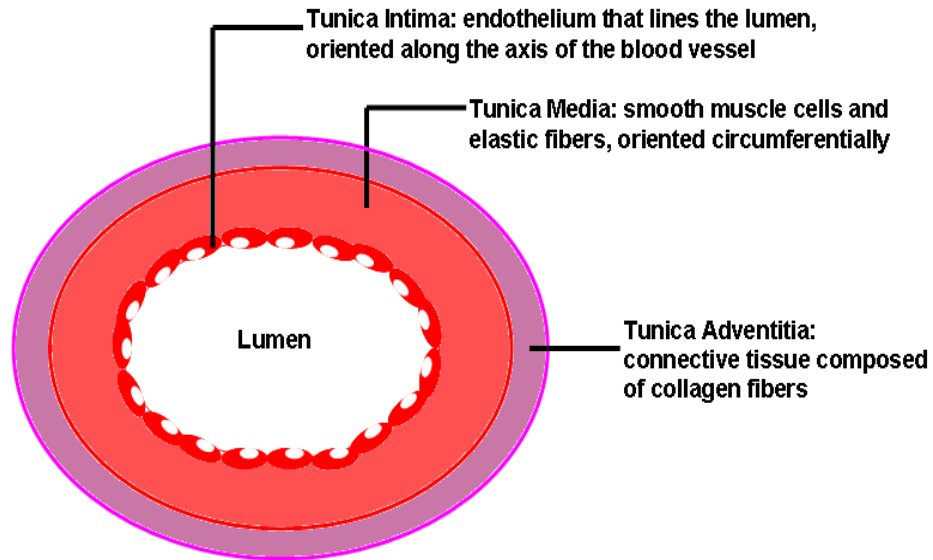


Figure 1.1. General organization of a blood vessel.

1.2. Vascular Disease

One of the major causes of death western society is cardiovascular disease that affects small and medium sized blood vessels (Tu et al., 1997). Most common among these diseases is atherosclerosis, caused by a lesion involving a raised focal plaque within the intima (Figure 1.2). This plaque consists of a lipid core, surrounded by an extracellular matrix (ECM) and smooth muscle cells and is covered by a fibrous cap (Benditt and Schwartz, 1988). This lesion increases in size, restricts blood flow and eventually clogs the vessel. The option at this stage is generally the removal of the diseased vessel and replacement with a homograft or a synthetic vascular graft. Many of the advances in vascular therapy have been made possible by the development of synthetic or reconstituted biological vascular grafts which are used to replace diseased or injured vessels.

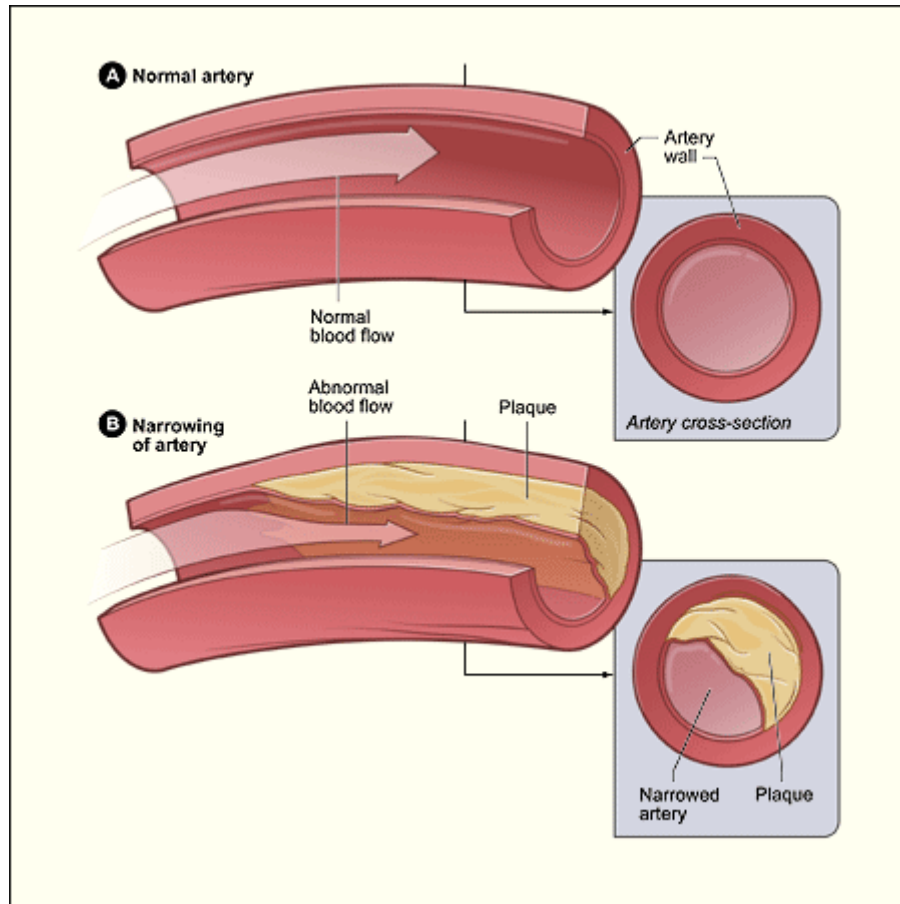


Figure 1.2. Comparison of healthy (a) and atherosclerotic (b) artery.
 (www.web-books.com/.../Images/Athero.gif)

According to the Department of Health and Human Services of the United States Center for Chronic Disease Prevention, cardiovascular disease is the predominant cause of death in the USA, killing more people than cancer every year, with 685,000 deaths in 2003 (National Center for Chronic Disease Prevention and Health Promotion). In Turkey, the total number of patients in 2004 was 2.8 million and it is estimated to be 5.6 million in 2015, with an annual increase rate of 7.2 %. 140,000 of these patients undergo arterial reconstruction surgery every year (Turkish Society of Cardiology, 2004).

The ideal vascular graft has not yet been found; autogenous grafts are currently the best conduits in use but are not always available or suitable (Ratcliffe et al., 2000). There is, therefore, a continuous search for a graft that is fully biocompatible and able to take over the function of the diseased or injured vessels.

1.3. Approaches for Vascular Reconstruction

Vascular reconstruction can be achieved via vascular grafts which can be separated into four broad groups: autogenous grafts, synthetic prosthetic grafts, biological prosthetic grafts and tissue engineered vascular grafts.

1.3.1. Autogenous Grafts

Autogenous grafts are harvested from and implanted into the same individual, and may be either arterial or venous. Arterial autografts have many advantages such as retaining viability, proportional arterial growth when used in children, no degeneration with time, healing in an infected region and good mechanical properties including flexibility at joints (Ferrari and von Segesser, 2006). However, widespread use of arterial autografts is limited due to unavailability and the short lengths of autogenous arteries, unavailability of autogenous veins either because of disease or because previous surgery and need for second surgeries for both. Therefore, common autografts used clinically are the veins which are more available in adequate length, easily harvested and adapt well to placement in arterial circulation (Farsak et al., 2003). The saphenous vein is generally the first choice because of its adequate diameter, relatively thick walls and is the longest vein in the body.

1.3.2. Synthetic Prosthetic Grafts

For vascular reconstruction homografts are currently the best choice but as stated above their availability is limited, and many factors including multiple bypass surgery, repeat procedures and age of the patient decrease their suitability (Thomas et al., 2003). Therefore, there is a continuous search for a vascular substitute which can be used instead of autogenous grafts, and numerous different prosthetic vascular grafts have been developed over the years. Synthetic vascular grafts are generally made from polymers such as Dacron, expanded poly(tetrafluoroethylene) (ePTFE) and polyurethane (Kannan et al., 2005).

Dacron or poly(ethylene terephthalate) is a polyester, and can be produced as continuous multifilaments to make the graft soft, elastic and easy to handle (Figure 1.3 a). Dacron can be tailored into a vascular graft by weaving or knitting (Figure 1.3 b). Woven Dacron grafts are fabricated in a simple over and under pattern both in lengthwise and circumferential directions to produce grafts with little or no stretch in any direction, low porosity and relatively high strength and stiffness. Low porosity reduces bleeding and the relatively high stiffness decreases elongation and dilatation observed after implantation. However, their low porosity leads to reduced perigraft healing. Knitted Dacron grafts can have a structure oriented mostly in the longitudinal (warp knitted) or circumferential (weft knitted) direction. The knitted grafts generally have a higher porosity, enhanced healing, improved compliance, superior handling characteristics and a lower tendency to wear than the woven grafts (Kannan et al., 2005). However, they need pre-clotting to prevent blood leakage due to their high porosity.

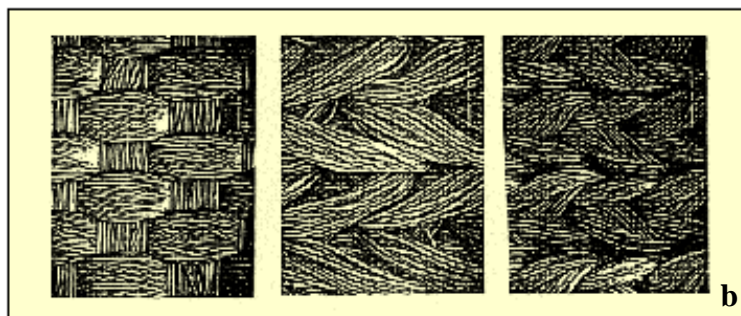


Figure 1.3. a) Dacron vascular graft (https://.../disease/marfan/actual2_graft.jpg), b) Woven (left) and knitted (center and right) fabrics used for Dacron vascular grafts (www.devicelink.com/mpb/archive/98/01/9801b16e.gif).

ePTFE is a fluorocarbon polymer that can be formed into porous sheets that have solid nodes interconnected by fine fibers with variable intra-nodal distances that can be used to change the graft porosity. The grafts in clinical use are impervious to blood, resistant to dilatation, chemically inert, highly electronegative and highly hydrophobic (Figure 1.4) (Zdrahala, 1996). ePTFE is better than Dacron for venous reconstruction.



Figure 1.4. ePTFE vascular graft
(www.terumo-cvs.com/images/products/10658.jpg)

Polyurethane has been used in the production of vascular grafts (Figure 1.5) because of its smooth and relatively low thrombogenic surface, and handling characteristics (Kim and Jacobs, 1996). However, patency rates have not been high mostly due to elongation of the polymer, leading to weakening and aneurysm formation, and degradation upon implantation (Santerre et al., 1994, Marois et al., 1996, Zhang et al. 1997). Therefore, new generation polyurethane grafts, which are currently in clinical trials, were designed by using polycarbonate based polyurethanes without ether linkages, and therefore, more resistant to biodegradation (Tanzi et al., 2000, Kannan et al., 2005).



Figure 1.5. Polyurethane vascular graft
(www.devicelink.com/.../media/Raumedic.jpg)

1.3.3. Biological Prosthetic Grafts

Biological grafts obtained from other humans (allografts) or from non-human species such as pig or bovine (xenografts) are also studied and used. These grafts undergo special treatment before they can be utilized in humans and have, therefore, been classified as prosthetic grafts. Allografts preserved by formalin, gamma irradiation or freeze-drying gave better results in the short term than fresh allografts but subsequently underwent degeneration and aneurysm formation (Callow, 1996). Unsatisfactory results with synthetic grafts, especially with small diameter vessels, due to a need for revision surgery and graft infection, has led to a renewed interest in allografts. Cryopreservation with liquid nitrogen and dimethyl sulfoxide (an oxygen radical eliminator) decreased the host immunological response and increased patency but degeneration could not be prevented (Borne et al., 1977). Glutaraldehyde treated human umbilical vein graft (Biograft-Biovascular Inc.) was introduced in 1975. Despite the good results reported (Dardik et al., 1988), there is not much evidence that the biological grafts have superior patency than small diameter synthetic grafts. Xenografts have the same disadvantages of rejection and degeneration as allografts (Brems et al., 1986). The risk of transmission of viral disease is a further complication of xenograft use.

1.3.4. Tissue Engineered Grafts

All of the prosthetic grafts have a lower patency than the autogenous vascular grafts (Geeracrt and Callaghan, 1977, Nunn et al., 1979, Chakfe et al., 1996, Miller et al., 2004). The major reasons for this low rate of patency are clogging, compliance mismatch and fibrous tissue formation. All materials are thrombogenic to some extent and clogging of the implanted grafts is a common problem. Another major problem is fibrous tissue formation at the interface between the graft and the tissue due to the natural healing process (Henze et al., 1996). To solve these problems many different approaches have been tried including the application of a variety of anti-thrombogenic coatings (Rhee et al., 1996), endothelial cell seeding (Thompson et al., 1994, Sarkar et al., 2007), and modifying pore size, surface texture, anatomical location and material biocompatibility (Hellener et al., 1994, Sandusky et al., 1995, Marois et al., 1996). These approaches improved the performance of prosthetic grafts (both synthetic and biological) to a certain extent but can only be applied in the treatment of the pathology of large arteries (>6 mm inner diameter). There is, therefore, a significant clinical need for an alternative source of vessels to replace the diseased, smaller diameter vessels. Tissue engineering offers a solution for this problem (Ratcliffe et al., 2000). By this approach limitations in reconstructing small diameter prosthetic vascular grafts such as thrombosis, thromboembolism, compliance mismatch, anticoagulant-related haemorrhage, neointimal hyperplasia and aneurysm formation can be overcome.

1.4. Tissue Engineering

Last decades the field of biomaterials has developed in a new direction, involving the use of cells and biodegradable carriers, generally termed tissue engineering. Tissue engineering is an interdisciplinary biomedical field that aims to produce substitutes to replace injured or diseased tissues, by using a multicomponent system, biomaterials, ECM components and cells (Langer and Vacanti, 1993). The general approach in tissue engineering is to harvest cells from tissue, proliferate them *in vitro* and seed on an appropriate carrier before

implantation into the patient. The carrier is called a scaffold, and should be able to mimic the natural ECM in providing the volume and sites for cell attachment, proliferation, migration and function. When this construct, i.e. carrier and cells, has matured to a defined degree it is implanted. Over time, the carrier degrades in the body, leaving only seeded and infiltrated cells, the natural ECM and the blood vessels produced by them (Freyman et al., 2001).

1.4.1. Cell Types and Sources Used in Tissue Engineering

The cells used in tissue engineering can be divided into 3 general categories; cell lines, primary cells and stem cells. They should be specific to the tissue targeted for regeneration and can be derived from different sources. Basically there are four different cell sources for tissue engineering; autogenous cells, allogenic cells, xenogenic cells and stem cells. The ideal cell source for this purpose is the patient himself, whose own cells, autogenous cells, are used in the process. The main advantage of use of mature autogenous cells is the prevention of the risk of immunological response. However, these cells are limited especially when the tissue is damaged or diseased, harvesting is not painless and poses the risk of infection. When the risk is high, different cell sources such as stem cells, allogenic or xenogenic cells should be considered (Nishida et al., 2004, Buma et al, 2004).

The use of stem cells in tissue engineering is a novel and promising approach since these cells can differentiate into different cell types with stimulation, and they have a higher proliferative capacity. But their utilization depends on, and is limited to, advances in stem cell research (Sun et al., 2005). Multipotent mesenchymal stem cells can be obtained from adult human tissues and can be used to obtain cells suitable for the engineering of the target tissue. Most commonly used mesenchymal stem cells sources are the bone marrow and Wharton's Jelly (the umbilical cord matrix).

Allogenic cells are cells from a different individual of the same species; another person for humans. Their use is limited due to an immunogenic response (rejection) caused by the host (Niemeyer et al., 2004).

Xenogenic cells are cells from species different than the target organism. Their use is infrequent since they can induce severe inflammatory and immunological responses leading to the rejection by the tissue or serve to transmit of infectious diseases (Tebken et al., 2000, Leyh et al., 2003). Xenogenic cells are generally used for research purposes.

1.4.2. Scaffolds Used in Tissue Engineering

Eukaryotic cells are anchorage dependent; therefore, they need a surface to attach. In tissue engineering, polymers of natural or synthetic origin are usually used to provide this surface which is called a carrier or a scaffold.

1.4.2.1. Synthetic Polymers

Constructing scaffolds from synthetic polymers has advantage of large scale production, low cost and processing. The most commonly used ones in tissue engineering are poly(α -hydroxy acids) such as poly(lactic acid) (PLA), poly(glycolic acid) (PGA) and their copolymers poly(lactic acid-*co*-glycolic acid) (PLGA). They are approved by the United States Food and Drug Administration for human clinical use (Langer, 2000). However, they have to be prepared under strictly controlled conditions and extensively purified of the catalysts, initiators, solvents and unreacted monomers. Also, they lack the binding molecules that can be recognized by cells for attachment, therefore; in most cases their surfaces need to be modified to increase the attachment efficiency of cells.

1.4.2.2. Natural Polymers

Among the natural polymers most commonly used in tissue engineering are collagens which are the most abundant animal protein (Lee et al., 2001, Hasirci et al., 2006), chitosan, a derivative of natural protein chitin (Shi et al., 2006) and poly(β -hydroxy acids) such as polyhydroxyalkanoates (PHA) which are the intracellular energy and carbon storage products found in various microorganisms,

and after genetic modification, in plants (Williams et al., 1999). In pure form PHAs are biodegradable and biocompatible; and therefore are being used in biomedical applications including tissue engineering. The most commonly used PHA is poly(3-hydroxybutyrate) which can be produced by a variety of bacterial strains in large amounts. Among the PHA, copolymers of 3-hydroxyvalerate and 3-hydroxybutyrate are found in different ratios (PHBV) and are among the most studied (Kose et al., 2003, Kenar et al., 2006, Zorlutuna et al., 2006, Ndreu et al., 2008).

1.4.2.2.1. Collagen

Collagen is the major protein in mammals constituting 20-30 % of the total body proteins (Harkness, 1961). It provides mechanical support to tissues and is found as an assembly of fibrous supramolecular aggregates in the ECM. Collagen is a triple helix of polypeptide chains with a large number of repeat sequences of Gly-X-Y; where X is often proline or hydroxyproline (Figure 1.6). Each collagen polypeptide chain comprises 1000 amino acid residues and the entire molecule is about 3000 Å long. These triple helices further polymerize into fibrils of several micrometer length and 50-200 nm thickness (Branden and Tooze, 2006). There are more than 20 different types of collagens differing in the amino acid sequences of each polypeptide chain and crosslinkage within the three dimensional structure (Bosman et al., 2003).

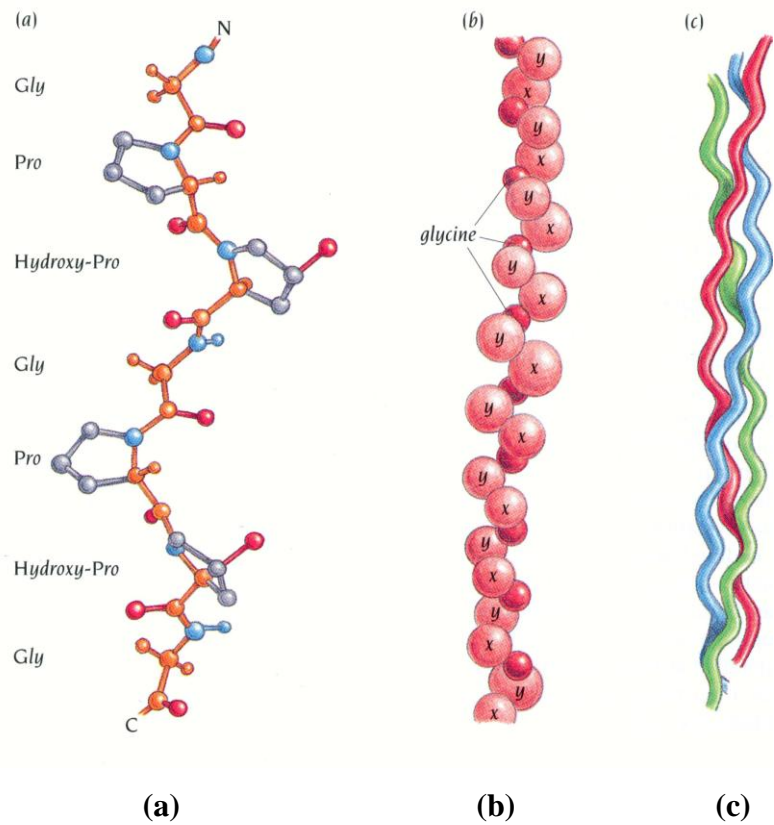


Figure 1.6. Structure of collagen. (a) Ball and stick model of two turns of one polypeptide chain, (b) model of a single collagen chain, (c) collagen superhelix (Branden and Tooze, 2006).

Since it is a natural molecule, collagen is biodegradable, offering the facility for regulating degradation rate by the degree of crosslinking. It is nontoxic and biocompatible when properly treated. It can easily be obtained in large amounts from various sources in contrast to most other natural materials used in the biomedical field. It easily can be obtained in pure form (pure Type I, II etc.). Also, since it is a part of the natural ECM it has the signal molecules required for cell attachment (Lee et al., 2001).

1.4.2.3. Processing, Modification and Characterization of Scaffolds

Scaffolds used in tissue engineering can be 2 or 3 dimensional depending on the nature of the tissue to be reconstructed. The 2 dimensional (2D)

carriers are generally in the form of membranes or films and the 3 dimensional (3D) ones are mostly foams or sponges of high porosity or multilayers of the 2D films.

The conventional and the simplest method for producing 2D scaffolds is solvent casting; a process that involves pouring a polymer solution onto a mold or a template and evaporating the solvent leaving behind a polymer sheet (Zorlutuna et al., 2006). Foams or sponges are the most common form of 3D scaffold and are produced by freeze-drying of a polymer solution. By this method high porosity interconnected foams can be produced. In order to have more control on the porosity and pore distribution particulate leaching is used in combination with freeze drying (Kose et al., 2003). In particulate leaching, a particle insoluble in the solvent for the polymer is incorporated into the foam structure and then leached out by immersing the sponge in a solvent for the particle and a non-solvent for the polymer. Recent approaches to scaffold preparation include rapid prototyping (RP) and electrospinning. RP is a computer-controlled production method borrowed from the manufacturing industry (e.g. automotive) and first used in the biomedical field to produce models that could be used in the design and manufacture of various prostheses including tailor-made prosthesis for individual patients (Bibb et al. 2000). This method allows the scaffold to be in a specific 3D shape to fit into an irregular defect site, to provide strictly defined porosity, pore size and pore distribution within the scaffold and through this to control the mechanical properties. Although the most commonly used polymers in this method are the synthetic ones (Zein et al., 2002, Vozzi et al., 2003, Yilgor et al., 2008), the method enables the use of polymers with aqueous solvents and enable production of well-defined structured hydrogels as well (Landers et al., 2002). The technology was also investigated for single cells and cell aggregates, to achieve direct organ printing (Mironov et al., 2003). Electrospinning is another method borrowed from other industry (e.g. textile industry) and produces micro and nano sized fine fibers but the product properties cannot be controlled as accurately as in RP. It is a technique that uses electrical potential to draw these fine fibers from a polymer solution. Its product is a very thin fibrous mesh (mat) that can be made thicker by using multilayers, rolling or folding into 3D forms. Although initially investigated with collagen in an attempt to mimic collagen matrices (ie. ECM) of natural tissues

(Huang et al., 2001, Matthews et al., 2002), later collagen was used blend with synthetic polymers like poly(ethylene oxide) (Huang et al., 2001, Zhang et al., 2005). Thus, electrospun synthetic polymers became at least as much studied as the natural ones and promising results were obtained when used as scaffold materials (Kenawy et al., 2003, Xu et al., 2004, Badami et al., 2006, Ndreu et al., 2008). The scaffold need not only provide a surface for attachment but can also act as a reservoir for the release of bioactive molecules like hormones, cytokines or growth factors as in the natural ECM. Although direct incorporation of the bioactive molecules into the scaffold materials was tried (Hile et al., 2000), more control of the release profile of the agents was achieved by incorporating controlled release techniques (micro-nano capsules, liposomes, etc.) into the scaffolds (Eiselt et al., 1998, Perets et al., 2003) and even by sequentially delivering more than one active agent (Zisch et al., 2003, Basmanav et al., 2008, Yilgor et al., 2009).

1.4.2.3.1. Surface Modifications

The surfaces of the scaffolds have been modified in many different ways since the beginning of tissue engineering. The first modifications were made to improve cell adhesion and spreading, mainly on scaffolds made from synthetic polymers because these kinds of polymers are mostly either too hydrophobic for the cells to properly attach to or do not possess the appropriate binding sites that the ECM provides for cells to interact with and used to attach to the surface. Among the most preferred but nonspecific methods used to modify the surface chemistry of the scaffolds is plasma treatment (O₂ or monomers) (van Wachem et al., 1989, Nitschke et al., 2002, Ozcan et al., 2008). Attachment of surface molecules which are either more hydrophilic, or hydrophobic than the original surface material or molecules that contain the appropriate cell attachment motifs (RGD, IKVAV etc.) for cell adhesion is another approach (Vleggeert-Lankamp et al., 2004).

Modifying the scaffold surface to mimic the architecture and chemistry of natural tissue is a relatively recent approach. This is done with physical and/or chemical cell guidance which can be used to orient cells in a predefined manner. In physical guidance, surface topography is organized in such a way that improves cell

localization, attachment or orientation by the physical restraints created (Curtis et al., 1978). Since it is known that the cell morphology also affects its functionality, obtaining layers of cells with morphologies close to their natural morphology in the target tissue is important (Jackman et al., 1998, Walboomers and Jansen, 2001). Thus, surface topography control also leads to improvements in cell functionality (Shen et al., 2006). Using scaffold surfaces with 3D patterns for cell guidance has been used by a number of researchers (Takayama et al., 1999, Pins et al., 2000, Dalton et al., 2001, Kenar et al., 2005, Zorlutuna et al., 2006). Most of the patterns used to this end were in the micron-scale because of the limitation of the methods used to create the desired patterns and also due to cells being micron scale, too. Nano-scale modification of surfaces of cell carriers is a more recent approach and it enables researchers to mimic the molecular level interactions of natural ECM (Craighead et al., 2001, Diehl et al., 2005).

Chemical guidance of the cells is achieved by 2D chemical patterns created on a scaffold surface (i.e. microcontact printing). This creates regions of different chemistry on the scaffold surface. For example, molecules containing RGD sequences and other cell adhesive molecules, or molecules that increase hydrophilicity are introduced in a predetermined design on the surface to obtain cell adhesion in these regions (Schmalenberg et al., 2004).

1.4.2.3.2. Nano-scale Modification of Scaffold Surfaces

Nanotechnology and nanobiotechnology are among the most novel research fields of the 21st century. Nanotechnology is defined as “research and technology development at the atomic, molecular, or macromolecular scale, leading to the controlled creation and use of structures, devices, and systems with a length scale of 1-100 nanometers” (McNeil, 2005). Since this range is at the scale of biomolecules, nanotechnology offers many new applications in the biomedical field. Physical or chemical manipulations of materials at the nano-scale has led to the design of novel drug delivery systems, image contrast agents and diagnostic systems, all important applications in the field of nanomedicine (Yang et al., 2004, Morawski et al., 2004).

Soft lithography, hot embossing lithography and dip-pen nanolithography (DPN) are some of the current methods used to create nano-scale features on a polymer surface (Hasirci et al., 2006). These methods have their limitations as well as advantages. For example, hot embossing lithography can achieve features as small as 10 nm (Schift et al., 2002), but involves application of heat and pressure which may not be desirable for many biopolymers. Soft lithography does not have this disadvantage since it is carried out under mild conditions but the resolution is not as good (Kane et al., 1999). Sub-100 nm sized patterns can be created by this method (Choi et al., 2005). DPN utilizes an atomic force microscope (AFM) in tapping mode to transfer the desired molecules from solution to a substrate surface according to a predetermined design. 30 to 50 nm features were successfully created by this method (Wilson et al., 2001). AFM was also used to create 3D nanopatterns by scratching a surface in contact mode (Tang et al., 2004, Yang et al., 2006). Alternatively, 3D nanopatterns were fabricated on silicone or acrylate based polymers by using x-ray interference lithography which provides periodic patterns on large areas in short processing times (Heyderman et al., 2004) or e-beam lithography which can be used to create complex arbitrary structures relatively slowly (Robinson et al., 1999) to produce features with sizes less than 30 nm and 10 nm, respectively (Figure 1.7).

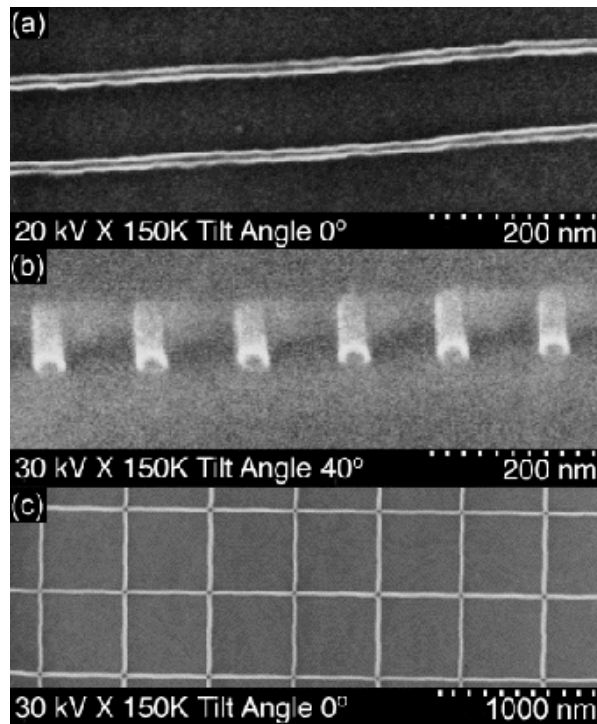


Figure 1.7. SEM micrograph of silicon wafers created by e-beam lithography. a) 14 nm wide lines, b) 30-40 nm dots and c) \sim 20 nm lines (Robinson et al., 1999).

1.5. Vascular Tissue Engineering

Proper functioning of a tissue engineered vascular graft depends on several conditions. An important requirement is adequate mechanical properties that approach that of native vessels. Another is that it should consist of a continuous layer of endothelium to prevent thrombosis and consequent clogging. A tissue engineered vascular graft must also have a highly organized structure consisting of collagen for strength and elastin to provide compliance and recoil. Organized layers of crosslinked collagen and elastin are a necessity for strong and elastic vessels (Mitchell and Niklason, 2003).

A general approach in vascular tissue engineering is to produce tubular constructs constituted of both a degradable scaffold and autogenous vascular cells (Boccafroschi et al., 2007) to achieve a structure with high mechanical strength and continuous lining of endothelial cells (Greenwald and Berry, 2000) (Figure 1.8).

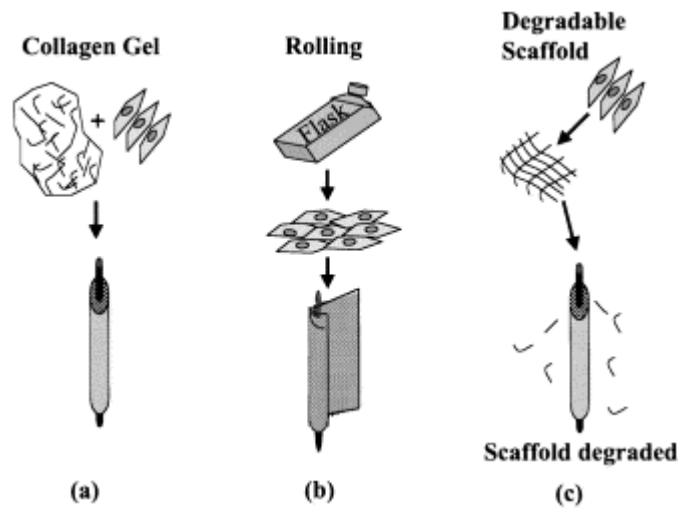


Figure 1.8. Development of (a) collagen gel-based, (b) rolled sheet and (c) degradable scaffold vascular grafts (Mitchell and Niklason, 2003).

The choice of the scaffold material is critical since stiff materials cause compliance mismatch which leads to formation of neointimal hyperplasia and atherosclerosis. On the other hand, materials with low ultimate tensile strength (UTS) rupture under normal blood pressure (Salacinski et al., 2001). As a result, many different materials were studied for their suitability for vascular tissue engineering purposes in terms of cell viability and mechanical properties both in the form of films and tubes.

Use of synthetic polymers as the scaffold material has the advantage of high mechanical strength but treatment of the scaffolds for enhanced cell interaction is generally required. Poly(ϵ -caprolactone) (PCL) films were tested after seeding with VSMC (Chong et al., 2007), and to increase the cell adhesion the films were modified either with collagen immobilization or surface hydrolysis (by immersion in sodium hydroxide), the latter causing a UTS drop. A collagen immobilized surface gave the best result in terms of VSMC adhesion and proliferation. Polyglyconate based electrospun tubular scaffolds with a random fiber distribution and 200-400 nm fiber diameter were mechanically tested and found to have enough mechanical strength for vascular tissue engineering applications (Thomas et al.,

2007). Polyglyconate had to be blended with biopolymers such as gelatin and elastin to mimic the natural artery and a layered structure was obtained by stepwise electrospinning. The UTS dropped to 2.5 MPa from 14.5 MPa after blending, still a value comparable to those of the natural arteries. In one study, tissue engineered vascular grafts that were prepared by using autogenous cells and biodegradable polyglycolic acid and polyhydroxyalkanoate polymers were tested as ovine pulmonary arteries which resulted in adequate mechanical strength with collagen and DNA content approaching to that of the native artery over time upon implantation to systemic circulation without any surface modification (Shum-Tim et al., 1999). Grenier et al. tested 3D porous polyurethane scaffolds with VSMCs and showed that these scaffolds promoted cell attachment and proliferation, however, they also caused uneven cell attachment and this was solved by coating the scaffold with Matrigel (Grenier et al., 2009).

An extreme case of vascular grafts is cell sheets rolled around mandrels (without any scaffold material), and they were found to possess good mechanical strength (burst strength of 2000 mm Hg) and suturability, but limited patency after 3 to 4 weeks of transplantation (L'Heureux et al., 1998).

Using natural polymers as scaffold materials gave better results than with synthetic polymers in terms of cell-scaffold interactions but these had lower mechanical properties. Smooth muscle and endothelial cells seeded on electrospun silk fibroin scaffolds proliferated, preserved their phenotype and deposited ECM (Zhang et al., 2008). In another study, tubular electrospun silk fibroin scaffolds were sequentially seeded with VSMCs and endothelial cells and cultivated under physiological pulsatile flow (Zhang et al., 2009). Dynamic flow conditions gave better results when compared to static culture controls in terms of cell proliferation, alignment, phenotype and ECM production. To enhance endothelial cell retention under physiological shear conditions the tube was coated with Matrigel. A tubular scaffold made from collagen supported with an acellular crosslinked collagen sleeve to enhance its mechanical properties demonstrated viable cells and appropriate histology (Berglund et al., 2003). Tubes made from collagen seeded with endothelial and smooth muscle cells were investigated under shear conditions (4 dynes/cm^2) which resulted in changes in the morphology of the cells that were

facing the luminal surface (Takei et al., 2007). Elastin was also studied as a scaffold material for vascular tissue engineering (Kurane et al., 2007). Acellular elastin tubes prepared from porcine carotid arteries were implanted subdermally in adult rats and cell infiltration was studied for 28 days. Cell infiltration was more when the elastin tubes were filled with agarose gel releasing basic fibroblast growth factor and most of the infiltrated cells were fibroblasts.

There are many studies showing that endothelial cells adhere to and proliferate well on many different materials including polyesters (Kwon et al., 2005, Miller et al., 2004) and natural polymers like silk fibroin (Bondar et al., 2008) and collagen (Vartanian et al., 2008). However, a major concern is that similar cell behavior is required under the hemodynamic conditions of the natural blood vessel (Li et al., 2005). More specifically, the endothelial cells need to be retained on a supporting scaffold during blood flow and under the resultant physiological shear force.

Another complication to obtaining a continuous layer of functional endothelial cells is biomaterial-induced toxicity. Kader and Yoder (2008) showed in their recent work that synthetic biomaterials cause endothelial cell death due to anoikis, a form of apoptosis caused by an inflammatory reaction due to an inappropriate interaction of cells with the surface (Kader and Yoder, 2008). They proposed that endothelial cells on synthetic biomaterials like PTFE, polyethylene terephthalate, polyester, or polyethylene produce increased amounts of superoxides and other reactive oxygen species which in turn induce a local inflammatory response and cell death. Since collagen is a part of the natural ECM and has the required molecular motifs for proper cell attachment, it is a good candidate as a scaffold material for endothelial cells (Lee et al., 2001).

As a scaffold material, collagen type I has a special place since it is the predominant protein in the natural ECM of the blood vessels. It is secreted by VSMCs and is essential for mechanically strong vessels (Mitchell et al., 2003). Collagen type I is hemocompatible; it does not enhance blood coagulation, modify the viscoelastic properties of the blood or cause excessive platelet adhesion and aggregation (100 mmHg, Boccafosci et al., 2005). However, engineered vascular grafts from reconstituted collagen possess lower mechanical properties than the

natural vessels (Berglund et al., 2003). Even though the artificial blood vessels consist mainly of collagen as the natural blood vessel this low mechanical strength could be related with the loss of the fibrillar nature and organization of the natural vessels.

It was also suggested that circumferential orientation of natural smooth muscle cells could be the reason for the observed mechanical strength, so mimicking this could improve the mechanical strength of the engineered vessels (Tranquillo et al., 1996). Mimicking of natural tissues was attempted by cell guidance using physical cues in many studies (Dalton et al., 1999, Pins et al., 2000, Kenar et al., 2006, Zorlutuna et al., 2006). In this approach surface topography is modified to improve attachment, orientation and morphology of the seeded cells. It was shown that cell orientation affects its morphology and this in return affects their function, and mechanical properties of the construct, therefore, achieving an organization similar to that in their natural environment is important (Walboomers et al., 2001, Zorlutuna et al., 2007, Vrana et al., 2007). A support in this direction was obtained when alignment of VSMCs with the help of microchannels in a pattern similar to their natural organization resulted in cells with the “contractile phenotype” which is necessary for functional blood vessels, rather than the “synthetic phenotype” (Shen et al., 2006). Patterns created on the surfaces for this purpose were at micron-scale because the cells were of micron dimension and also the techniques used to create the desired patterns had micron scale resolution. Nano-scale modification of cell carriers became possible only recently through the use of developments in nanotechnology and thus the topography of the natural ECM could be mimicked at the molecular level (Craighead et al., 2001, Diehl et al., 2005). The major question now was “Can nano-patterns guide cells?”. Previously, guidance of VSMCs was accomplished by using electrospun poly(L-lactide-co-ε-caprolactone) (75:25) scaffolds with 500 nm fiber diameter (Xu et al., 2004). This alignment was suggested for probable mechanical property enhancement, but the correlation of cell guidance and mechanical properties was not studied experimentally. There are also studies showing that endothelial cells could be aligned by micropatterns (Duncan et al., 2007, Vartanian et al., 2008). However, endothelial cell alignment is also reported to result in apoptosis due to cell

anisotropy and resultant inadequate cell attachment to the surface (Hu et al., 2004, Wu et al., 2007). Nano-scale topographies were also tried, mainly to increase endothelial cell adhesion on synthetic surfaces. PLGA surfaces having nano-scale controlled roughness rather than patterns, were tested for improved endothelial cell adhesion but this resulted in lower cell adhesion than the unmodified planar surfaces (Miller et al., 2004). Nano-scale modification of other vascular graft materials including polyurethane derivatives (Punshon et al., 2005) and titanium (Lu et al., 2008) were also tried, and these succeeded in increasing endothelial cell attachment and proliferation, apparently through increased surface area. The difference in responses to Miller et al.'s (2004) material, to Punshon et al.'s (2005) and Lu et al.'s (2008) must be due to the surface chemistry differences between these surfaces.

The effect of cell seeding on the mechanical properties of tissue engineered constructs has been studied from different angles. The presence of fibroblasts in collagen gels increased the mechanical properties starting with Day 3 of culture, up to a few weeks by contracting the collagen fibers in the gel, an effect that decreased as the culture period increased (Feng et al., 2003). The presence of cells could affect the mechanical properties of the tissue engineering scaffolds through interfering with their metabolism as well. In one study it was shown that seeding of fibronectin-null myofibroblasts on collagen gels loaded with fibronectin resulted in polymerization of fibronectin into ECM and increase in mechanical strength (Gildner et al., 2004).

A mechanical stimulus was also used to enhance the mechanical properties of cell seeded scaffolds. Although it was not effective at 2 weeks, cyclic distention was shown to increase the mechanical properties of smooth muscle cell seeded collagen-based scaffolds after 5 weeks of incubation (Isenberg and Tranquillo, 2003). Alignment of fibroblasts by static mechanical stimuli was also shown to increase the mechanical strength of cell sheets (Grenier et al., 2005). Earlier studies on cell guidance for corneal tissue engineering had shown that seeding with keratocytes enhanced the mechanical properties of micropatterned polymeric films but seeding with epithelial cells did not, suggesting that the presence of the cells was not enough, rather, the ECM secreted by the guided cells

was needed to enhance the mechanical properties of the scaffold (Zorlutuna et al., 2007, Vrana et al., 2007). Thus, increase of mechanical strength due to guidance of cells was only possible if that cell type secreted its own ECM.

The cell source for tissue engineered vascular grafts is an important issue. Common autografts used in the clinics are the veins; they are more available in adequate length, easily harvested and adapt well to placement in arterial circulation (Farsak et al., 2003). The saphenous vein is the first choice of the surgeons because of its appropriate diameter, relatively thick walls and providing sufficient length (due to being the longest vein in the body). Therefore, cells harvested by a small biopsy sample from the saphenous vein could be a suitable cell source for vascular tissue engineering both because of these properties and also since the cells can be isolated with high efficiency and can be proliferated and passaged without dedifferentiation.

1.6. Approach and Novelty of the Study

The aim of this study was to produce a tissue engineered vascular graft with appropriate mechanical properties using nanopatterned tubular collagen scaffolds populated with smooth muscle cells on the outside and endothelial cells in the inside of the tube. The approach followed to this end was to first test the 2 cell types individually on the collagen films patterned with 322.5-650 nm wide nanochannels, knowing that these 2D films can be effectively converted into tubes by rolling and crosslinking. Nanopatterned films with various dimensions were seeded with commercial endothelial cell line Human Microvascular Endothelial Cells (HMEC) and vascular smooth muscle cells (VSMC) isolated from human saphenous vein and tested for vascular tissue engineering purposes in terms of cell proliferation, viability, phenotype, alignment, small molecule diffusivity (4-acetaminophenol and oxygen) and mechanical properties under tensile conditions. After these individual tests, both cell types were seeded sequentially (first VSMC) on the two sides of the nanopatterned tubular scaffolds and co-cultured. The tubes containing both the endothelial cells and the smooth muscle cells were further investigated for cell proliferation, phenotype and histology of the tissue engineered

construct. The hypothesis was that cells aligned on the biodegradable films will strengthen them mechanically as a result of the metabolic products and the ECM secreted by them. Mechanical test results showed that aligning smooth muscle cells, and probably the ECM that was secreted by them, just as in the natural ECM of the vessels indeed improved the mechanical properties bringing them into the range of the natural vessels. Using nanopatterns on the inside of the tube enhanced endothelial cell retention under physiological shear conditions. Therefore, this study showed that cell guidance can be used to enhance the mechanical properties of engineered vessels as proposed several times in the literature and overcome one of the most important challenges in vascular tissue engineering; the adequate mechanical properties, while using nanopatterns enhanced endothelial cell retention leading to formation of a continuous endothelial layer even under flow shear conditions, which is the other major challenge in the field.

Novelty of the study:

Effect of VSMC alignment with the help of nanosized topographical cues on the mechanical properties of engineered vascular grafts has not been reported yet. Also, the influence of nanopatterns on cell retention on the films under dynamic culture conditions (shear), too, was not earlier shown. These two aspects are very important in constructing a viable vascular graft.

CHAPTER 2

MATERIALS AND METHODS

2.1. Materials

N-hydroxysuccinimide (NHS) was purchased from Aldrich Chem. Co. Inc. (USA). Poly(dimethylsiloxane) (PDMS) was supplied by Dow Corning (Sylgard 184 Elastomer Kit, USA). Fetal calf serum (FCS) and Dulbecco's Modified Eagle Medium (DMEM) were obtained from Hyclone (USA). Ham-F12 and MCDB 131 Medium was obtained from Gibco Invitrogen Co. (New Zealand). Alamar Blue was purchased from Biosource (USA). Cacodylic acid (sodium salt), ascorbic acid, glutaraldehyde (Grade I, 25 % aqueous solution), trypsin-EDTA (0.25 %), sodium azide, gelatin, endothelial cell growth supplement (ECGS), poly(L-lysine), dimethyl sulfoxide (DMSO), Monoclonal Anti-Actin α -smooth muscle, Monoclonal Anti-PECAM-1 (CD31), 4',6-diamidino-2-phenylindole (DAPI), L-glutamine, streptomycin-penicillin (10000 units), acrylamide-bisacrylamide, Coomassie Brilliant Blue and 4-acetaminophenol were supplied by Sigma Chem. Co. (USA). Ethyldimethylaminopropyl carbodiimide (EDC) and dialysis tubings were purchased from Pierce (USA). Formaldehyde (37 %), acetic acid and Tween 20 were obtained from Merck KGaA (Germany). AlexaFluor 488, calcein AM and ethidium homodimer-2 were supplied by Molecular Probes Inc. (USA). Bovine serum albumin (BSA) was purchased from Fluka (Germany). Triton X-100 was supplied by Applichem GmbH (Germany). Human Microvascular Endothelial Cells were obtained from Center for Disease Control (CDC) of USA (CDC, Ref. No: E-036-91/0). Human Internal Thoracic Artery Endothelial Cells

and their growth medium were purchased from European Collection of Cell Cultures (UK). Rank cell was supplied from Rank Brothers Ltd (UK), platinum wire from and silver/silver chloride electrode from Bioanalytical System Inc., (UK). Human saphenous vein segments were obtained from Bayındır Hoapital (Ankara, Turkey) under the supervision of their ethical committee.

2.2. Methods

2.2.1. Scaffold Preparation

2.2.1.1. Collagen

As the scaffold material type I collagen isolated from rat tails according to the following procedure was used.

2.2.1.1.1. Isolation

Type I collagen was isolated from male Sprague Dawley rats after terminating the rats by ether inhalation. Rat tails were dissected and tendons were placed in cold acetic acid (0.5 M) for a couple of days at 4°C with stirring to dissolve the tendons and after that the solution was filtered to remove any insoluble material. Then the collagen solution (500 mL) was dialyzed (10,000 MWCO, Pierce, USA) against a buffer (5 L, 12.5 mM NaH₂PO₄, 11.5 mM Na₂HPO₄, pH: 7.2) at 4°C. After the collagen precipitated out of the solution as a white solid it was centrifuged (Hettich Zentrifugen, Germany) at 16000 x g for 10 min at 4°C. Pellet was dissolved in cold acetic acid (500 mL, 0.15 M) at 4°C overnight. NaCl (25 g, Solid) was added to give a final concentration of 5% and this was incubated at 4°C overnight to dissolve the salt. Collagen was precipitated after this step. The final pellet was dissolved in cold acetic acid (500 mL, 0.15 M) at 4°C overnight and dialyzed for 5 consecutive days at 4°C. Collagen solution was centrifuged again and the pellet was stirred in 70% EtOH for 48 h. After a final centrifugation step, the

final pellet was frozen at -80°C and lyophilized by freeze drying (FreeZone[®] 6 Liter Freeze Dry System, Labconco Co., USA) for 12 h.

2.2.1.1.2. SDS-PAGE Analysis of Isolated Collagen Type I

The purity of the isolated type I collagen was determined by SDS-PAGE. Separating (10 % acrylamide/bisacrylamide) and stacking (4.2 % acrylamide/bisacrylamide) gels were prepared and the isolated collagen and commercial type I collagen (BD Biosciences, USA) were loaded in 0.2 % (in 0.15 M acetic acid) concentration after denaturing at 95°C for 5 min. Samples were run at 30 mA for 2.5 h. Later the gel was stained with 0.2 % Coomassie Brilliant Blue by incubating overnight on a shaker and destained in a solution of 40 % water, 50 % methanol and 10 % acetic acid.

2.2.1.2. Template Preparation

X-ray interference lithography was used to create the templates with the nano-channels. Briefly, a photoresist (AZ 5214) is coated in 500 nm thickness on a silicon wafer (2 cm^2), exposed to a laser of $\lambda=325\text{ nm}$ for 10 min and developed revealing patterns in the form of channels. Later, these patterns were transferred to silicon by using an epoxy replica of the original template. The designs obtained were parallel channels with 650 nm equal groove and ridge widths with 300 nm depth, equal groove and ridge widths of 500 nm with 250 nm depth and equal groove and ridge widths of 332.5 nm with 200 nm depth.

To prepare PDMS replicas, PDMS and the curing agent were mixed 10 to 1 (w/w) and poured onto the silicon templates. After removing the bubbles under vacuum, PDMS was cured at 65°C for 3 h.

2.2.1.3. Film Preparation

2.2.1.3.1. Single-Side Nanopatterned Films

Films patterned on one side and unpatterned films were prepared by solvent casting collagen solution (200 $\mu\text{L}/\text{cm}^2$, 15 mg/mL, 0.5 M, in acetic acid) on PDMS templates. After overnight drying at room temperature, films were peeled off the surface.

Chemical crosslinking was performed using EDC and NHS dissolved in NaH_2PO_4 (50 mM, pH 5.5) at concentrations of 33 mM EDC and 6 mM NHS. Films were immersed into the crosslinking solution for 2 h at room temperature. Films were washed with Na_2HPO_4 (0.1 M, pH 9.1) for 1 h, with 1 M NaCl for 2 h and with 2 M NaCl for 1 day with a minimum of five solution changes. Films were finally washed with distilled water, dried and stored at room temperature in a desiccator (Staros et al., 1986).

2.2.1.3.2. Double-Side Nanopatterned Films

In order to prepare double sided patterned collagen films collagen solution (150 μL , 20 mg/mL, in 0.5 M acetic acid) was placed onto one of the templates and allowed to partially dry for 3 h and then the second template was placed on the top with its patterns perpendicular to the one on the bottom. It was allowed to dry for 4 days and after drying, films were peeled off the surface and stored at room temperature in a desiccator.

2.2.1.4. Preparation of Tubular Scaffolds

Films prepared as described in Sections 2.2.1.3.1. or 2.2.1.3.2., were rolled around Teflon mandrels (dia. 3.5 mm) and chemically crosslinked in this position as described in Section 2.2.1.3.1.

2.2.2. Characterization

2.2.2.1. Atomic Force Microscopy

Silicon templates and collagen films (650 nm channel width) were examined with AFM (Universal SPM, Quesant, Ambios Inc., USA) in non-contact mode with silicon tips (at 2 Hz, 40 x 40 mm² maximum scan area).

2.2.2.2. Scanning Electron Microscopy

Collagen films and the tubular scaffolds prepared from these films were spin coated with a thin layer of gold under vacuum and characterized with SEM (Quanta 400F Field Emission SEM, Netherlands).

2.2.2.3. Stereomicroscopy

Tubular scaffolds were examined by stereomicroscopy (SMZ 1500, Nikon, USA) before and after incubating under cell culture conditions for 28 Days.

2.2.2.4. Diffusivity

Diffusivity of the collagen film towards oxygen and 4-acetaminophenol was measured in order to estimate nutrient transport through the films. 4-acetaminophenol was used as a model molecule to glucose since their molecular weights are similar (180 and 151.6). Collagen films were placed over a 2 mm diameter platinum working electrode of a Rank cell (Figure 2.1). A platinum wire (MW-1032, 0.5 mm diameter, 75 mm length) was used as the counter electrode and the reference electrode was a silver/silver chloride electrode (MF-2052). Autolab PGStat10 potentiostat instrument (Eco Chemie, (Netherlands)) was used for the amperometric measurements. Diffusion coefficients were calculated according to Rong et al. (2006) by fitting the experimental data to Fick's Second Law:

$$\partial C / \partial t = D \partial^2 C / \partial x^2$$



Figure 2.1. Rank cells. www.rankbrothers.co.uk/images/oxyelec.jpg

For 4-acetaminophenol diffusivity measurements phosphate buffer saline (5 mL, pH: 7.4, 10 mM) was placed in the Rank cell and stirred with a magnetic stirrer. After application of a polarizing voltage of + 0.65 V versus the reference electrode, 4-acetaminophenol was added into the buffer in the Rank cell to yield a final concentration of 1 mM. Test groups for 4-acetaminophenol measurements included a) unseeded films, b) human microvascular endothelial cell (HMEC) seeded films, c) HMEC seeded and fixed films, and d) unseeded and fixed films, ($n=3$). The films themselves were already crosslinked (fixed) with EDC/NHS. Cell fixation was done with 4% formaldehyde for 30 min which can further crosslink the collagen films. Unseeded and fixed films were included to both tests to see the effect of the additional formaldehyde crosslinking.

Diffusivity of the collagen films to oxygen (MW 32) was also determined. This time first PBS (2.5 mL, pH: 7.4, 10 mM), that was deoxygenated by bubbling argon gas through it, was placed in the Rank cell and stirred. After application of polarizing voltage 2.5 mL oxygenated PBS was added. Test groups for oxygen included: a) unseeded films, b) unseeded and fixed films, and c) HMEC seeded and fixed films ($n=3$). Cell fixation was done with formaldehyde as before (Section 2.2.3.1.2.2).

2.2.3. *In Vitro* Studies

2.2.3.1. Human Microvascular Endothelial Cells (HMEC)

2.2.3.1.1. HMEC Cell Culture

HMECs (passage 15) were cultured in MCDB 131 Medium supplemented with 5% FCS, 200 mM L-glutamine, 1 % penicillin-streptomycin at 37 °C in a carbon dioxide incubator (5 % CO₂, MCO-17AIC, Sanyo Electric Co. Ltd., Japan). The cells were passaged using 0.05 % trypsin-EDTA solution at subconfluency.

2.2.3.1.2. Studies with HMECs on Collagen Films

Collagen films (1 cm²) were placed into 24-well plates, sterilized by incubating in EtOH (70%) for 2 h, washed 4 times with PBS (10 mM, pH 7.4) and dried under sterile conditions in a laminar flow cabin (LaminAir Safe 2000, Holten A/S, Denmark). HMECs were detached from the tissue culture flasks by using 0.05% trypsin for 5 min at 37⁰C, then centrifuged (Sigma Laborzentrifugen GmbH, Germany) for 5 min at 3000 rpm and resuspended in MCDB 131 Medium supplemented with 5% FCS, 200 mM L-glutamine, 1 % penicillin-streptomycin. Cell number was counted using NucleoCounter (ChemoMetec A/S, Denmark). 3 different seeding densities; 2x10⁴, 5x10⁴ and 1x10⁵ cells/film were used. First, cells in these densities were seeded on each film in 50 µL medium (MCDB 131 Medium supplemented with 5% FCS, 200 mM L-glutamine, 1 % penicillin-streptomycin) and the films were not disturbed for 30 min to allow cell attachment. After 30 min, 500 µL of the same medium was added. They were incubated at 37 °C in a carbon dioxide incubator (5 % CO₂, MCO-17AIC, Sanyo Electric Co. Ltd., Japan) for 24 or 48 h. Same density of cells was also achieved on tissue culture polystyrene (TCPS) control.

2.2.3.1.2.1. Cell proliferation

The samples that were seeded with 3 different seeding densities, 2×10^4 , 5×10^4 and 1×10^5 cells/cm², were examined after 48 h with Alamar Blue assay to compare the cell amount on the films and on the control. For the Alamar Blue assay the cells were incubated in 5 % Alamar Blue solution in complete medium for 4 h and the fluorescence was measured at an excitation wavelength of 544 nm and emission wavelength of 590 nm.

2.2.3.1.2.2. Microscopy (SEM, Fluorescence)

The cells on the films (1 cm²), which were seeded with 2×10^4 cells/cm² on each, were fixed after 24 h with 4% formaldehyde and stained with DAPI to examine cell alignment. Also, to determine cell viability, cells were double stained with Calcein AM (for live cells) and ethidium homodimer-2 (for dead cells) without any fixation at 24 h. After 48 h of seeding, the samples were crosslinked with 4% formaldehyde and dehydrated in a graded series of EtOH (50%-95%) and examined with SEM after coating with a thin layer of gold under vacuum.

2.2.3.1.2.3. Flow-Shear Studies

After 48 h of incubation under static cell culture conditions in a CO₂ incubator (37⁰C, 5% CO₂), flow-shear studies were performed by using a custom made flow chamber and a pump (Watson Marlow Pumps, 205U). 5×10^4 cells/cm² seeded on nanopatterned (332.5 nm and 650 nm wide channeled) and the unpatterned films were subjected to flow-shear stress. Average shear stress value on a flat section of an artery is reported to vary between 10 to 20 dynes/cm² (Nerem et al., 1998). Films were placed in the flow chamber and the complete medium flow rate 0.72 mL/min was achieved exerting a flow shear stress of 12 dynes/cm² on the film surfaces according to the following equations:

$$(1) \quad V_m = \frac{Q}{A}$$

$$(2) \quad V = 2V_m \left\{ 1 - \left(\frac{y}{a} \right)^2 \right\}$$

$$(3) \quad \tau_\omega = \mu \frac{\partial V}{\partial y} = \mu 2V_m \cdot \frac{2y}{a^2} \Big|_{y=a}$$

$$(4) \quad Q = \frac{\tau_\omega \cdot A \cdot a}{4\mu}$$

where V_m the maximum velocity in the channel (mm/s), Q is the flow rate (mL/min), A is the cross-sectional area (mm²), $2a$ is the depth of the channel (mm), y is displacement coordinate (depth), τ_ω is the flow shear stress (dynes/cm²) and μ is the viscosity (cp). After 1 h of stress application in a CO₂ incubator at 37⁰C and 5% CO₂, cells were fixed with 4% formaldehyde, permeabilized with Triton-X 100 and stained with DAPI for fluorescence microscopy ($n=3$). Cell number on these films as well as the control films (seeded at the same time with same density but not subjected to shear stress) were quantified by obtaining images with a fluorescence microscope (Leica Microsystems, Germany) with x 10 objective, from 6 random areas (each area was calculated to be ~ 2 mm²) of the film and counting the stained cell nuclei with Image J (NIH).

2.2.3.2. Human Vascular Smooth Muscle Cells (VSMC)

2.2.3.2.1. Cell Isolation

Human saphenous vein segments (~5 cm in length) were obtained from patients who under went by-pass surgery at Bayındır Hospital (Ankara, Turkey) following the guidelines of the Ethical Committee of Bayındır Hospital (Appendix A). The vein piece was put into the transport medium (DMEM:Ham F12-1:3 supplemented with 10% FCS and 10 µL/mL penicillin-streptomycin) and stored at RT (not more than 3 h). Vein was washed with PBS, cut longitudinally and the endothelial cells were scraped off the tissue with a # 15 scalpel blade. The vein was

then cleaned with a sterile gauze soaked in PBS to remove any remaining endothelial cells. Then the de-endothelialized vein was cut into smaller pieces (~ 4 mm²) and put with luminal surface facing down into 35 mm Petri dishes which were pre-coated with gelatin (Grenier et al., 2003).

For gelatin coating, briefly, gelatin solution (1% in distilled H₂O) was warmed to 55⁰C and filtered for sterilization. 3 mL of this solution was added into the 35 mm Petri dishes, incubated for 3 h at 37⁰C and washed with PBS before explant culture. To enhance the adhesion of explants onto the gelatin-coated Petri surface, a small volume (500-700 µL) of DMEM-Ham F12 (3:1) supplemented with 30 % FCS, 75 µL/mL ECGS and 10 µL/mL penicillin-streptomycin was added and CO₂ concentration of the incubator was increased from 5 to 8% until the cells migrated out of the biopsy samples. Extreme care was taken during the manipulation of the dishes to keep the explants attached to the surface.

2.2.3.2.2. Culturing

When the explant culture cells reached subconfluency (90%), they were trypsinized by incubating for 1 min in 0.25 % trypsin-EDTA solution and counted with the NucleoCounter. 2.5x10⁴ cells were seeded on poly(L-lysine) coated cover slips for immunostaining and the rest of the cells were transferred into a T75 tissue culture flask and incubated in the standard medium (3:1-DMEM:HAM F12 supplemented with 10 % FCS and 1 % penicillin-streptomycin) until they reached confluency. At sub-confluency, cells were passaged until passage 6 or they were frozen at lower passage numbers for future use. The freezing medium for the cells was, 10 % DMSO in standard medium.

2.2.3.2.3. Characterization

VSMCs at passages 4, 5 and 6 were immunostained to show that the cells were not dedifferentiating due to passaging. Cells were seeded on the poly(L-lysine) coated cover slips and then stained for α-smooth muscle actin by using AlexaFluor 488 as the secondary antibody to show the cell phenotype. These were

also stained with DAPI for the cell nuclei to show that all of the cells in the culture were VSMCs since DAPI would have shown the nuclei of other cells as well if there were any. After fixing the cells with formaldehyde (4%) for 30 min at RT, cells were permeabilized with Triton X-100 (1%) for 5 min and washed 3 times with PBS (10 mM, pH 7.4). Then they were incubated in blocking solution (0.5% BSA, 0.1 % Tween 20, 0.1 % FCS, 0.1% sodium azide in PBS) for 30 min at RT and in primary antibody solution (anti- α -smooth muscle actin diluted in blocking solution to achieve a concentration of 10 μ g/mL for 2 h at 37°C). After washing 3 times with PBS cells were incubated 1 h in secondary antibody solution (Alexa 488 diluted 1:400 in blocking solution) which also contains DAPI (1:5000 diluted) at 37°C. After 3 final washes with PBS, cells were examined with a fluorescence microscope (TCS SPE, Leica, Germany).

2.2.3.2.4. Studies with VSMCs on Collagen Films

Collagen films were placed into 24-well plates, sterilized by incubating in EtOH (70%) for 2 h, washed 4 times with PBS (10 mM, pH: 7.4) and dried under sterile conditions in a laminar flow cabin. VSMCs (passage 4) were detached from the tissue culture flasks by using % 0.25 trypsin-EDTA for 1 min at 37°C, then centrifuged for 5 min at 3000 rpm and resuspended in their standard medium (3:1-DMEM:HAM F12 supplemented with 10 % FCS and 1 % penicillin-streptomycin). Cell number was determined using NucleoCounter. 5000 cells/film were seeded on each film in 50 μ L of standard medium and the films were not disturbed for 30 min to allow cell attachment. After 30 min, 500 μ L of the same medium was added. They were incubated at 37 °C in a CO₂ incubator for 21, 45 and 75 days. Medium was changed every other day. Same density of cells was also seeded to TCPS as control.

2.2.3.2.4.1. Cell proliferation

On Days 1, 7, 14 and 21 Alamar Blue assay was performed in order to determine the live cell number on the films. Briefly, cells were incubated in 10 % Alamar Blue in colorless DMEM for 1 h and the optical density (OD) was measured at 570 and 595 nm with a kinetic microplate reader (Maxline Vmax[®], Molecular Devices, USA). From these OD values percent reduction of the dye was calculated according to the equation that was given by the Alamar protocol (Appendix B). These percent reduction values were further converted to cell numbers by constructing a calibration curve (Appendix C).

2.2.3.2.4.2. Microscopy (SEM, Fluorescence)

On Days 1, 7, 14 and 21, the cells on the films were fixed with formaldehyde (4%) and immunostained as described previously in Section 2.2.3.2.3. Also on the same days, cells on the films were crosslinked with glutaraldehyde (2.5 % in Cacodylate buffer 0.1 M, pH:7.4) before SEM examinations.

2.2.3.2.4.3. Mechanical Tests

Tensile properties of unseeded and cell seeded collagen films were determined using Instron 3366 (50 N load cell, Instron Engineering Co., U.S.A.) mechanical tester. Test groups consisted of unseeded wet films (Day 0) and VSMC seeded films (seeding density 5000 cells/cm²). Cell seeded samples included 2 different types of nanopatterned films (650 nm and 332.5 nm) and unpatterned films after 45 and 75 days of incubation ($n=6$). The cells on all the cell seeded samples were not fixed. Wet films were gently placed on a rubber base and a sharp triple-blade tool was used to cut two rectangular specimens (ca. 15 mm length, 4.2 mm width) from each film. The specimens were subsequently attached to the grips. After the attachment of each film, the length of the film portion between the grips were measured and recorded. Testing was performed at room temperature (ca.

21°C) in wet state on an Instron 3366 (Instron Engineering Co., U.S.A) with 50 N capacity load cell. The specimens were subjected to uniaxial tension with an elongation rate of 0.4 mm/min. This rate corresponded to a strain rate of 10%/min. Testing continued until the failure of the specimen was achieved.

2.2.3.2.5. Studies with VSMCs on Tubular Scaffolds

Tubular collagen scaffolds were placed into 24-well plates, with Teflon mandrels inside and Teflon sheets covering the bottom of the wells to prevent cell adhesion to the well bottoms, in an inclined fashion in order to allow the cells to adhere around the tubular structure (Figure 2.2). They were sterilized by incubation in EtOH (70%) for 3 h and wash 4 times with PBS (10 mM, pH: 7.4). VSMCs (passage 4) were detached from the tissue culture flasks by using % 0.25 trypsin for 1 min at 37°C, then centrifuged for 5 min at 3000 rpm and resuspended in their standard medium (3:1-DMEM:HAM F12 supplemented with 10 % FCS and 1 % penicillin-streptomycin). Cell number was counted using NucleoCounter. In order to optimize the cell seeding density 5×10^4 , 1×10^5 and 2×10^5 cells/tube were seeded on each tube in 2 mL of standard medium. They were incubated at 37 °C in a carbon dioxide incubator for 21 days. Medium was changed every other day. Cell numbers were determined as in Section 2.2.3.2.4.1 and microscopy conducted according to Section 2.2.3.2.4.2.

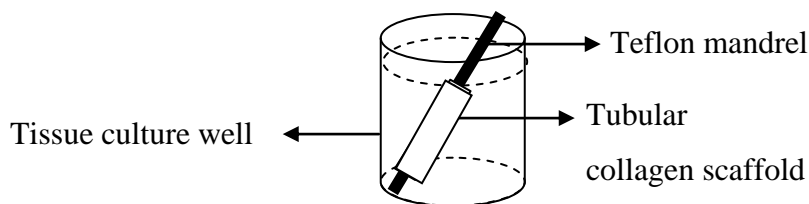


Figure 2.2. Schematic representation of tubular collagen construct in 24 well tissue culture plate.

2.2.3.3. Human Internal Thoracic Artery Endothelial Cells (HITAEC)

HITAECs (passages 2-10), which were obtained from European Collection of Cell Cultures, were cultured in HITAEC Growth Medium at 37 °C in a carbon dioxide incubator. The cells were passaged by incubation in 0.25 % trypsin-EDTA for 1 min at room temperature solution at subconfluency.

HITAECs were characterized by immunostaining as described previously in Section 2.2.3.2.3. by using anti-PECAM-1 (CD31), which is an endothelial cell marker, as primary antibody. Samples were also stained with DAPI for the cell nuclei.

2.2.4. Co-Culture of VSMCs and HITAECs on Tubular Scaffolds

Tubular collagen scaffolds were placed into 24-well plates, with Teflon mandrels inside and Teflon sheets covering the bottom of the wells, in an inclined fashion in order to allow the cells to adhere around the tubular structure. They were sterilized by incubating in EtOH (70%) for 3 h and washed 4 times with PBS (10 mM, pH: 7.4). VSMCs (passage 4) were detached from the tissue culture flasks by using 0.25 % trypsin-EDTA for 1 min at 37°C, then centrifuged for 5 min at 3000 rpm and resuspended in their standard medium (3:1 DMEM:HAM F12 supplemented with 10 % FCS and 1 % penicillin-streptomycin). Cell number was counted using NucleoCounter and 2×10^5 cells in 2 mL were seeded on each tube. They were incubated at 37 °C in a carbon dioxide incubator for 14 days. Medium was changed every other day. After 14 days, the mandrel was removed and the inside of the tube was seeded with HITAECs in a density of 0.5×10^5 cells/tube and incubated for another week. After HITAEC seeding the medium was changed to HITAEC medium and the medium was changed every other day. Alamar Blue assay was performed in order to determine the cell number on the tubes as described in Section 2.2.3.2.4.1.

2.2.4.1. Microscopy (SEM, Fluorescence)

On Day 1, 7, 14 and 21 the cells on the tubes were fixed either with formaldehyde (4%) or with glutaraldehyde (2.5 % in Cacodylate buffer 0.1 M, pH:7.4) for immunostaining and SEM, respectively. Immunostaining was done as described previously in Section 2.2.3.2.3. by using anti- α -smooth muscle actin as primary antibody for VSMCs and by using anti-PECAM-1 (CD31) as primary antibody for HITAECS. Immunostained samples were also stained with DAPI for the cell nuclei.

2.2.4.2. Histology

On Day 21, co-culture samples were examined histologically. The cells on the tube were fixed with formaldehyde (4 %) for 24 h and incubated in EtOH (96 %) for 5 h with 5 solvent changes. Then the tubes were transferred into xylol and incubated for another 2 h with 2 solvent changes and embedded in paraffin for 4 h at 62 °C. Five μ m thick sections were obtained with a microtome (RM 2125RT, Leica, Germany) and deparaffinized by incubating in 70 °C for 25 min and in xylol for 30 min. After immersing in EtOH (96 %, each for 2 min) 5 times and washing with dH₂O, the sections were stained with Hematoxylin-Eosin (Biooptica, Italy) by incubating in Hematoxylin for 5 min, washing with dH₂O and incubating in Eosin for 2 min. After a final wash in EtOH (96 %) and in xylol, the sections were examined under a light microscope (IX70, Olympus, Japan).

2.2.5. Statistical Analysis

Data from flow-shear experiments were analyzed for their statistical significance by values defined as $p < 0.05$ based on one-way analysis of variance (ANOVA) followed by Tukey's test for determination of the significance of difference between different groups ($p \leq 0.05$).

CHAPTER 3

RESULTS AND DISCUSSION

3.1. Characterization of Templates

Silicon templates possessing nanochannels with 90° walls were characterized with AFM. Three different templates with channel (and ridge) widths of 332.5 nm (Figure 3.1), 500 nm (Figure 3.2) and 650 nm (Figure 3.3) were designed to study whether the cells of the blood vessels can sense and orient themselves with the nano-level topographical features. Smaller features could not be tested due to the limitations of the methodology.

In the figures data and various views of the templates are presented. It is observed that patterns on the templates and the dimensions of these patterns were as designed.

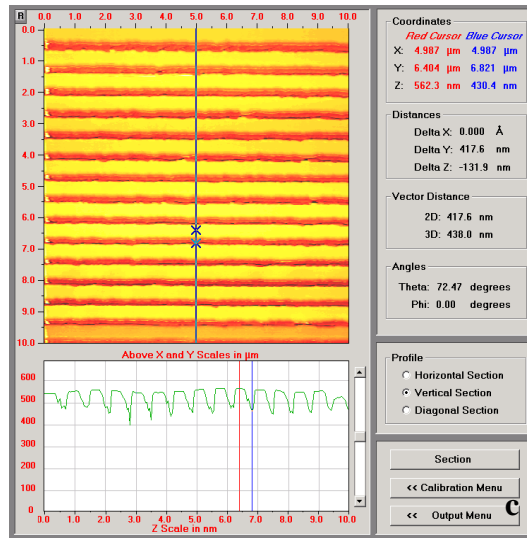
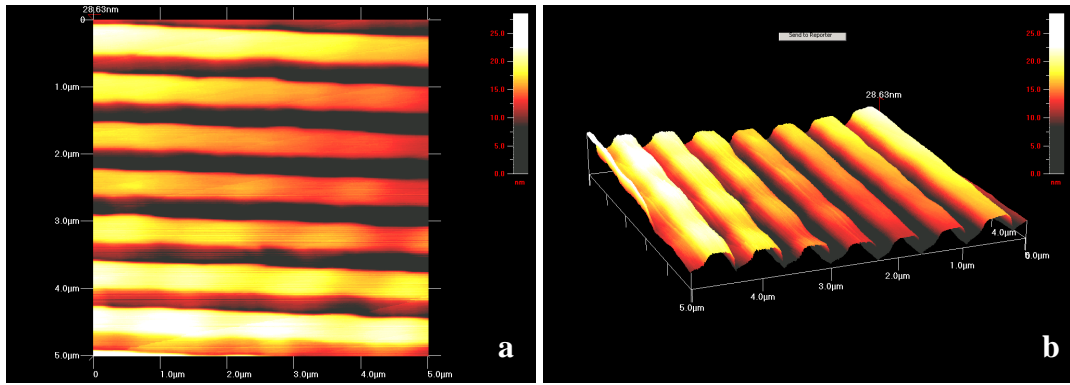


Figure 3.1. Silicon template with 332.5 nm channel width. a) top view, b) 3D view, c) view and dimensions.

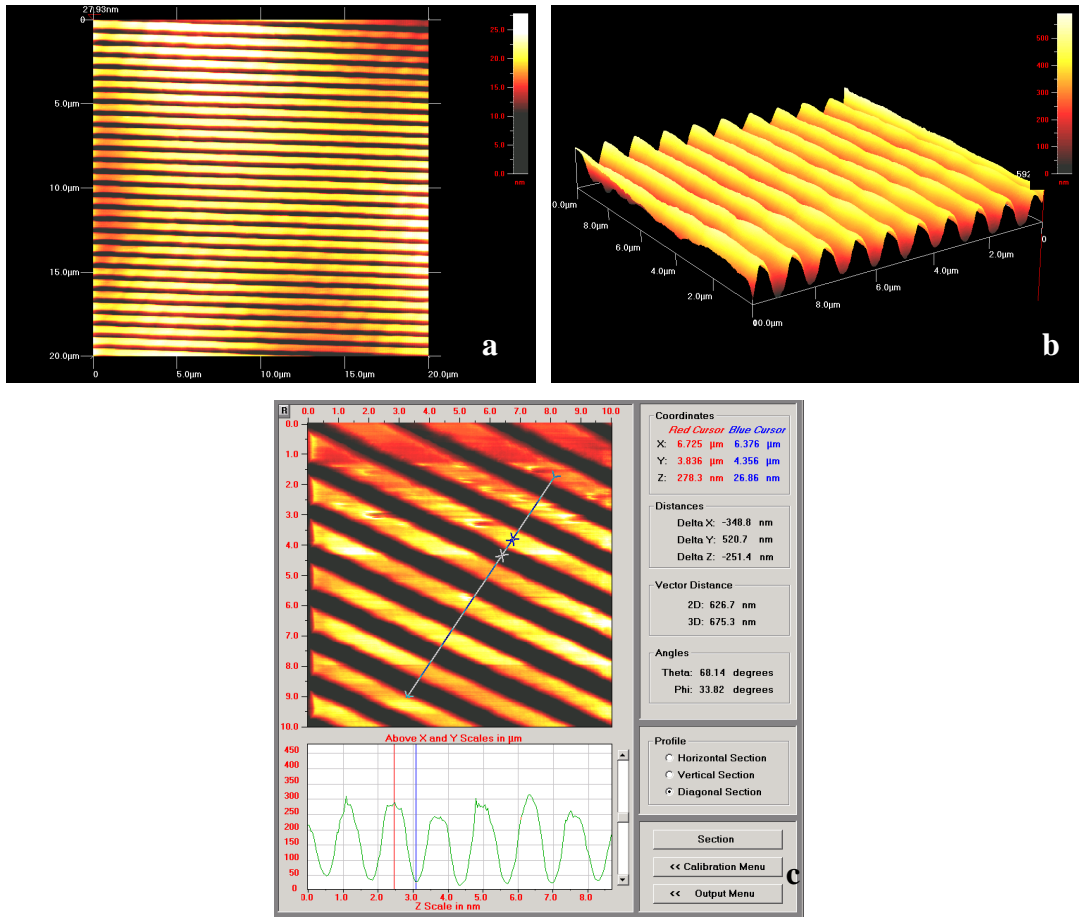


Figure 3.2. Silicon template with 500 nm channel width. a) top view, b) 3D view, c) top view and dimensions.

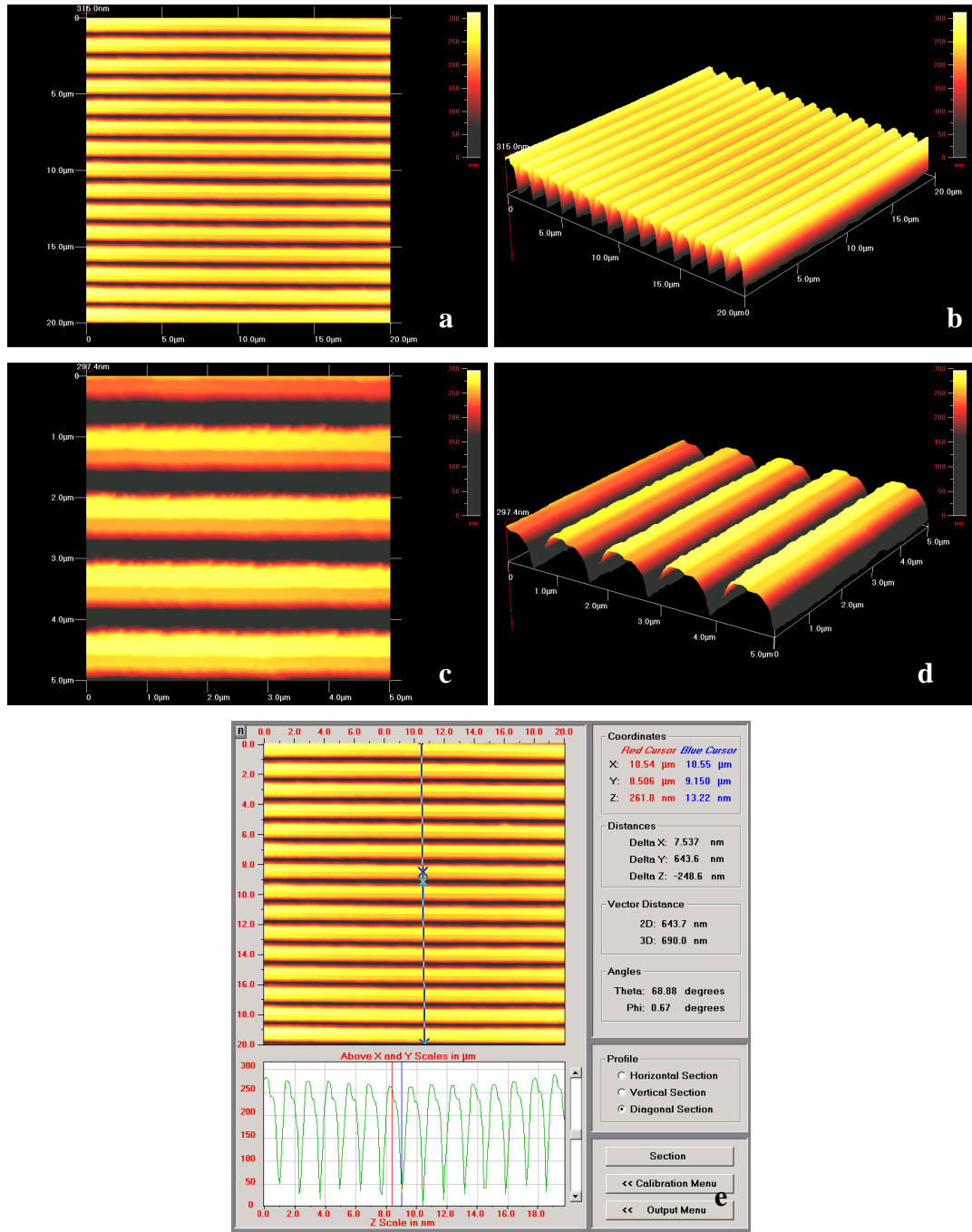


Figure 3.3. Silicon template with 650 nm channel width. a) top view, b) 3D view, c) top view, hard zoomed, d) 3D view, hard zoomed, e) top view and dimensions.

3.2. Characterization of Collagen films

3.2.1. SDS-PAGE of Isolated Collagen Type I

The purity of the isolated type I collagen was shown by SDS-PAGE (Figure 3.4). Column 1 shows the protein marker, where the bands are 260 kDa, 140 kDa, 100 kDa and 70 kDa (top to bottom). Both the isolated collagen (columns 2 and 4) and the commercial samples (columns 3 and 5) had doublets at apparent molecular weights of 115 and 130 kDa and at 215 and 235 kDa which is the typical band pattern for type I collagen. The absence of any other bands indicates that the collagen isolated from rat tails is pure Type I collagen.

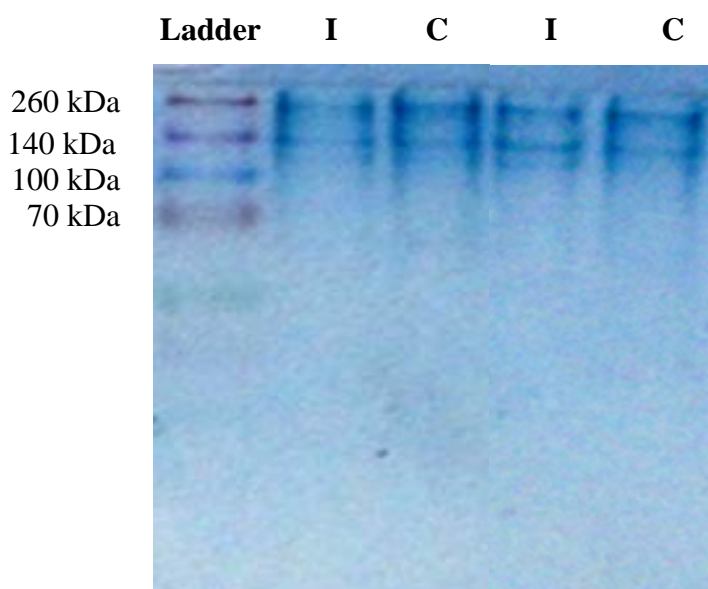


Figure 3.4. SDS-PAGE of type I collagen isolated from rat tail. Column 1 is the protein marker (ladder), Columns 2 and 4 are isolated collagen (I) (same sample applied as duplicate), 3 and 5 are commercial pure type I collagen (C) (duplicate).

3.2.2. Microscopic Characterization

Collagen films prepared on silicon templates were studied with SEM and AFM to show the fidelity of the pattern transfer, and its preservation after the crosslinking procedure (with EDC/NHS, Section 2.2.1.3).

SEM examination of the collagen films with 650 nm (Figure 3.5 a and b) and 332.5 nm (Figure 3.5 c and d) wide nanopatterns before crosslinking showed that the resolution of the patterns was satisfactory and that the patterns were quite sharp.

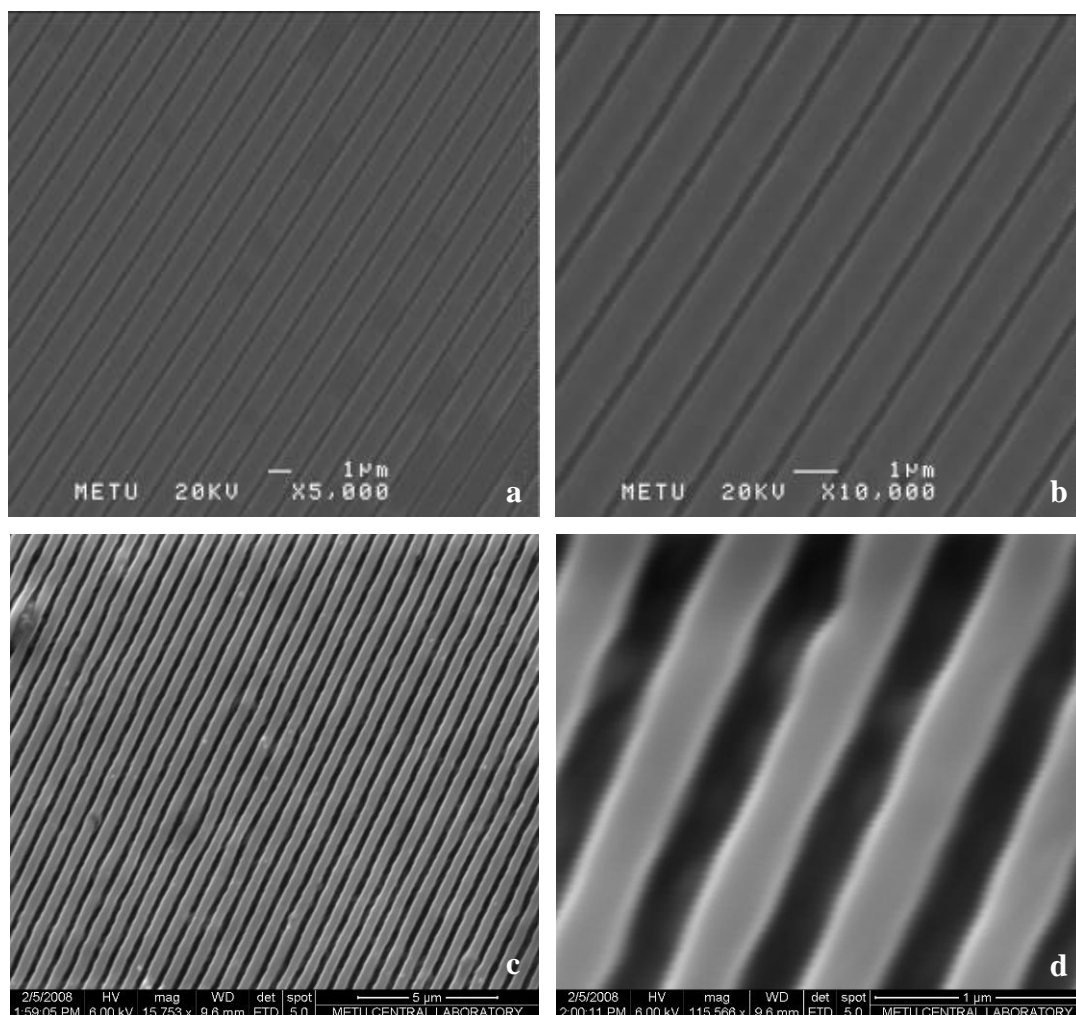


Figure 3.5. SEM images of the nanopatterned collagen films before crosslinking. a) 650 nm channel width (x 5000), b) 650 nm channel width (x 10000), c) 332.5 nm channel width (x 15753), d) 332.5 nm channel width (x 115500).

However, after crosslinking (the films were crosslinked while on the silicon templates) the patterns deteriorated (Figure 3.6). After the films were prepared and crosslinked on PDMS replicas of the original templates, high fidelity crosslinked patterns were obtained (Figure 3.7).

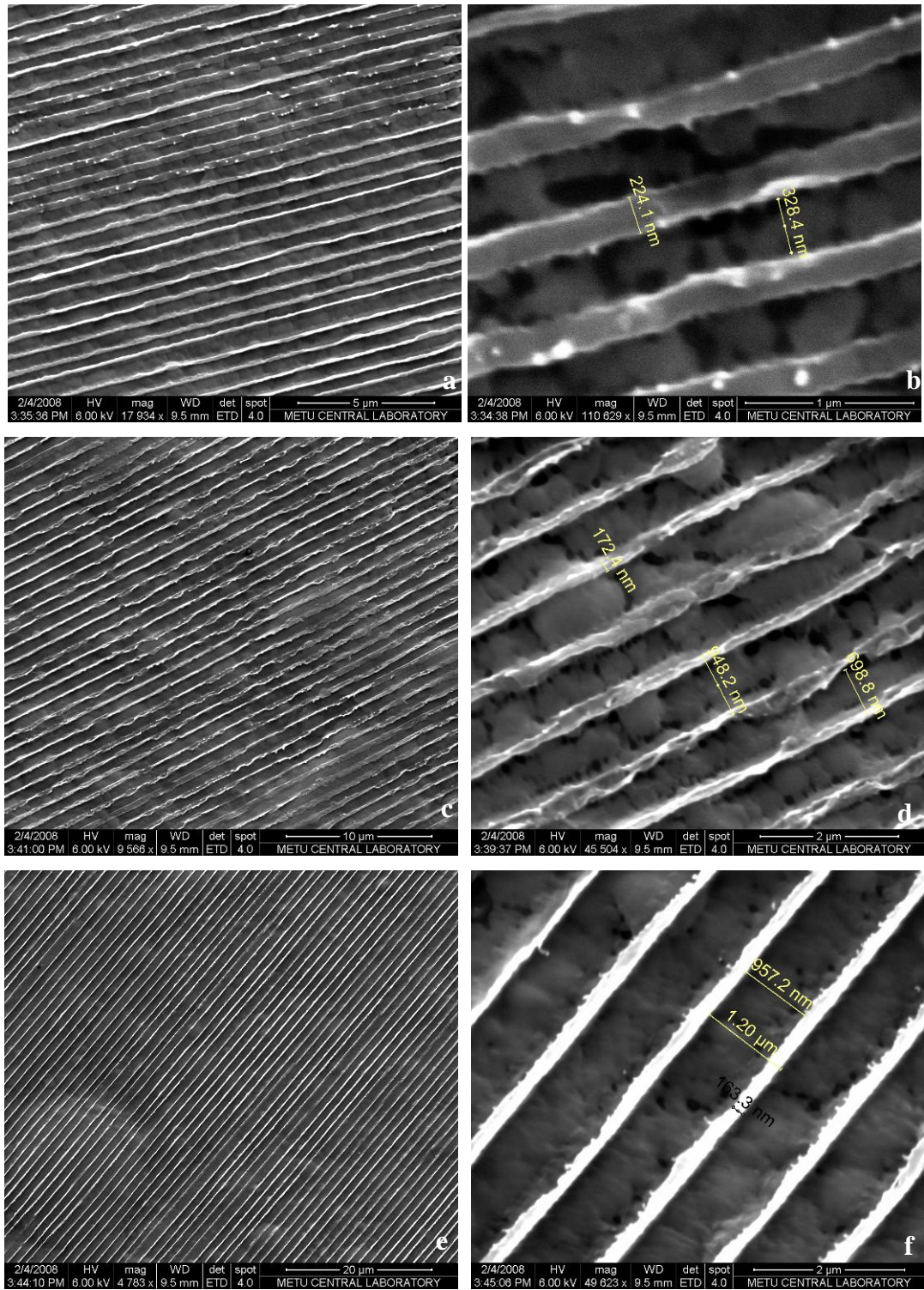


Figure 3.6. SEM images of collagen films crosslinked while on silicon templates. a) 332.5 nm channel width (x17934), b) 332.5 nm channel width (x110629), c) 500 nm channel width (x9500), d) 500 nm channel width (x45504), e) 650 nm channel width (x4753), f) 650 nm channel width (x40623).

Therefore, PDMS templates were used in the preparation of nanopatterned films in rest of the study (Figure 3.7).

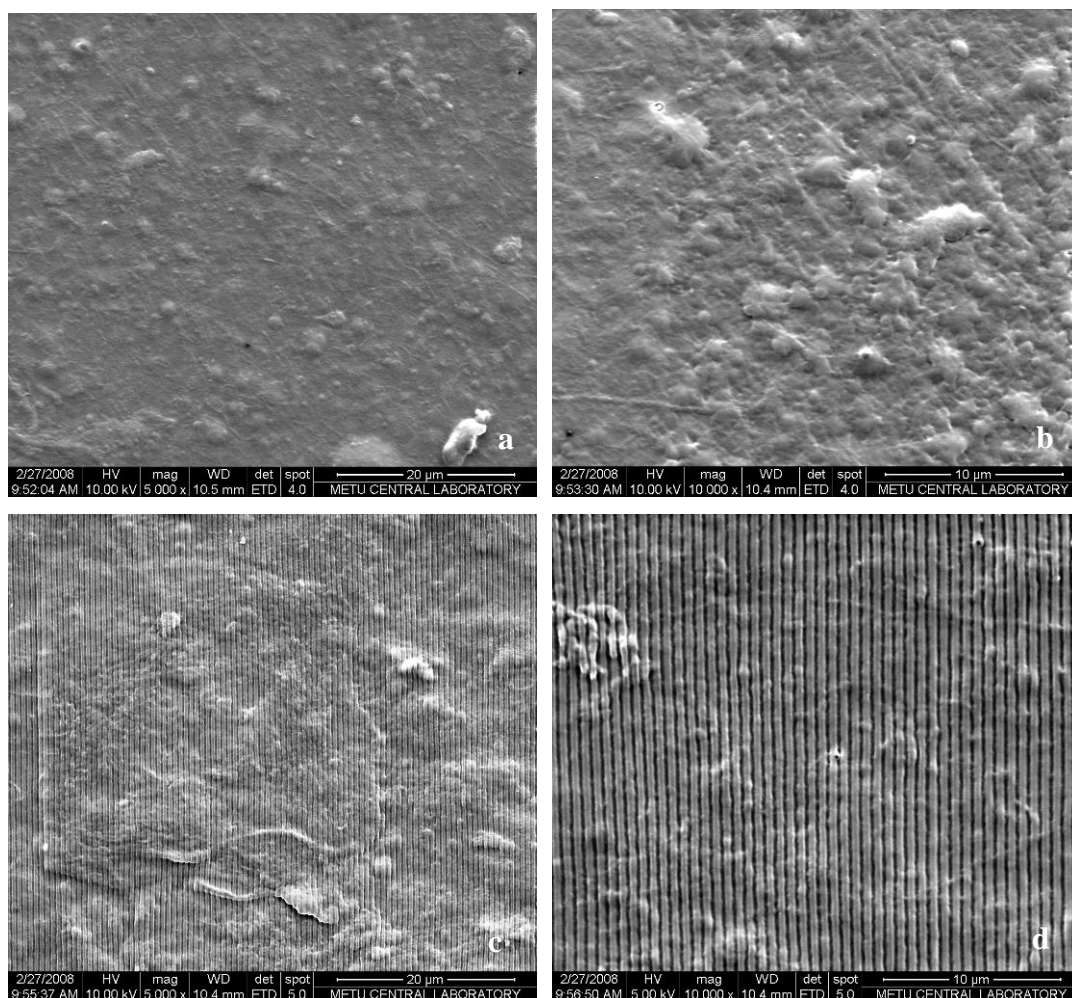


Figure 3.7. SEM images of crosslinked collagen films prepared on PDMS replicas. a) unpatterned (x5000), b) unpatterned (x10000), c) 332.5 nm channel width (x5000), d) 332.5 nm channel width (x10000), e) 500 nm channel width (x5000), f) 500 nm channel width (x10000), g) 650 nm channel width (x5000), h) 650 nm channel width (x10000).

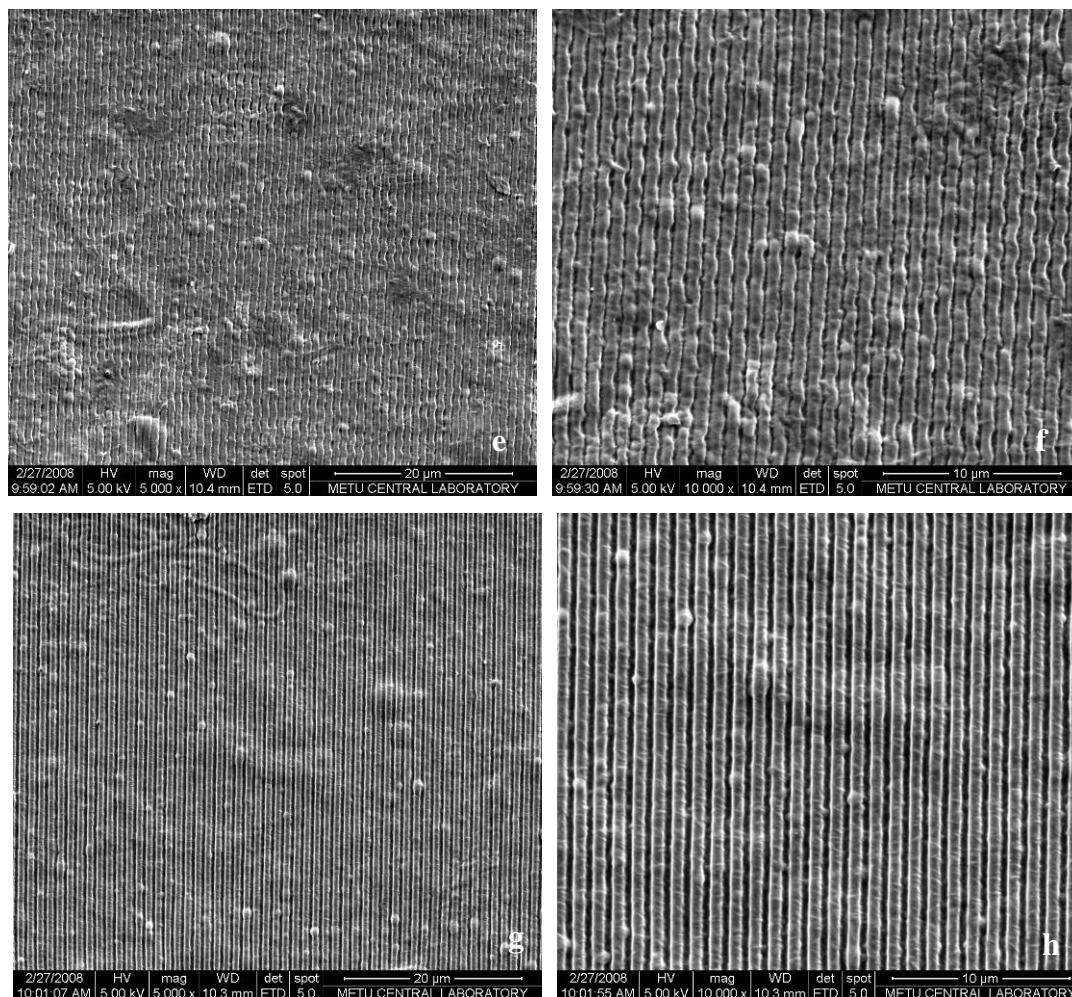


Figure 3.7. (Continued)

The patterns on one of the collagen films (650 nm channel width) were examined with AFM to confirm the SEM results, before (Figure 3.8 a and b), and after crosslinking (Figure 3.8 c and d). With AFM, the depth of the patterns on the collagen film could also be measured (Figure 3.8 e). Due to the difficulty of examining the nanopatterned collagen surfaces with AFM, only the AFM of the film with the largest pattern (650 nm) is presented. The width of the channels on the collagen film was same as the original silicon template. The pattern depth on the other hand was more shallow (250 nm instead of 300 nm) than that on the original silicon template, but was considered satisfactory and used in the *in vitro* tests.

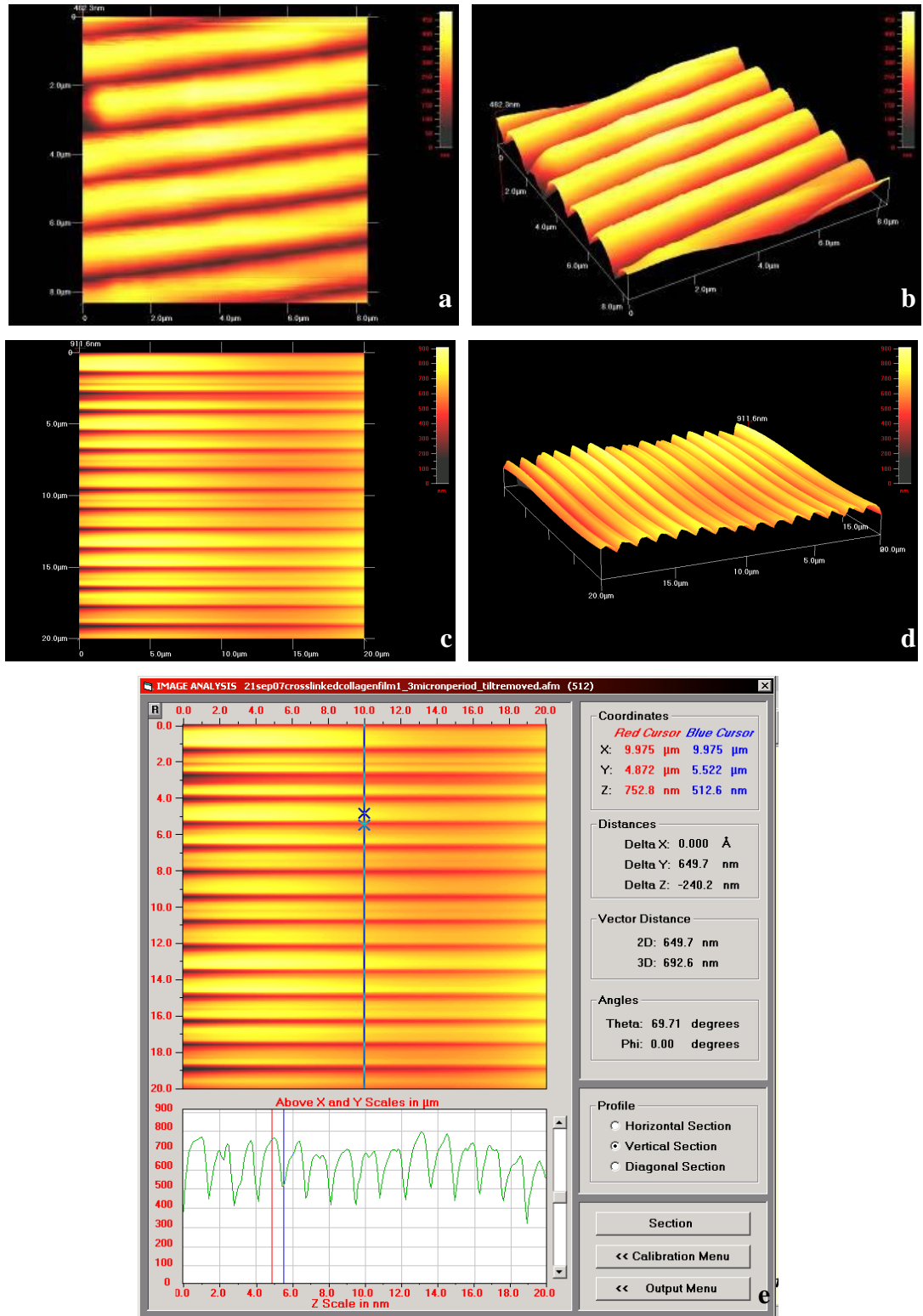


Figure 3.8. Collagen film with 650 nm channel width. Uncrosslinked film a) top view, b) 3D view. Crosslinked film c) top view, d) 3D view, e) top view showing the dimensions.

The other challenge was to prepare films possessing patterns on both sides. After several trials, this was achieved. Collagen solution (20 mg/mL 150 $\mu\text{L}/\text{cm}^2$) was placed onto the template and allowed to partially dry for 3 h then another template was placed on top of the semi-dry film with patterns perpendicular to each other. This was allowed to dry for 2 days. After drying, the films were examined macroscopically and with SEM (Figure 3.9). Patterns were reproduced properly, and therefore, this method was used in the rest of the study in the preparation of the both sides-patterned films.

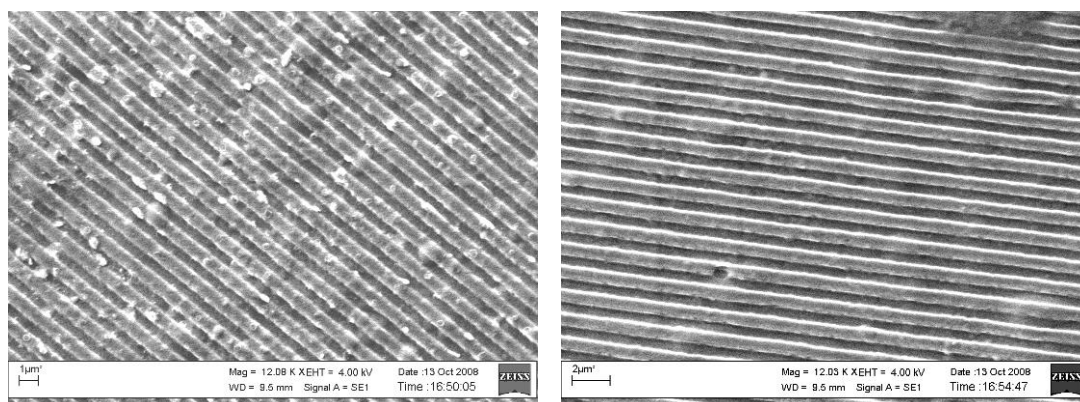


Figure 3.9. SEM images of two sides of the both side patterned collagen films (before crosslinking).

These films were crosslinked by immersion in the crosslinker solution and patterns were examined by SEM which showed patterns with high fidelity (Figure 3.10).

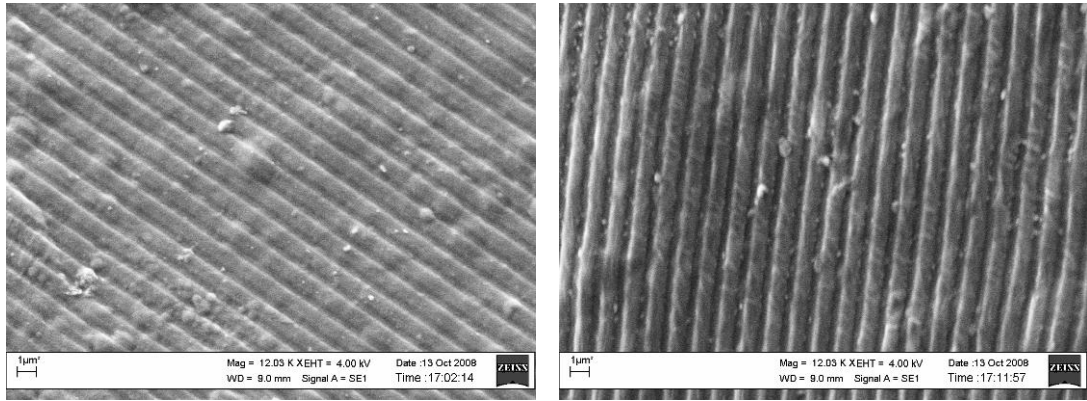


Figure 3.10. SEM images of two sides of the both side patterned collagen films after crosslinking.

3.2.3. Diffusivity of Collagen films

The diffusion of 4-acetaminophenol (as a model molecule for glucose) and to oxygen through the collagen films were calculated after fitting the measured amperometric currents to experimental data using a derivation based on Fick's Second Law (see Section 2.2.2.4).

3.2.3.1. Acetaminophenol Diffusivity

Initially, a control measurement was done without the collagen film in place to show that the response is very rapid when there is no barrier (Figure 3.11). The test is based on the delay in the measurement of the conductivity caused by a barrier (in this case the collagen films). Diffusion coefficients of the films were calculated from this delay after fitting the experimental data to the mathematical model, Fick's Second Law.

Two film groups were tested for their diffusivity to microsolute; unseeded collagen films and unseeded collagen films "further crosslinked" with formaldehyde. Films further crosslinked with formaldehyde were included in the test groups to consider the effect of further crosslinking when comparing unseeded films with cell seeded (and fixed with formaldehyde) samples.

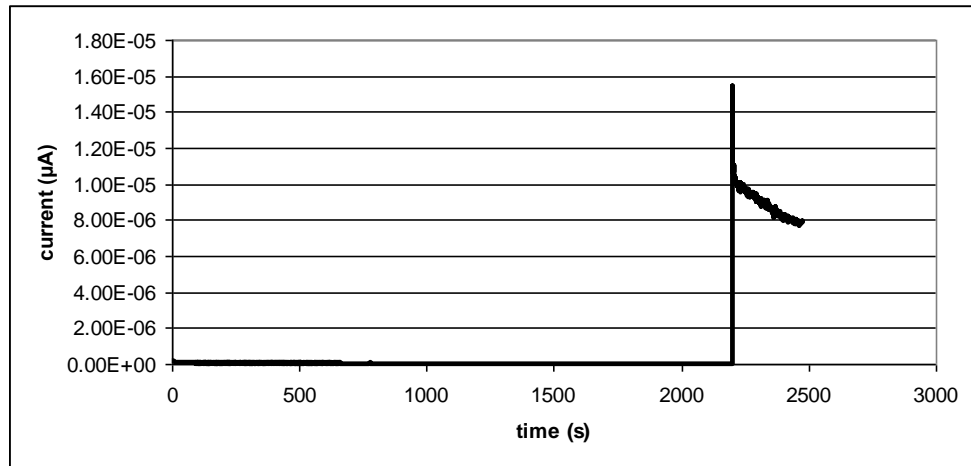


Figure 3.11. Control measurement for 4-acetaminophen diffusion (without the collagen film in place).

Representative curves for 4-acetaminophen diffusion of both test groups are given in Figure 3.12. From these figures it can be seen that the calculated data and the experimental curves are in agreement.

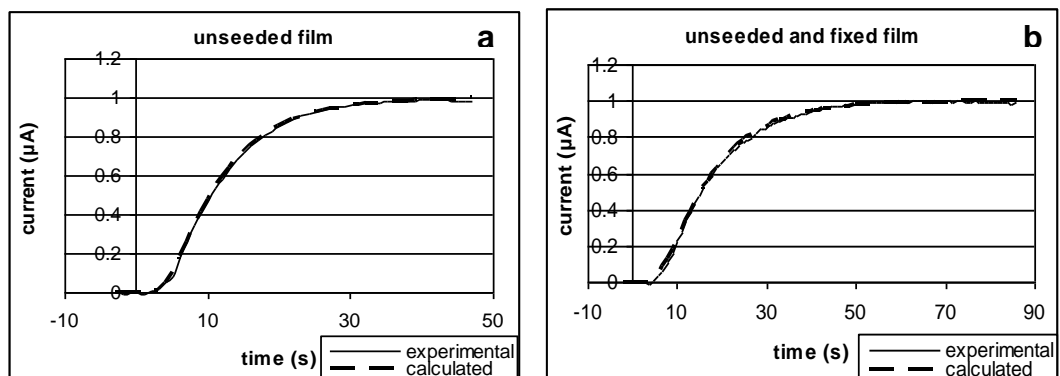


Figure 3.12. 4-acetaminophen diffusivity of collagen films. a) unseeded, b) unseeded and fixed.

Table 3.1 shows the diffusion coefficients calculated using these curves. The diffusion coefficients for 4-acetaminophen of unseeded films (crosslinked once) were calculated as $1.86 \times 10^{-7} \pm 3.9 \times 10^{-8} \text{ cm}^2 \cdot \text{s}^{-1}$. This value is in the range of biological diffusion coefficient for glucose that varies between 1.6×10^{-6} and $3.8 \times 10^{-7} \text{ cm}^2 \cdot \text{s}^{-1}$ (Rong et al., 2006). When treated as in cell fixation, this value

dropped to nearly half of the unseeded samples. These results are further discussed and compared with diffusivity measurements with cell seeded films in Section 3.4.2.

Table 3.1. Diffusion of unseeded and unseeded and fixed collagen films to 4-acetaminophenol and oxygen.

Sample	Diffusivity x 10 ⁻⁷ (cm ² .s ⁻¹)	
	4-acetaminophenol	oxygen
Unseeded film	1.86 ± 0.39	5.41 ± 2.14
Unseeded and fixed film	1.12 ± 0.02	4.77 ± 0.78

3.2.3.2. Oxygen Diffusivity

Figure 3.13 shows the control measurement for oxygen. Representative curves for oxygen measurements are given in Figure 3.14 again showing the agreement between the experimental and the calculated data.

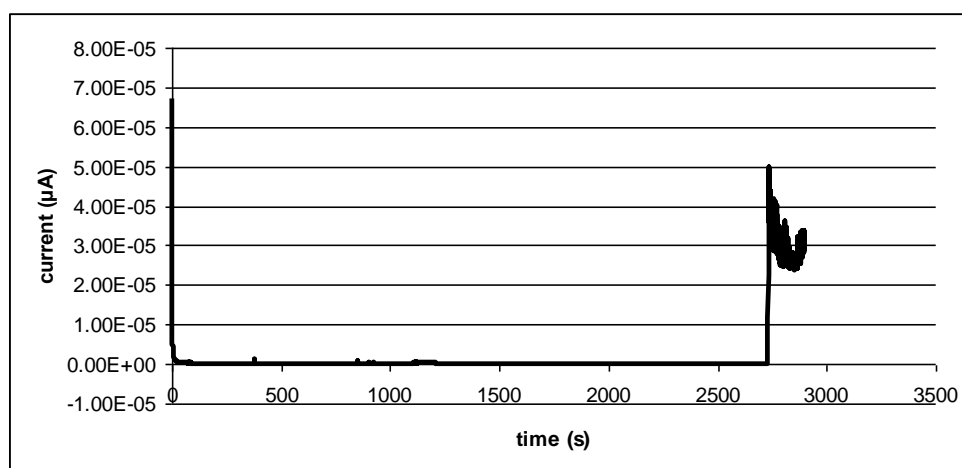


Figure 3.13. Control measurement for oxygen diffusivity (without the collagen film in place).

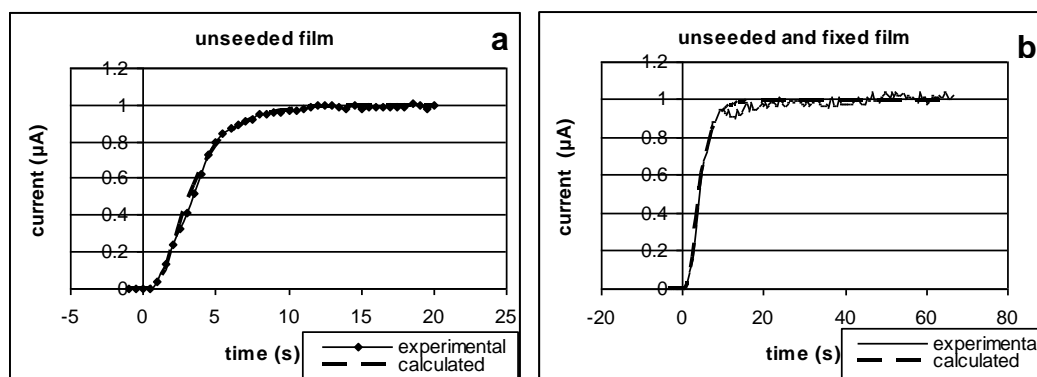


Figure 3.14. Oxygen diffusivity of unseeded collagen film. a) unseeded, b) unseeded and fixed film.

Diffusion coefficients for oxygen in unseeded films were calculated as $5.41 \times 10^{-7} \pm 2.14 \times 10^{-7} \text{ cm}^2 \cdot \text{s}^{-1}$ (Table 3.1). These values are much higher than for 4-acetaminophenol. Upon further fixation, the values decreased as before, but less dramatically, possibly because oxygen is a smaller molecule than 4-acetaminophenol and is therefore less affected by scaffold porosity. These results are also further discussed and compared to diffusivity of cell seeded films in Section 3.4.2.

3.3. Characterization of Cell-free Tubular Scaffolds

Tubular scaffolds were examined with SEM for their structural integrity, preservation of the layered structure and pattern fidelity after conversion of the films into tubes. The layered morphology and the intact structure of the scaffold can be seen on Figure 3.15.

Patterns on the inside and outside of the nanopatterned tubular scaffolds were also examined with SEM and compared with the unpatterned ones (Figure 3.16).

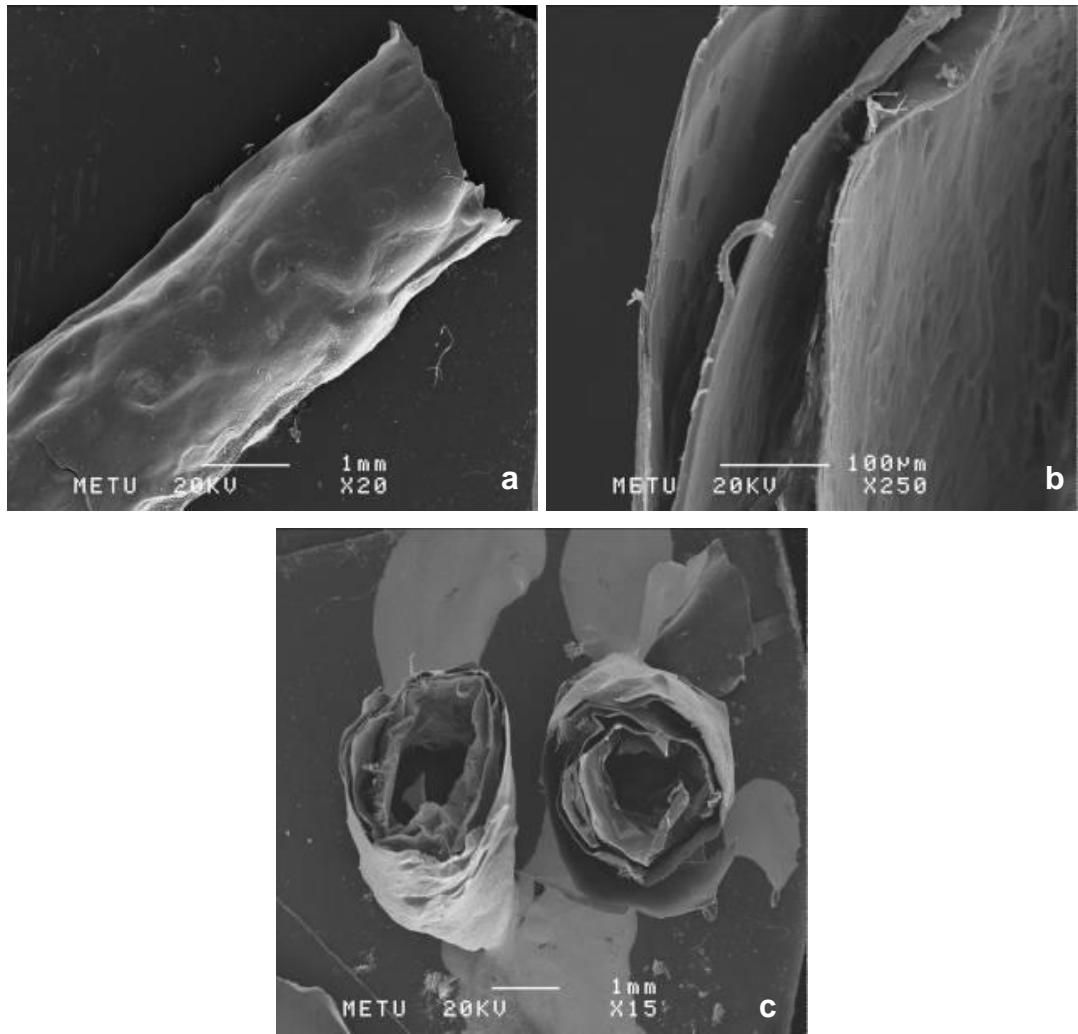


Figure 3.15. SEM images of tubular collagen scaffold. a) outside, b) inside, c) cross section.

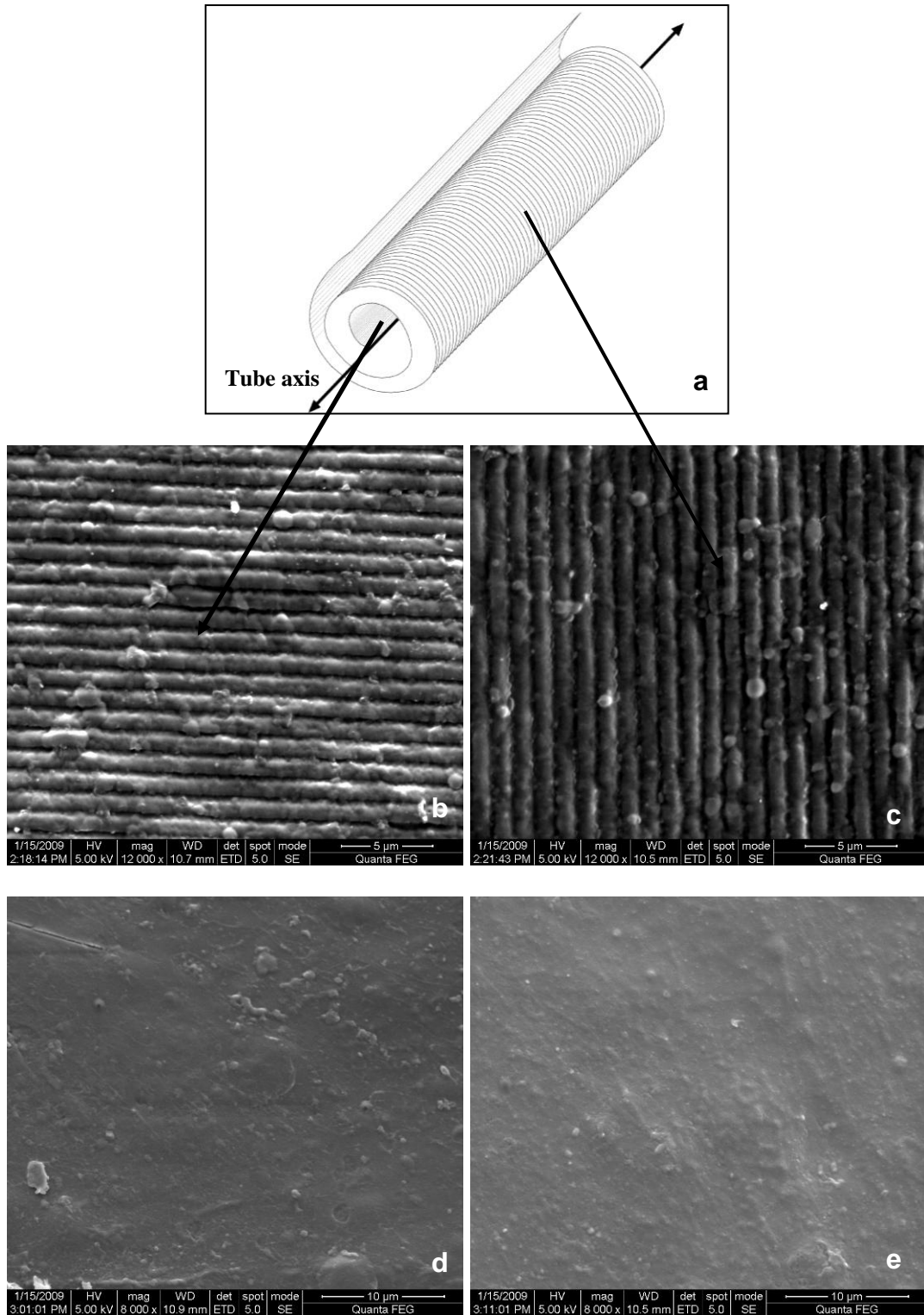


Figure 3.16. SEM images of tubular collagen scaffolds. a) drawing of the tubular scaffold, b) inside of the double side patterned tubular scaffold, c) outside of the double side patterned tubular scaffold, d) inside of the unpatterned tubular scaffold, e) outside of the unpatterned tubular scaffold.

The crosslinked tubular collagen scaffolds were incubated under cell culture conditions for 28 days and examined by stereomicroscopy (Figure 3.17) which showed that the scaffold maintained its form and integrity and was intact after this incubation period. This duration is enough for the growth of sufficient number of VSMCs which can secrete the ECM as observed in *in vitro* tests.

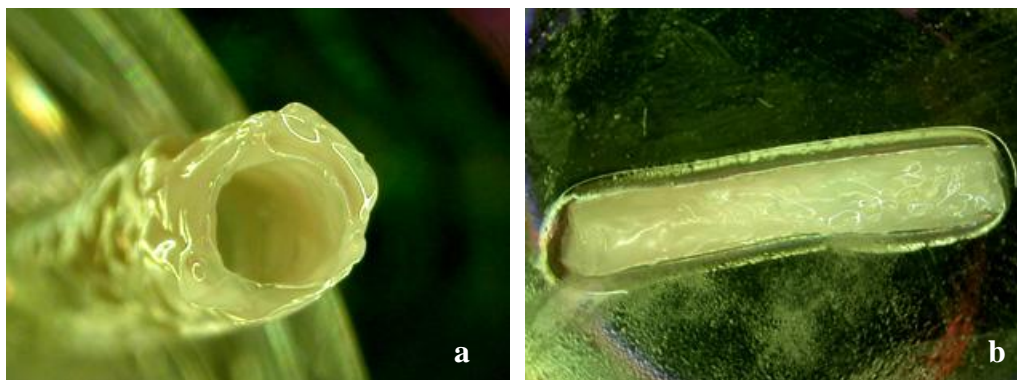


Figure 3.17. Stereomicrographs of tubular collagen scaffold after 28 days of incubation under cell culture conditions. a) cross-section, b) outside view.

3.4. Studies with HMECs

3.4.1. HMEC viability on Collagen Films

Cell viability was investigated qualitatively by staining with Calcein AM for live cells and ethidium homodimer-2 for dead cells without any fixation. Figure 3.18 (a) shows the live cells on the control, TCPS, and there was similarly a high number of live cells on the collagen film (Figure 3.18 b). There were very few dead cells indicating the suitability of the collagen films for *in vitro* use (Figure 3.18 c). There was no significant background fluorescence due to the film.

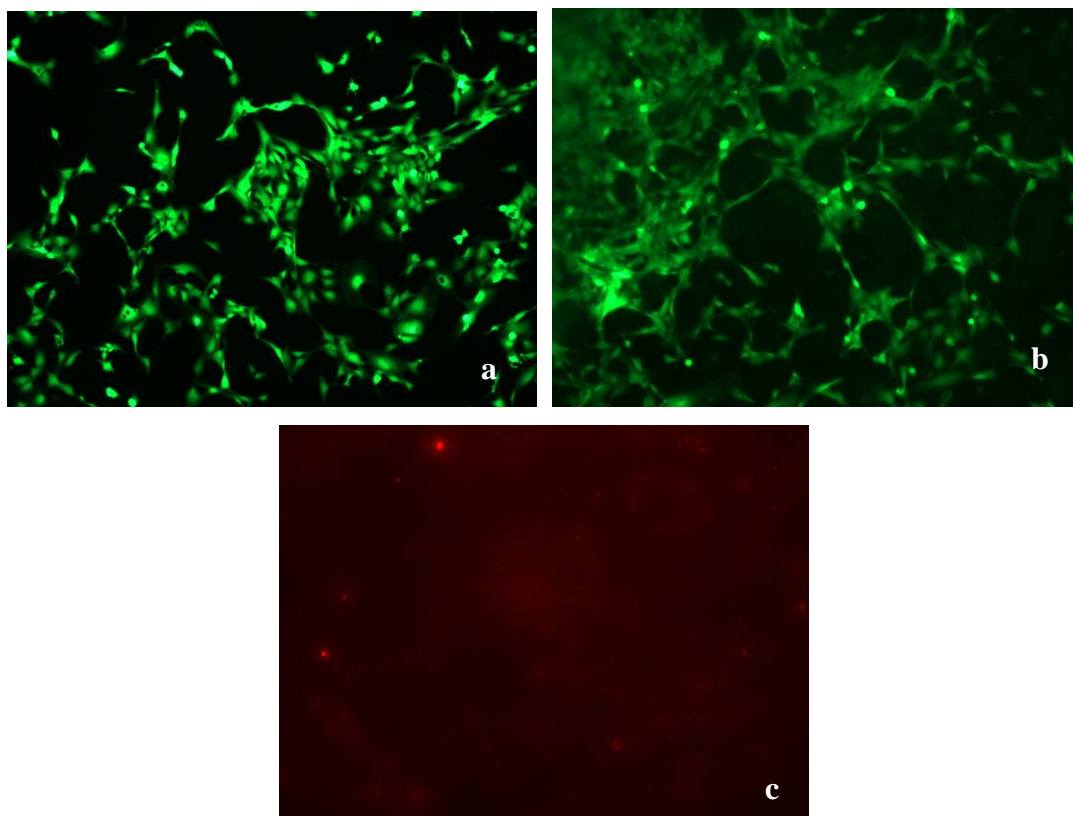


Figure 3.18. Calcein AM - ethidium homodimer-2 double staining. a) cells on the TCPS at the excitation wavelength for Calcein (488 nm), b) cells on the collagen film at the excitation wavelength for Calcein, c) cells on the collagen film at the excitation wavelength for ethidium homodimer-2 (590 nm).

3.4.2. Diffusivity of HMEC Seeded Films

The diffusion coefficients for HMEC seeded collagen films were calculated after fitting the simulated amperometric currents to experimental data. Measurements and calculations were performed as described in Section 3.2.2.

Two groups were tested for 4-acetaminophenol diffusivity of HMEC seeded collagen films; cell seeded collagen films, and cell seeded and fixed collagen films. For oxygen diffusivity, only cell seeded and fixed films were measured. Representative curves for these test groups are given in Figure 3.19. From these figures it can be seen that the calculated and the experimental data are in agreement.

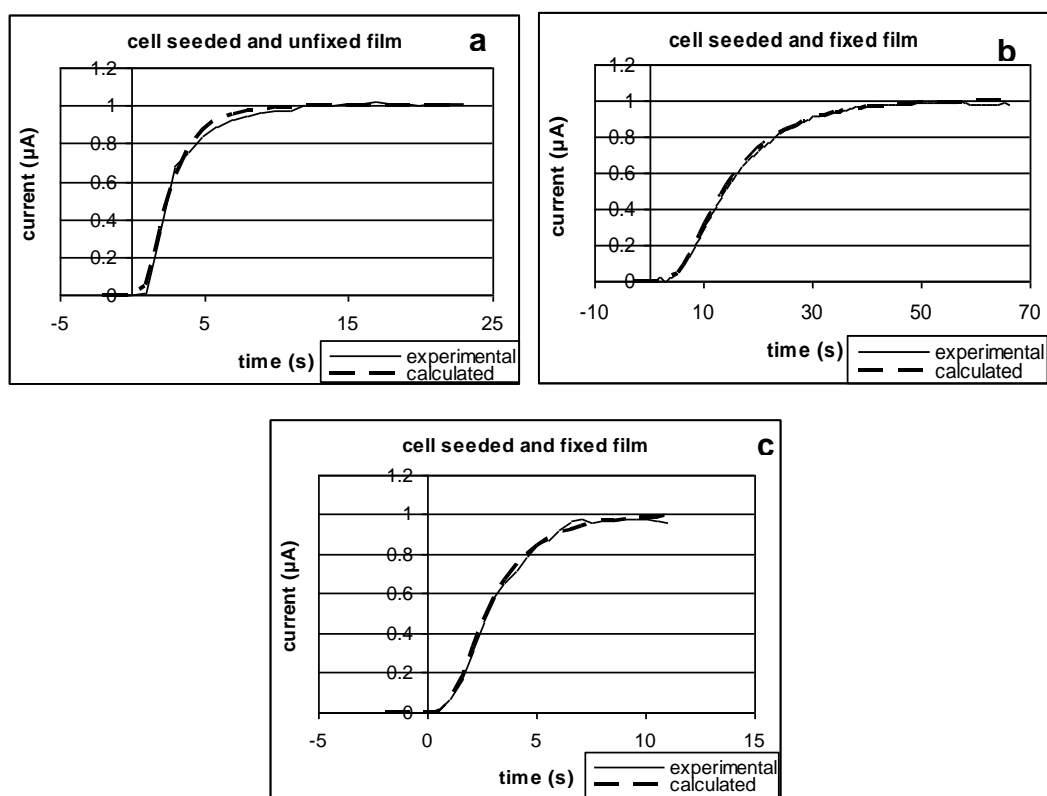


Figure 3.19. Diffusivity of cell seeded collagen films. a) 4-acetaminophen diffusivity of cell seeded, unfixed film and b) 4-acetaminophen diffusivity of cell seeded and fixed film, c) oxygen diffusivity of cell seeded and fixed collagen film.

Table 3.2 shows the calculated mean diffusion coefficients using these curves. The diffusion coefficients for 4-acetaminophen of HMEC seeded films (crosslinked once) were calculated as $8.09 \pm 1.81 \times 10^{-7} \text{ cm}^2 \cdot \text{s}^{-1}$. Among cell seeded, and cell seeded and fixed films, there was also a similar 2 fold decrease caused by this second fixation of the collagen as was observed with the unseeded and unseeded and fixed samples. When cell seeded and cell seeded and fixed samples were compared (Table 3.2), the latter was observed to have nearly 4 times higher diffusion coefficients than unseeded samples and unseeded and fixed samples, respectively. A possible explanation for the higher diffusivity observed upon cell seeding could be the contraction of the collagen fibers of the film by the endothelial cells, increasing the pore dimensions, thus increasing the diffusivity. The support for this comes from Kelley et al. (1987) who have shown that microvascular endothelial cells can contract collagen substrates by upto 50 % depending on the

cell number and the fetal calf serum amount of the media. Even though the diffusivities of the collagen films are within the physiological range, cell seeding appears to further enhance this. Similarly the cell seeded samples had higher oxygen diffusivity values than the unseeded ones.

Table 3.2. Diffusivity of cell seeded, unseeded, fixed or unfixed collagen films to 4-acetaminophenol and oxygen.

Sample	Diffusivity x 10 ⁻⁷ (cm ² .s ⁻¹)	
	4-acetaminophenol	oxygen
Unseeded film	1.86 ± 0.39	5.41 ± 2.14
Unseeded and fixed film	1.12 ± 0.02	4.77 ± 0.78
Cell seeded and unfixed film	8.09 ± 1.81	-
Cell seeded and fixed film	4.37 ± 1.51	8.48 ± 2.45

3.4.3. Cell Proliferation

Alamar Blue test results showed that the number of cells on all patterned collagen films and the TCPS, regardless of the nanopattern dimensions, and number of cells seeded were similar (Figure 3.20). This suggests that the collagen films with different surface topography were suitable for growth of microvascular endothelial cells and the presence or the dimensions of the nanopatterns appeared to have no effect on cell proliferation or viability.

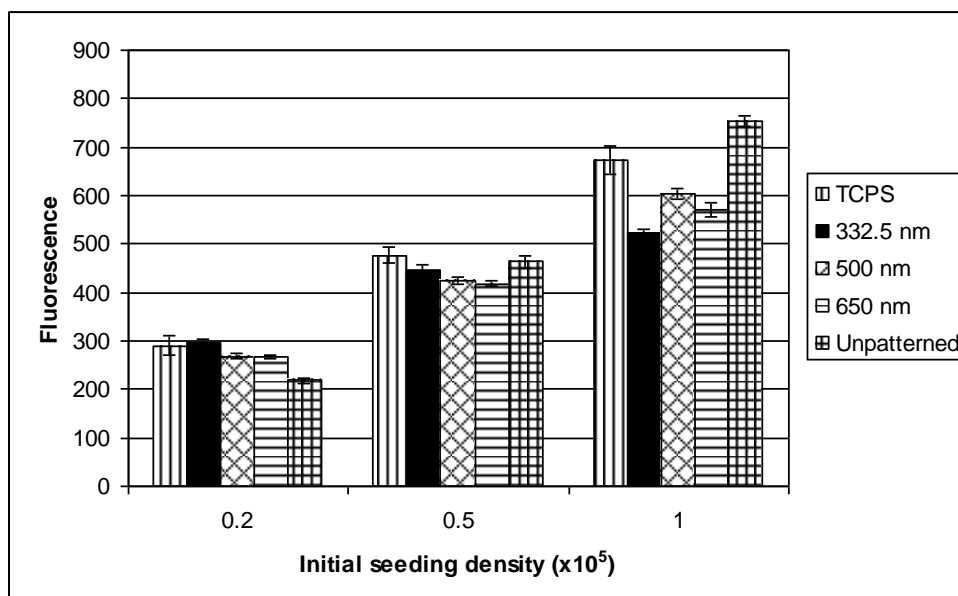


Figure 3.20. Alamar Blue test results showing the effect of seeding with HMEC with different initial seeding densities on cell proliferation on nanopatterned and unpatterned collagen films. (Incubation time: 48 h, $n=3$).

3.4.4. HMEC Orientation

At 24 h, cells on the unpatterned and nanopatterned films, which were seeded with 2×10^4 cells on each, were fixed by using 4% formaldehyde and stained with DAPI to examine the influence of nanopatterns on cell alignment. No such alignment was observed on any of the three nanopatterned film types. Cells were randomly oriented on the surface of these films as they had on the unpatterned film (Figure 3.21). Endothelial cell alignment has been previously studied using micropatterns and not on nano-channels. Wu et al. (2007) showed alignment with 15, 30 and 60 μm wide channels while Vartanian et al. (2008) showed the same effect with 25 μm . Nano-scale topographies that were used to modulate these endothelial cells were in the form of islands rather than channels and aimed to increase adhesion, spreading and proliferation rather than to achieve alignment (Dalby et al., 2002, Tajima et al., 2008). Alignment on nano-scale patterns was, however, shown by other types of cells. For example, alignment of vascular smooth muscle cells was achieved with the nano-scale dimension patterns (Zorlutuna et al., 2008). In the literature there is also data showing that fibroblastic cells align with

patterns in the nano-range (van Delft et al., 2008). Only in a recent study by Lu et al. (2008) endothelial cell alignment was shown on micro- and nano- scale features but here the channel dimensions ranged from 750 nm to 5 microns; larger than the largest dimension used in the current study. This implies that endothelial cells can respond to physical surface features, but only when the feature dimension is around 1 μm or larger.

SEM images supported these observations. Although there are a few aligned HMECs on the nanopatterned films (Figure 3.22 a), there was no extensive cell alignment on majority of the samples (Figure 3.22 b). Coverage of the films by the cells can be seen when SEM of samples with different initial seeding densities are compared (Figure 3.22 c to e).

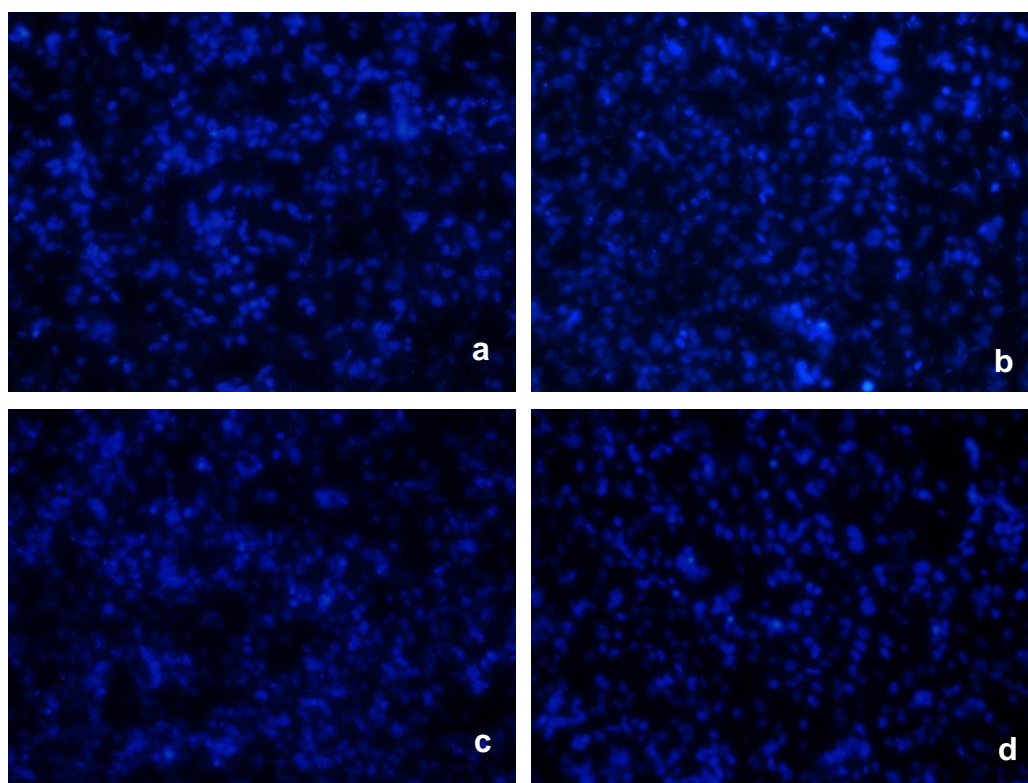


Figure 3.21. Fluorescence micrographs of HMECs on collagen films at 24 h (DAPI staining). a) unpatterned, b) 332.5 nm patterned, c) 500 nm patterned, d) 650 nm patterned (x 200).

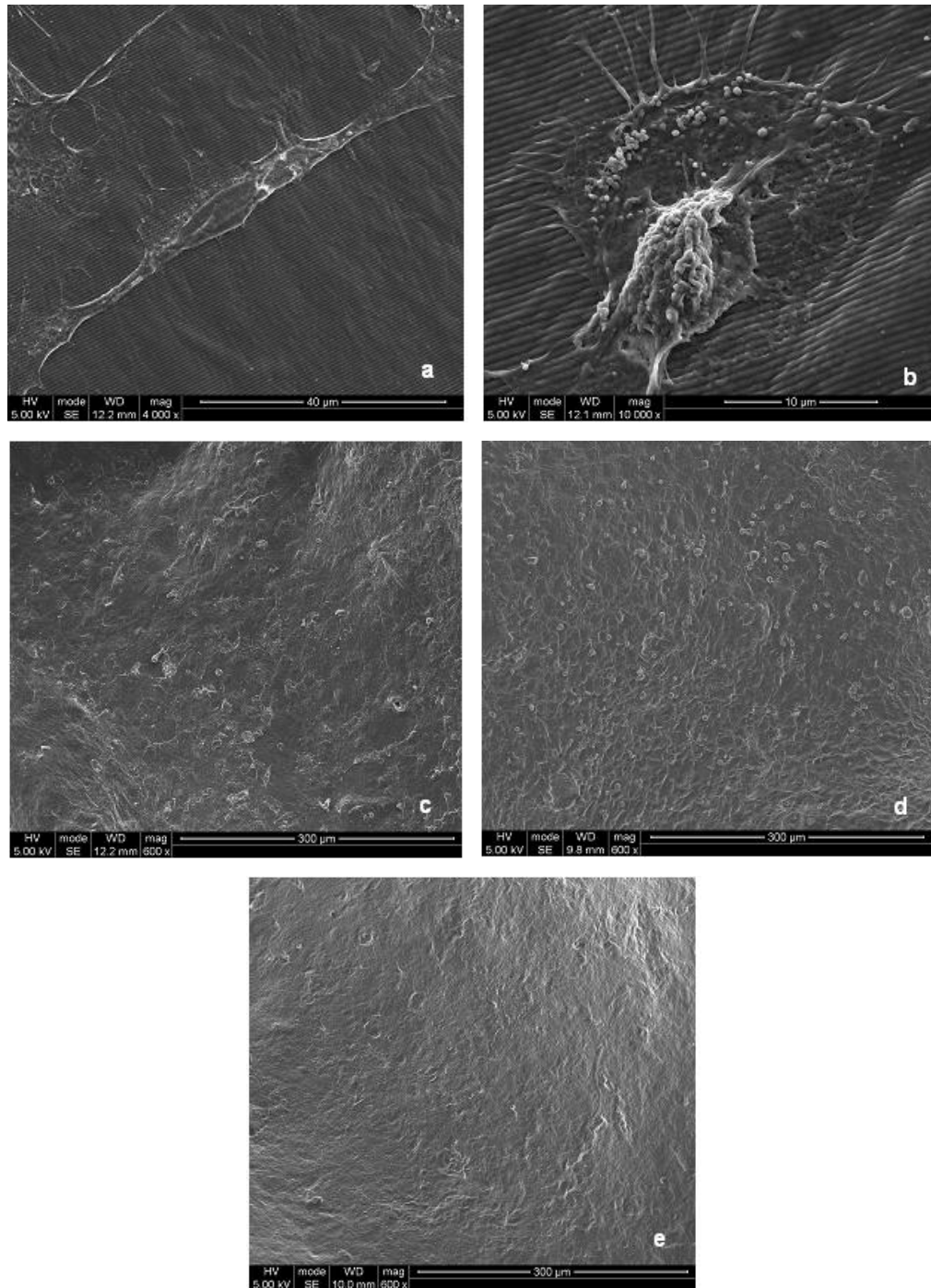


Figure 3.22. SEM images of HMECs seeded on 500 nm nanopatterned collagen films at 48 h. a) a single aligned cell, b) a single unaligned cell, c) initial seeding density of 2×10^4 , d) initial seeding density of 5×10^4 , e) initial seeding density of 1×10^5 .

3.4.5. Flow-Shear Test

The data presented earlier in this study refer to cell seeding and incubation under static conditions. The data presented in this section was obtained when the incubation was carried out under shear caused by fluid flow. In contrast to the microscopy and proliferation results obtained under static conditions, shear studies showed a significant difference ($p < 0.05$) between unpatterned, 332.5 nm patterned and 650 nm patterned films in terms of endothelial cell retention on the surface after application of shear stress, whereas the cell numbers on controls of these groups (static culture) were almost the same ($p > 0.05$) indicating that the presence of nanopatterns and their dimensions affect cell number only under flow-shear conditions (Figure 3.23). While the fraction of the cells that could be retained on unpatterned films was $35 \pm 10 \%$, it was $75 \pm 4 \%$ on 332.5 nm patterned films and even higher, $91 \pm 5 \%$, on 650 nm patterned films ($p < 0.05$). This increase in cell retention is probably due to an increase in the level or strength of individual cell attachment zones. Certainly the nanopatterned surfaces present a greater surface area for cells to interact with or attach to and thus resist the flow-shear. There was more cell retention on 650 nm patterned films than on 332.5 nm films, probably not just due to the higher width but also due to the lower depth of the 332.5 nm films. The narrower channels might be not deep enough for the cells to cling to. It was previously shown by Karuri et al. (2004) with corneal epithelial cells that nano-scale grooves enhance cell retention under shear stress by increasing the strength of cell attachment and this was proposed to be due to mimicking of the natural ECM. In the present study the increased surface area and higher molecular interaction between the cells and the surface appear to have helped the cells resist the flow.

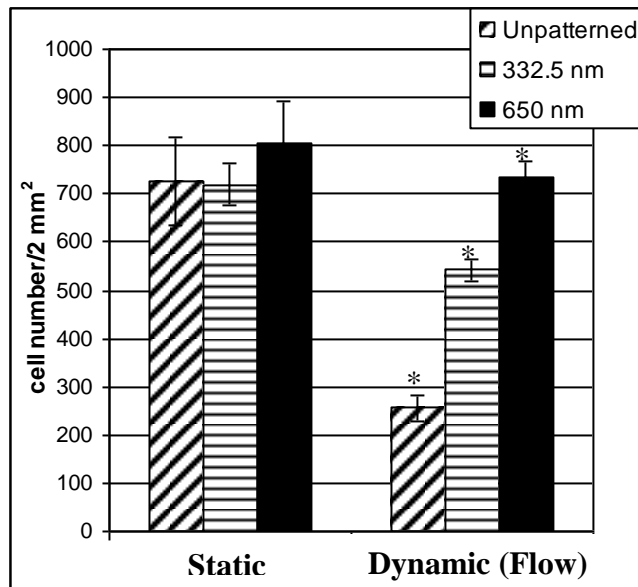


Figure 3.23. Cell numbers on flow-shear applied HMECs on nanopatterned and unpatterned films compared to cell numbers on films that were not subjected to shear. * indicates the significantly different values ($p < 0.05$).

3.5. Studies with VSMCs

3.5.1. Isolation and Characterization of VSMCs

Vascular smooth muscle cells were isolated from human saphenous vein by using explant culture techniques (Figure 3.24).

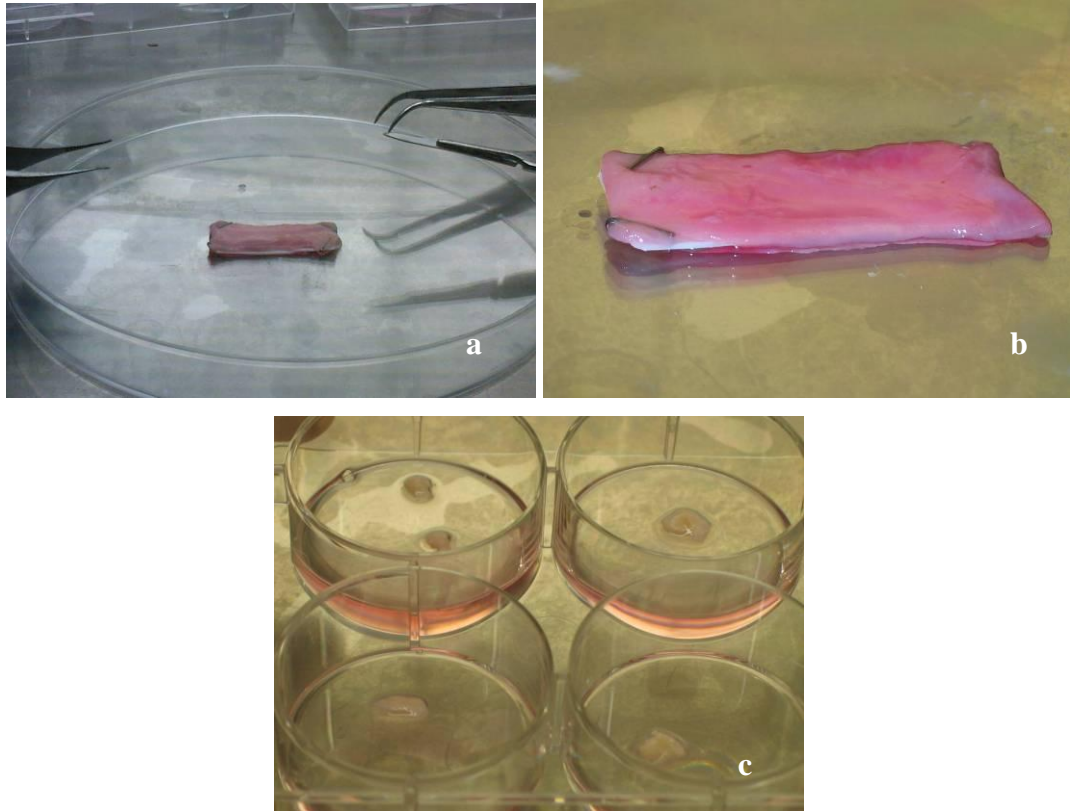


Figure 3.24. VSMC isolation from saphenous vein. a) intact saphenous vein after dissecting longitudinally, b) saphenous vein after removal of intima layer, c) fragments of the media layer of the saphenous vein (ready for explant culture).

VSMCs started to migrate out of the explant culture in about 2 weeks and were examined by inverted light microscopy (Figure 3.25).

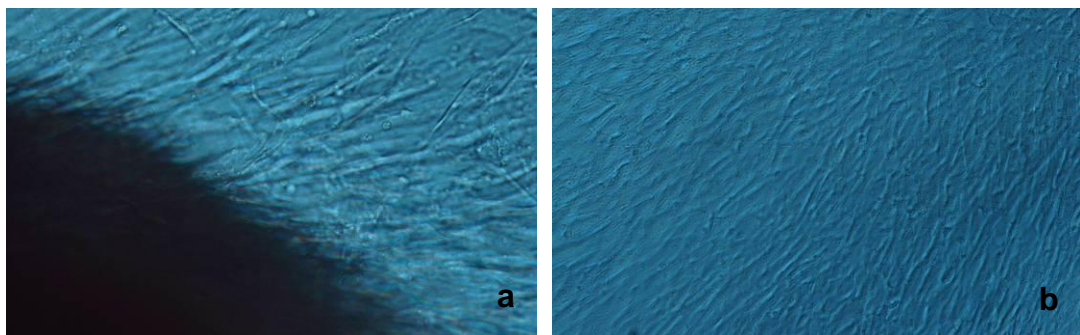


Figure 3.25. Light micrographs of VSMCs in explant culture. a) cells in the vicinity of the explant tissue (x 400) and b) cells in the medium (x 100).

VSMCs were stained with anti- α -smooth muscle actin which is a VSMC marker and examined with confocal microscopy to confirm the phenotype of the isolated cells and to observe their morphology since this staining shows the cytoskeleton (Figure 3.26).

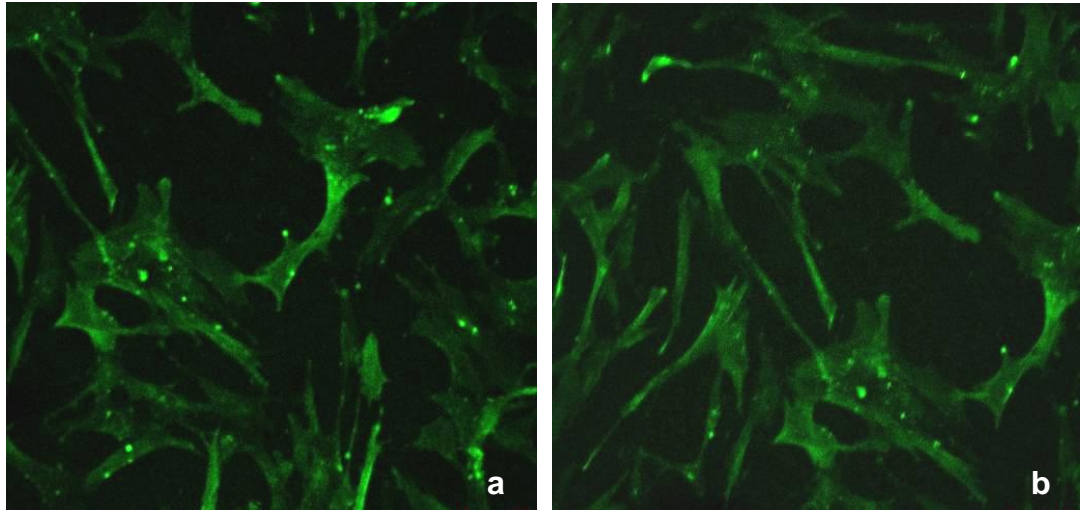


Figure 3.26. Confocal images of VSMCs with anti- α -smooth muscle actin staining (x 200).

Isolated VSMCs were stained for α -smooth muscle actin and cell nuclei through passages 4 to 6 in order to study the purity of the culture and the extent of de-differentiation during cell culture and passaging. Figure 3.27 shows that the cells in these three passages stained with both anti- α -smooth muscle actin and DAPI. There were no cells stained only with DAPI; this would have indicated impurities from cell isolation or de-differentiated cells. It was thus shown that the cells had maintained their VSMC character through passage 6.

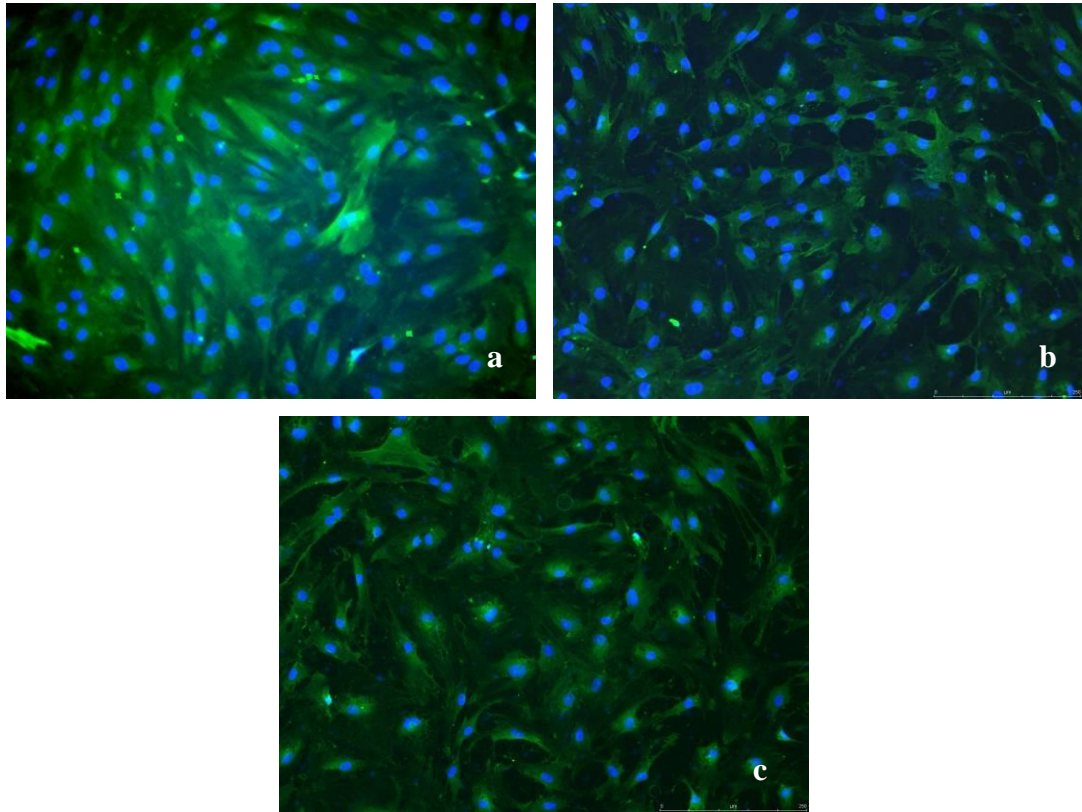


Figure 3.27. Fluorescence micrographs of VSMCs double stained with anti- α -smooth muscle actin and DAPI. Passages a) 4, b) 5 and c) 6 (x 100).

3.5.2. VSMCs on Collagen Films

3.5.2.1. Cell Proliferation

Cell numbers on the collagen films were calculated as “% reduction” of the Alamar Blue reagent. After the construction of a calibration curve (Appendix B), % reduction values were converted into cell numbers. Alamar Blue assay was performed on VSMC seeded samples on Days 1, 7, 14 and 21. Results showed that all the collagen films supported cell growth. Cell adhesion (Day 1) was higher when the pattern dimension was smaller (Figure 3.28). Unpatterned films and TCPS showed lower cell adhesion. Although initially the number of cells attached on the nanopatterned films was higher than on the TCPS control, the difference in the cell numbers gradually decreased until Day 21 when there was no appreciable

difference. This leveling off is probably due to an overall higher surface area of the TCPS (2.27 cm^2) compared to collagen films (1 cm^2), which allowed the cells on TCPS to proliferate in higher numbers before they were contact inhibited at confluency. Still, throughout the whole duration the highest number of cells was always found on the nanopatterned film with the smallest pattern dimension (332.5 nm). Vascular smooth muscle cells were previously shown to proliferate properly on collagen membranes without any topographical modifications (Elliott et al., 2005). On the other hand, when compared to synthetic polymeric scaffolds, VSMCs on nanopatterned collagen films proliferated twice as much in number as the human coronary artery smooth muscle cells on the poly(L-lactide-co-ε-caprolactone) nanofibrous electrospun scaffolds which have similar nano-scale guidance (500 nm diameter fibers) (Xu et al., 2004).

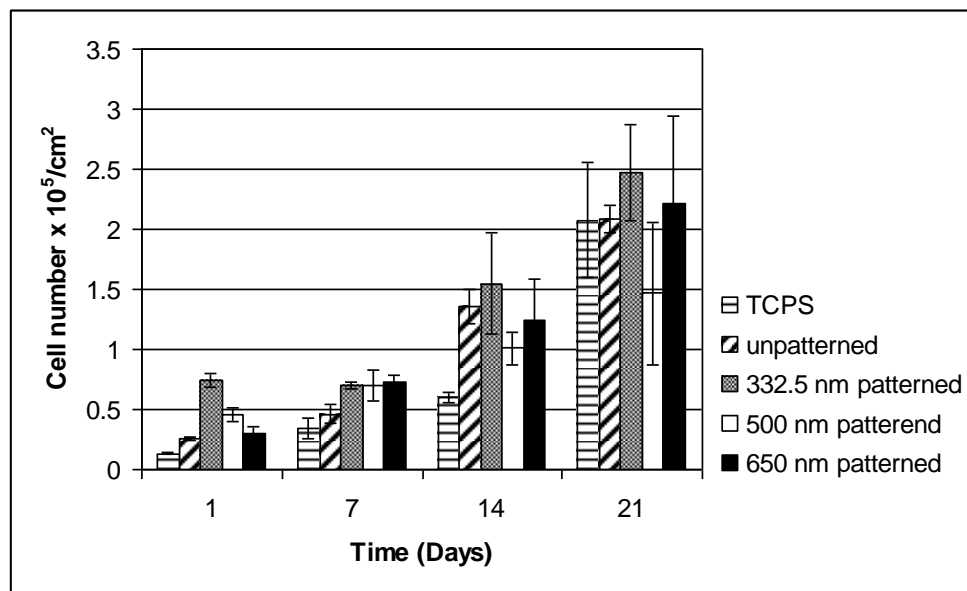


Figure 3.28. VSMC proliferation on collagen films. Alamar Blue assay ($n=3$).

3.5.2.2. Cell Morphology, Orientation and Phenotype

VSMCs on nanopatterned and unpatterned collagen films were stained with anti- α -smooth muscle actin on Days 1, 7, 14 and 21 in order to show the cell phenotype and also the alignment of cell cytoskeleton by the nanopatterns (Figures

29 to 32). Figures show the alignment of cell cytoskeleton by the nanopatterns since the marker used stains the cytoskeletal elements. The figures also show that the cell phenotype is maintained through out the experiment.

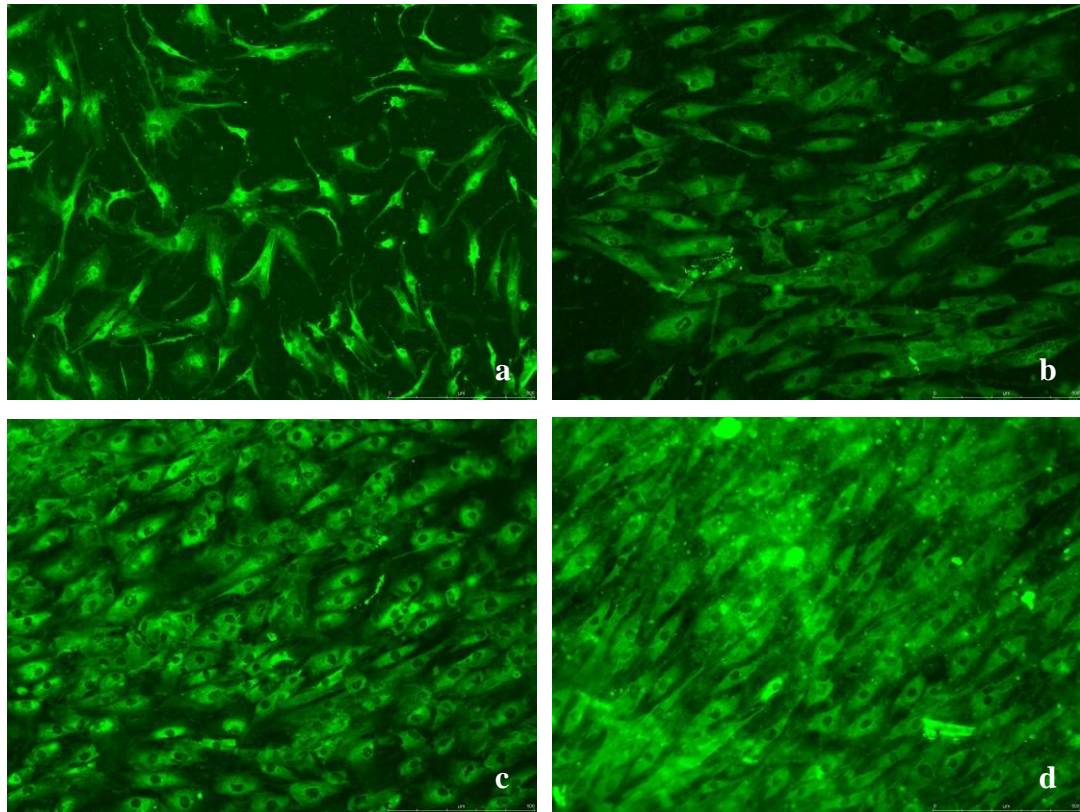


Figure 3.29. VSMC on collagen films. a) unpatterned, b) 332.5 nm, c) 500 nm, d) 650 nm (x 100). Day 1 anti- α -smooth muscle actin stain.

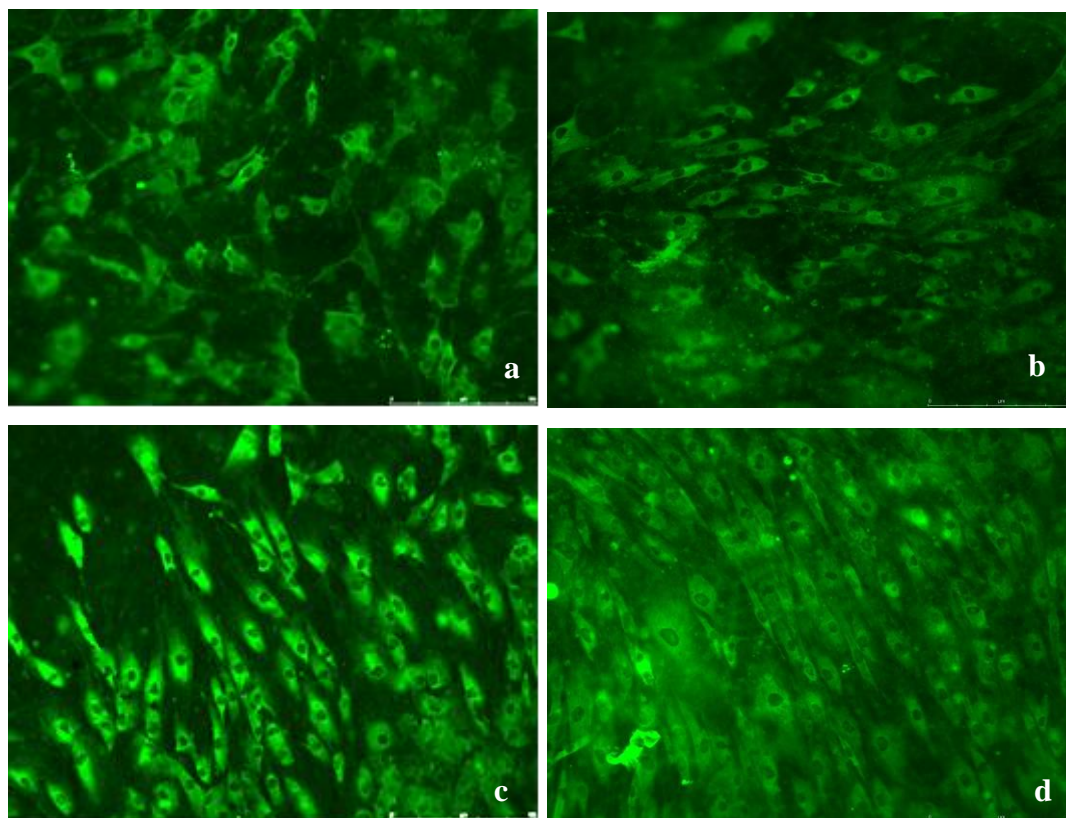


Figure 3.30. VSMC on collagen films. a) unpatterned, b) 332.5 nm, c) 500 nm, d) 650 nm (x 100). Day 7 anti- α -smooth muscle actin stain.

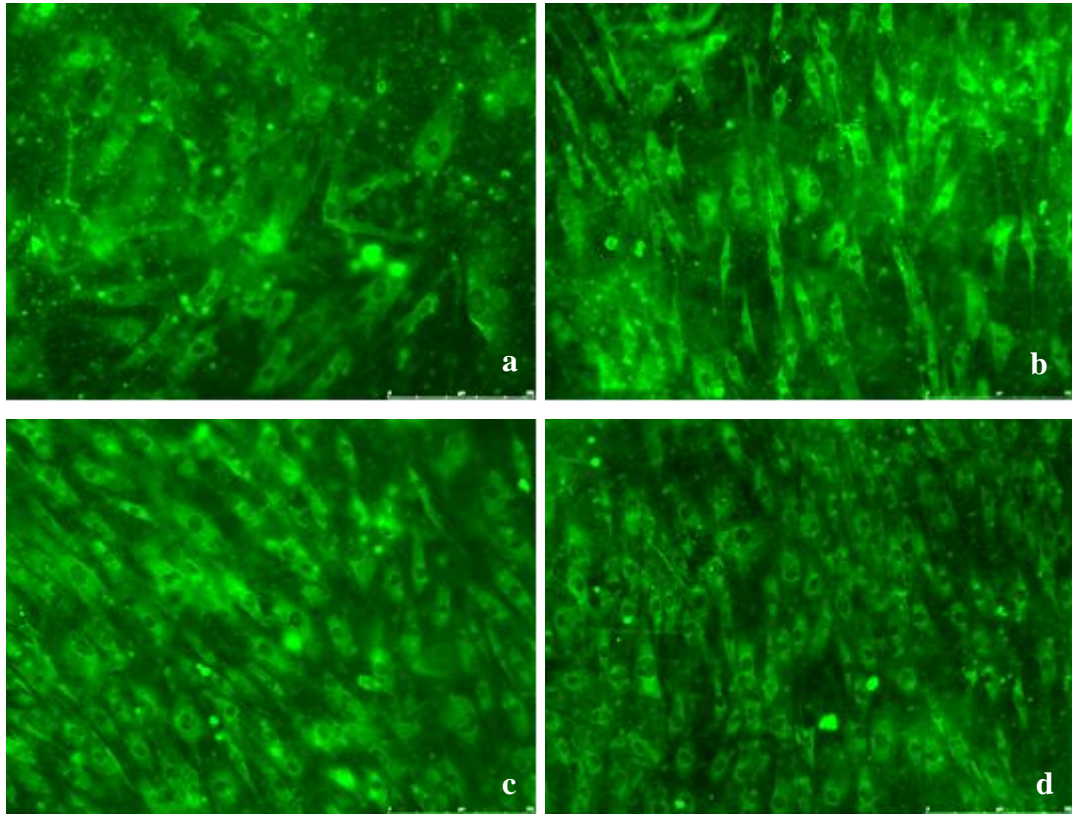


Figure 3.31. VSMC on collagen films. a) unpatterned, b) 332.5 nm, c) 500 nm, d) 650 nm (x 100). Day 14 anti- α -smooth muscle actin stain.

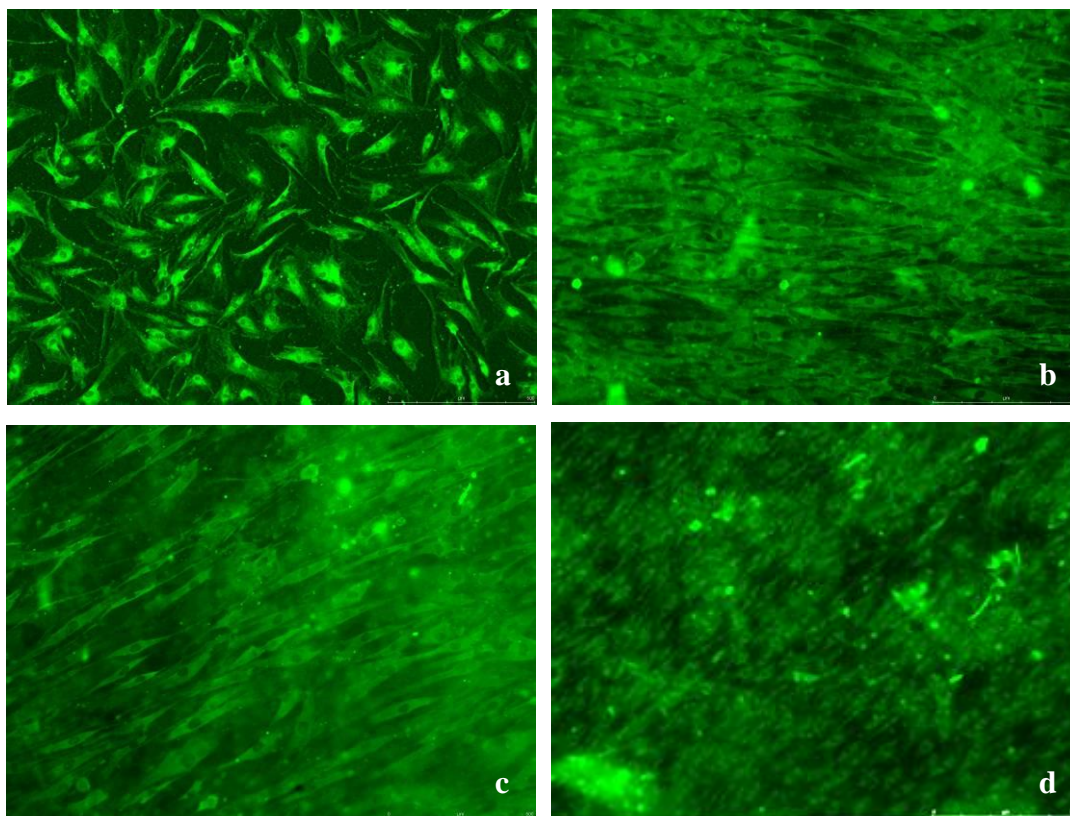


Figure 3.32. VSMC on collagen films. a) unpatterned, b) 332.5 nm, c) 500 nm, d) 650 nm (x 100). Day 21 anti- α -smooth muscle actin stain.

On Days 1, 7, 14 and 21, VSMCs on the nanopatterned and unpatterned films were fixed and examined by SEM in order to assess cell orientation (Figures 3.33 to 3.36). It is not possible to see both the alignment of the cells and the nanopatterns in a single micrograph since the patterns are in nanometer range while the cells are in the micron range. Therefore, images showing the film surfaces near the cells at a higher magnification were included in the figures.

VSMC alignment could be seen on all 3 types of the nanopatterned films, whereas cells were randomly oriented on the unpatterned films. This proves that patterns as small as 332.5 nm can effectively align cells which are at least 10 fold larger. Similar results were previously reported for bone marrow derived mesenchymal stem cells, where the cell alignment was achieved with polymethylmethacrylate nanochannels of 200 nm width (Engel et al., 2008). So, unlike micropatterns where physical restrictions larger than the cells lead to

aligning, on the nanochannels molecular level interactions are the aligning factors. Alignment of vascular smooth muscle cells by using micron-range surface features on collagen membranes was previously reported. Human umbilical artery smooth muscle cells were oriented by using collagen surfaces with 33, 13 and 7 micron wide channels (Vernon et al., 2005). Alignment on synthetic polymeric membranes ((poly(σ -caprolactone-*r*-L-lactide-*r*-glycolide) diacrylate) with 40, 80, 120, or 160 micron channels was also reported where the extent of orientation decreased with increased channel width (Shen et al., 2006). Alignment of human coronary artery smooth muscle cells on nano-scale topography was shown on synthetic polymeric fibers with 500 nm diameter (Xu et al., 2004). To the best of our knowledge the present study is the first that shows alignment of vascular smooth muscle cells on nano-scale patterned collagen membranes.

The SEM images of the film surfaces at higher magnification showing a region of the film not yet covered with cells clearly reveal good quality patterns maintained during the culture period. It can thus be concluded that collagen nanopatterns are effective in cell guidance and nanopatterns are quite stable in the growth medium under cell culture conditions for at least 21 days. This stability is specifically a result of crosslinking and is one of the key factors in achieving alignment on nanopatterns.

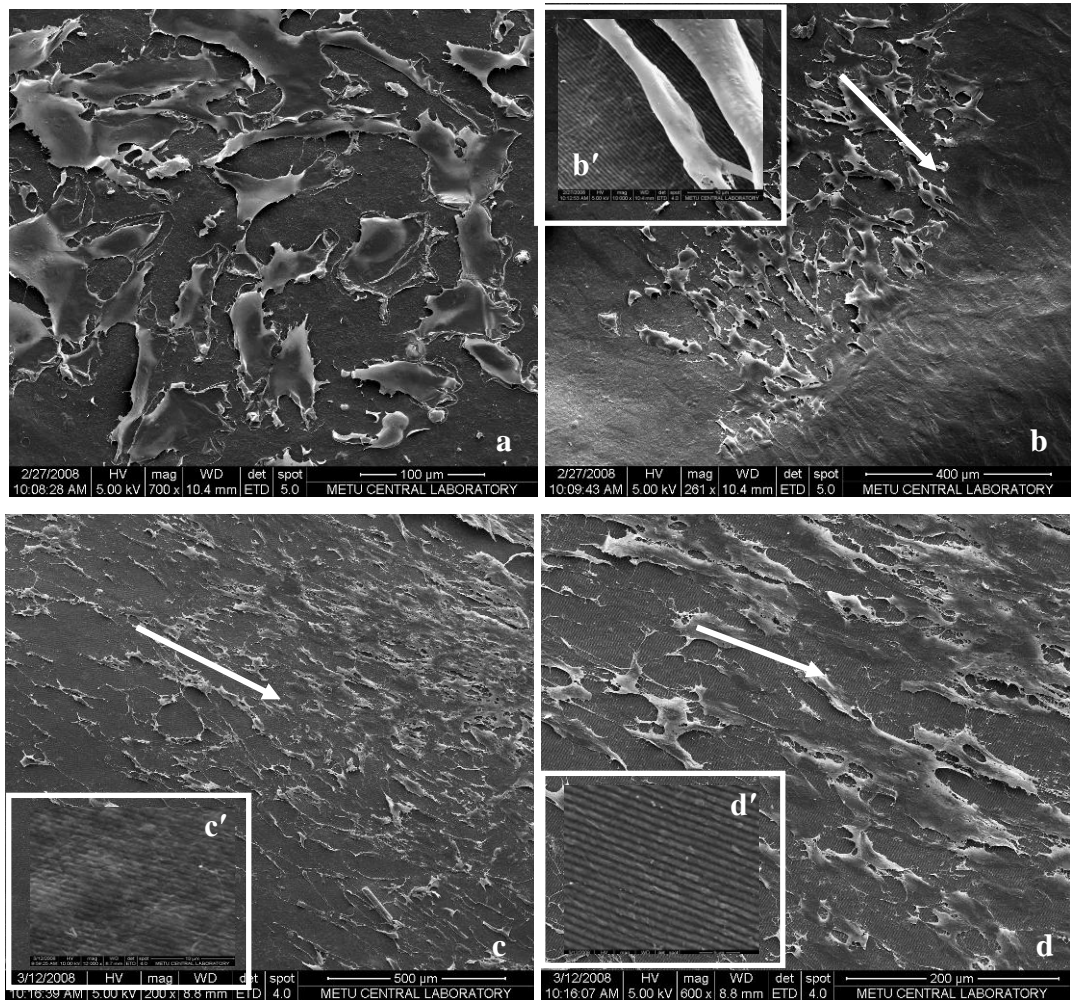


Figure 3.33. SEM micrographs of VSMCs on collagen films on Day 1. a) unpatterned film (x 700), b) 332.5 nm patterned film (x 261), b') 332.5 nm patterned film (region of the sample not occupied by the cells, x 10,000), c) 500 nm patterned film (x 200), c') 500 nm patterned film (region of the sample not occupied by the cells, x 10,000), d) 650 nm patterned film (x 600), d') 500 nm patterned film (region of the sample not occupied by the cells, x 12,000). White arrow indicates the direction of the patterns.

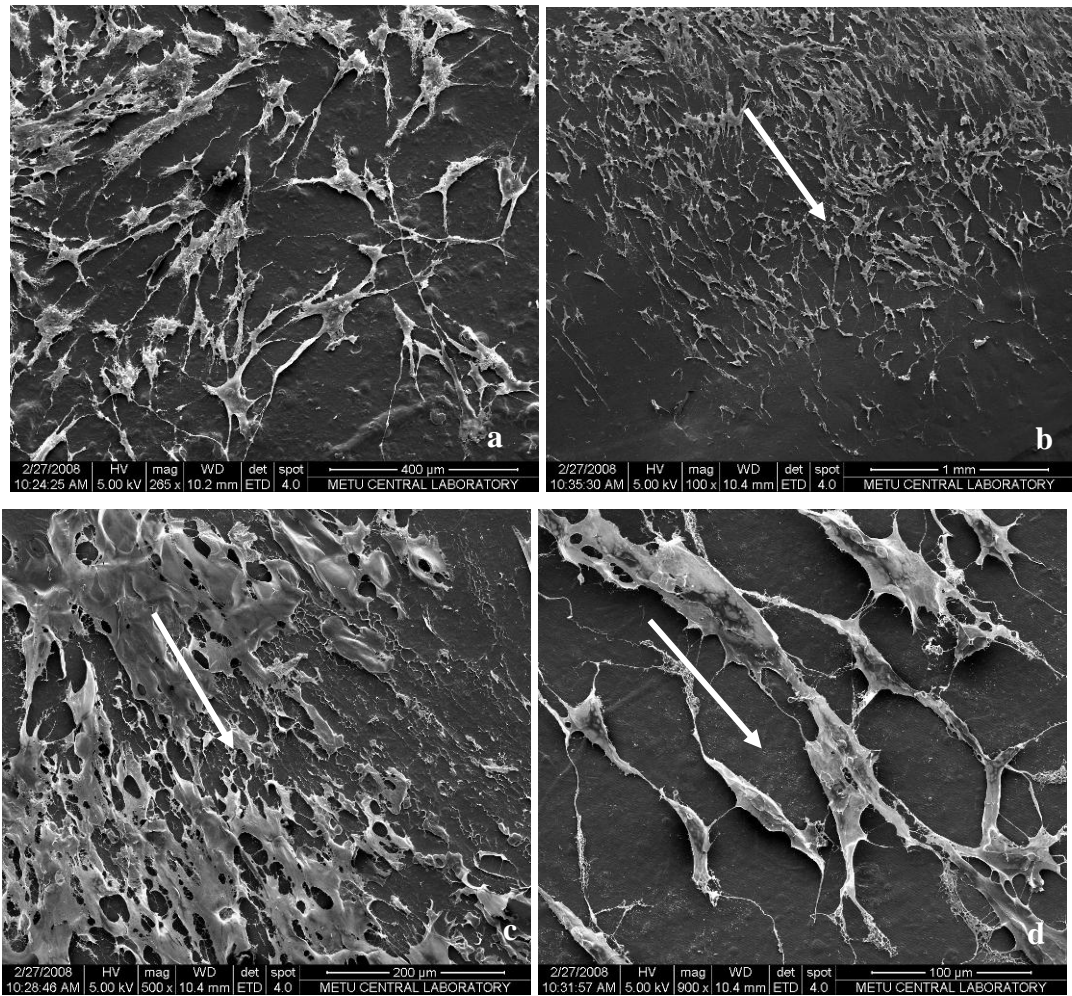


Figure 3.34. SEM micrographs of VSMCs on collagen films on Day 7. a) unpatterned film (x 265), b) 332.5 nm patterned film (x 100), c) 500 nm patterned film (x 500), d) 650 nm patterned film (x 900). White arrow indicates the direction of the patterns.

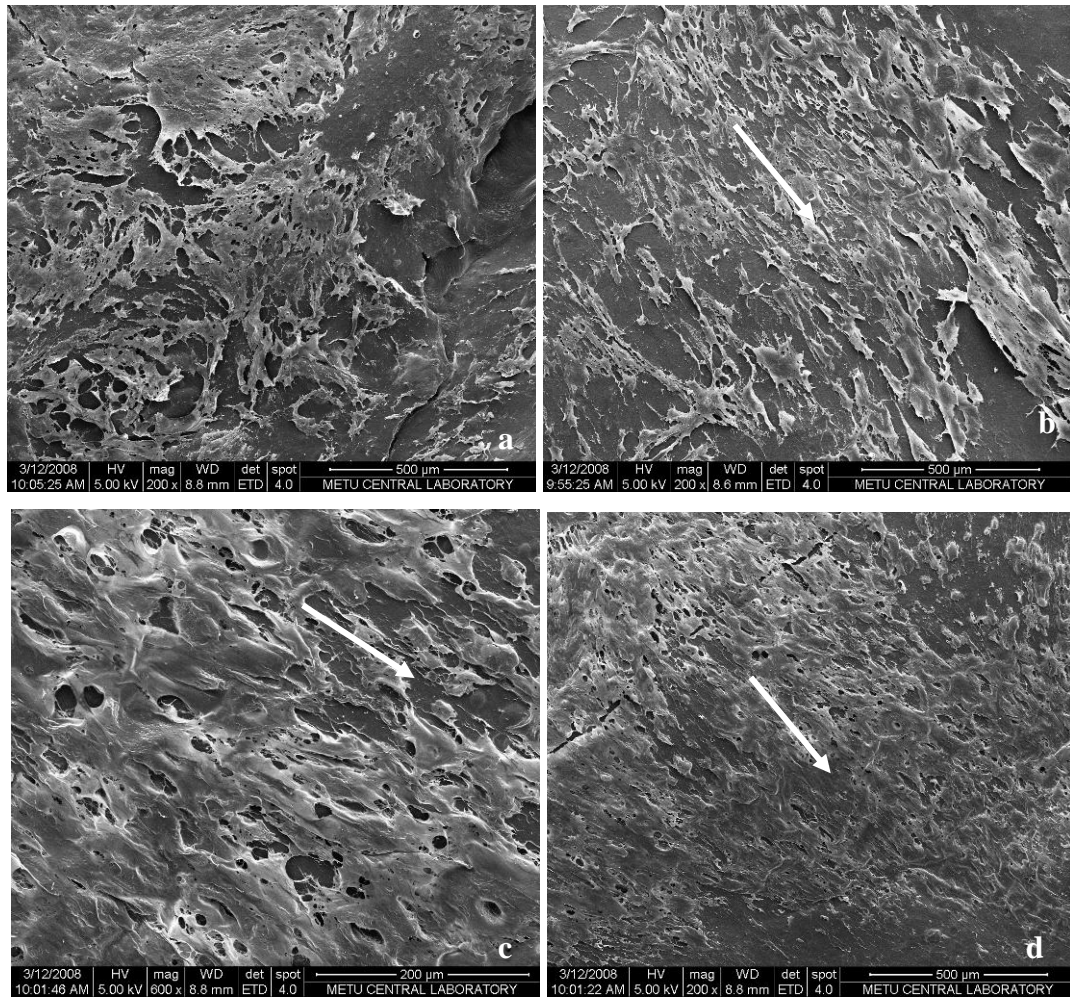


Figure 3.35. SEM micrographs of VSMCs on collagen films on Day 14. a) unpatterned film (x 200), b) 332.5 nm patterned film (x 200), c) 500 nm patterned film (x 600), d) 650 nm patterned film (x 200). White arrow indicates the direction of the patterns.

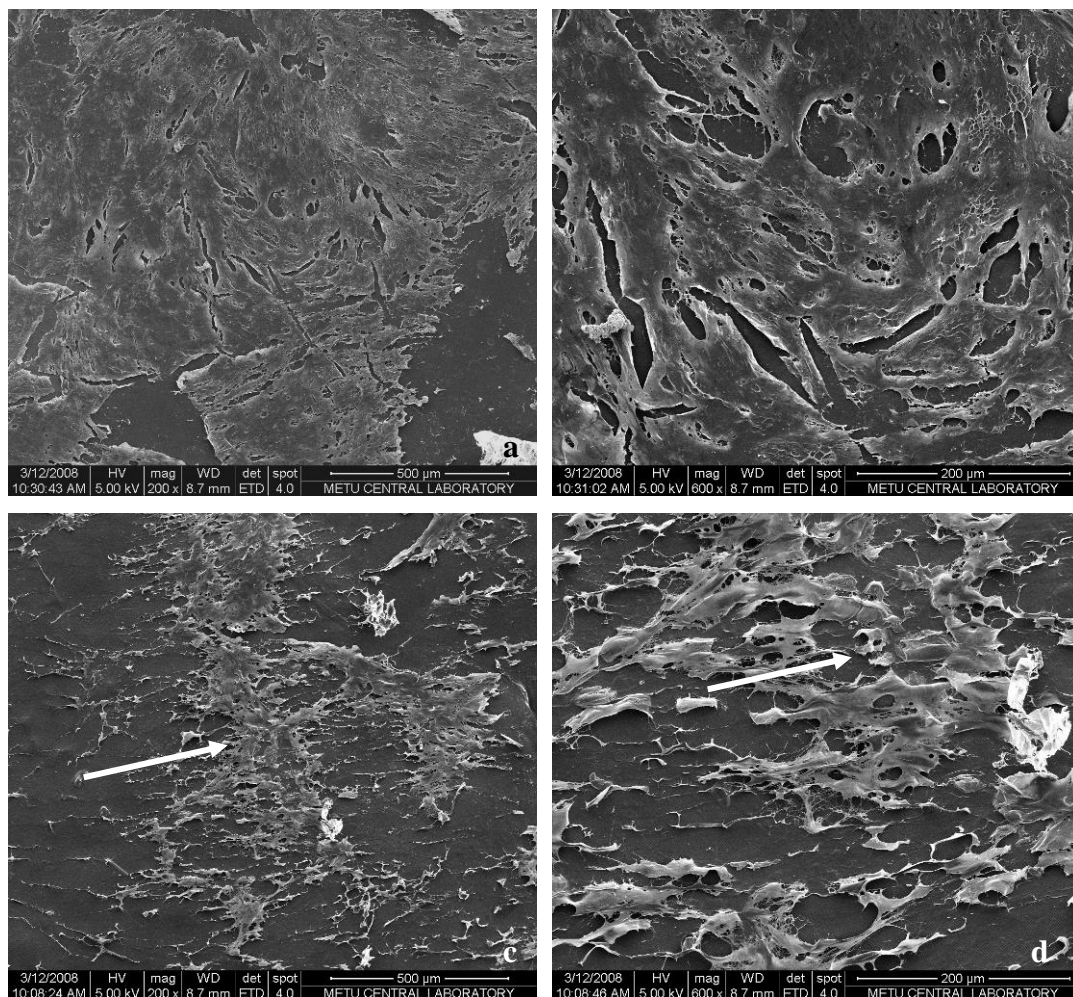


Figure 3.36. SEM micrographs of VSMCs on collagen films on Day 21. a) unpatterned film (x 200), b) unpatterned film (x 600), c) 332.5 nm patterned film (x 200), d) 332.5 nm patterned film (x 600), e) 500 nm patterned film (x 200), f) 500 nm patterned film (x 600), g) 650 nm patterned film (rolled by contraction by the cells, x 200), h) 650 nm patterned film (x 600). White arrow indicates the direction of the patterns.

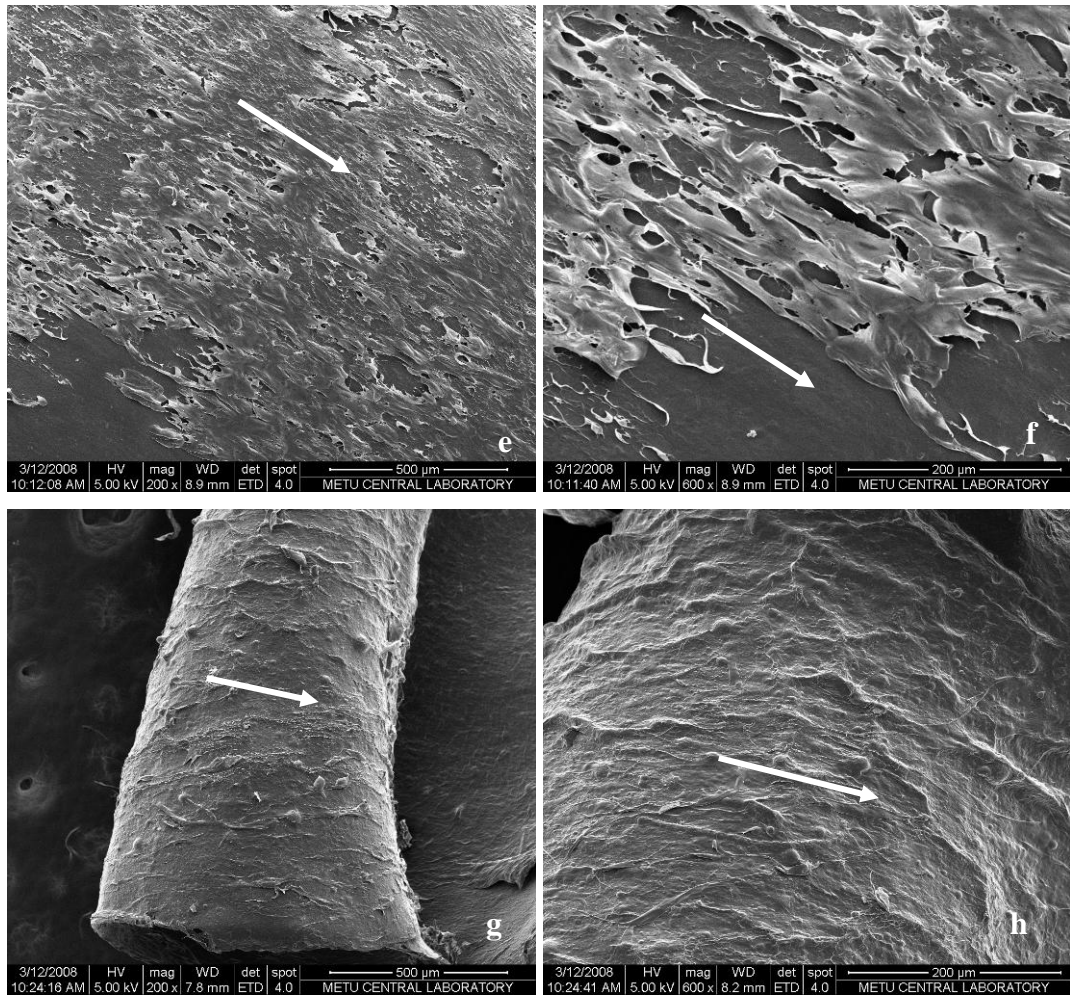


Figure 3.36. (Continued)

3.5.2.3. Mechanical Tests

Individual best curves (averages) for unseeded films, cell seeded and 45 day incubated films and cell seeded and 75 day incubated films were calculated using data obtained through tensile tests. Figure 3.37 shows the individual results and the mean curve for the unseeded collagen films.

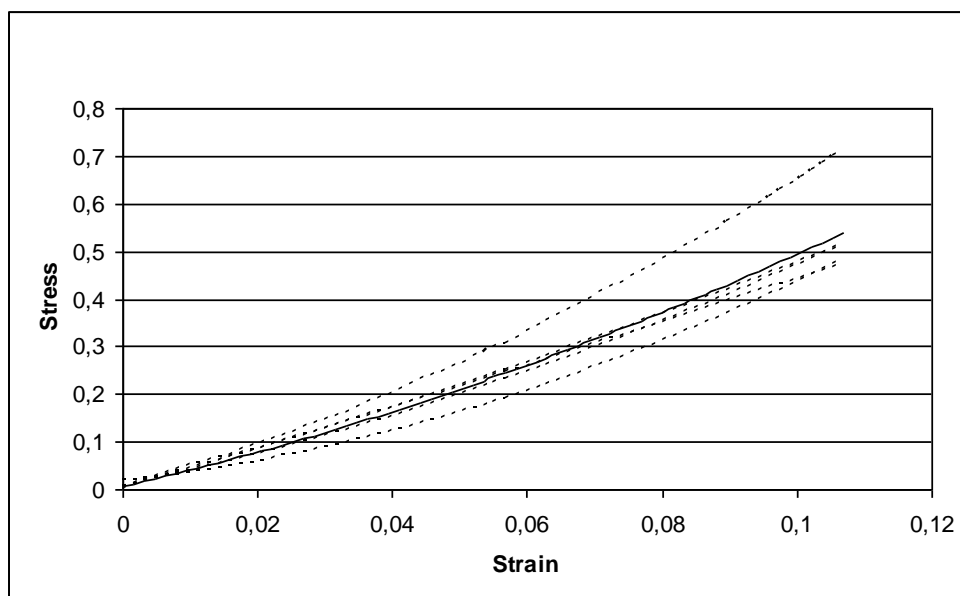


Figure 3.37. Stress-Strain plot of unseeded collagen films. Dashed curves are individual tests and the smooth curve is the average.

In the literature there are studies reporting the mechanical adequacy of scaffolds designed for vascular tissue engineering purposes. Yang et al. (2005), tested mechanical properties of biphasic scaffolds which were fabricated from poly(diols citrate) and found them to be similar to native vessels. The scaffold's Young's modulus and UTS values were both around 2 MPa, close to those of our VSMC seeded nanopatterned collagen films used in this study. In a recent work, Thomas et al. (2007), reported their electrospun polyglyconate tubular scaffolds as mechanically suitable for vascular tissue engineering which had UTS values around 2 MPa with a higher Young's Modulus of 9 MPa which is about 3 times higher, and therefore, stiffer than the natural vessels.

Tensile test results of the unseeded and cell seeded films incubated for 45 and 75 days are presented in Figure 3.38. Figure 3.39 shows the change in the UTS with time. Young's Moduli of the films were also calculated to assess the films hardness (Figure 3.40). Table 3.3 summarizes the overall UTS and Young's Modulus data.

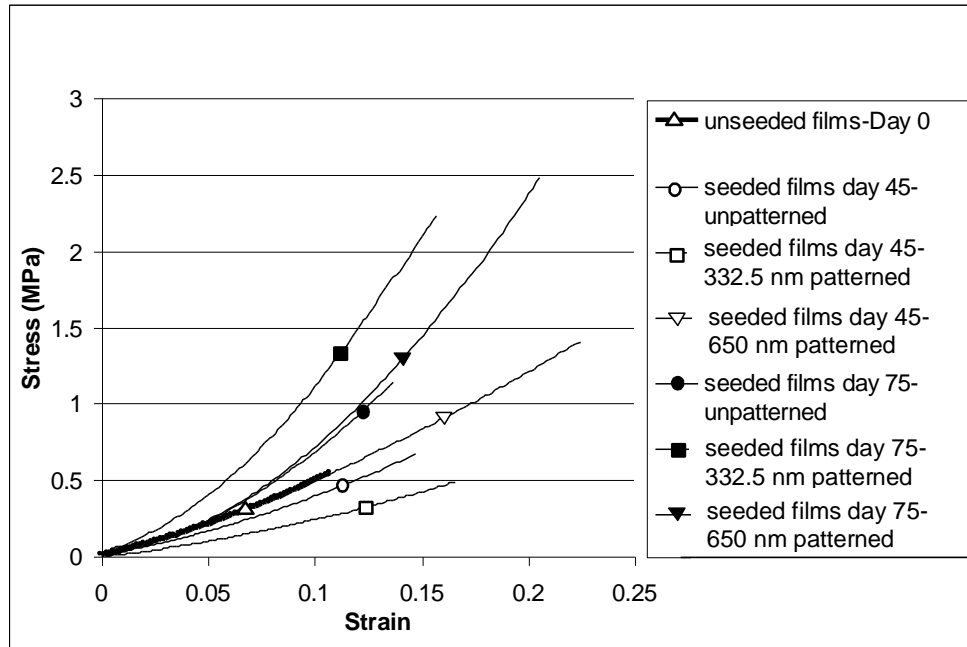


Figure 3.38. Stress-Strain graph of average curves of unseeded and VSMC seeded nanopatterned and unpatterned collagen films after 45 or 75 days of incubation ($n=6$).

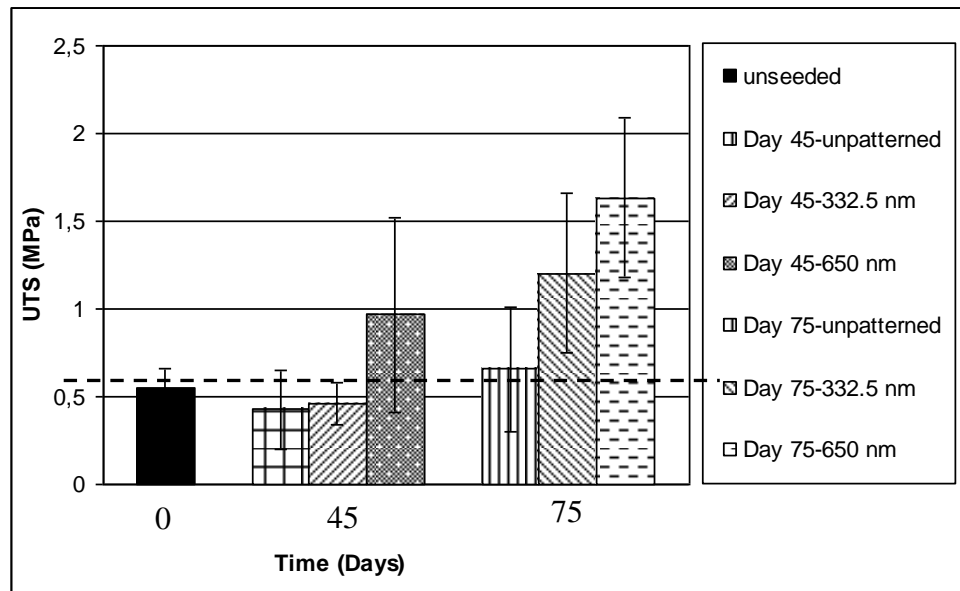


Figure 3.39. UTS values of VSMC seeded nanopatterned collagen films after 45 and 75 days of incubation.

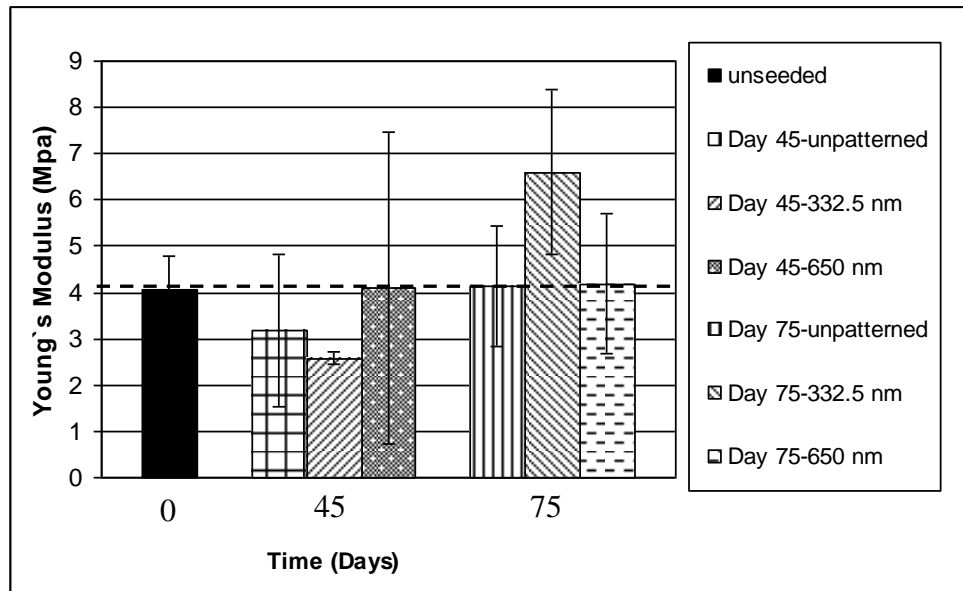


Figure 3.40. Young's Modulus values of VSMC seeded nanopatterned collagen films after 45 and 75 days of incubation.

Table 3.3. UTS and Young's Moduli of the seeded and unseeded collagen films ($n=6$).

Sample			UTS (MPa)	Young's Modulus (MPa)
Pattern (nm)	VSMC	Incubation Duration (Days)		
UP*	-	0	0.55 ± 0.11	4.05 ± 0.73
UP	+	45	0.43 ± 0.23	3.16 ± 1.65
332.5	+	45	0.46 ± 0.12	2.59 ± 0.12
650	+	45	0.97 ± 0.55	4.10 ± 3.36
UP	+	75	0.66 ± 0.35	4.12 ± 1.30
332.5	+	75	1.20 ± 0.46	6.60 ± 1.79
650	+	75	1.63 ± 0.46	4.19 ± 1.52

* UP: unpatterned

UTS of cell-free, collagen film was calculated as 0.55 ± 0.11 MPa. This value is consistent with the value in the literature which is around 0.7 MPa for EDC/NHS crosslinked collagen (Faraj et al., 2007). Since the depth of the patterns are at the most 200 nm and this value is insignificant when compared to the thickness of the film (ca. 35 μm), and the thickness is the only parameter that affects mechanical properties in the case of surface nanopatterns, nanopatterned and unpatterned films were not tested separately on Day 0 and assumed to have same mechanical properties. Upon cell seeding and incubation in the culture medium for 45 days the UTS decreases from 0.55 to 0.46 MPa for the 332.5 nm patterned film. However, after 75 days the UTS is measured as 1.2 MPa indicating a substantial gain in the strength due to ECM secretion by the VSMCs (Table 3.3). Also by day 75 there was a significant difference between the UTS of unpatterned and nanopatterned films (0.66 ± 0.35 MPa versus 1.20 ± 0.46 for 332.5 nm and 1.63 ± 0.46 for 650 nm) suggesting that cell alignment and resultant ECM organization along with the cells increased the strength of the collagen films. This difference was particularly distinct when the results of 650 nm patterned samples for Day 75 were compared with unpatterned films. In this case UTS value was 1.63 ± 0.46 MPa when cells were seeded on nanopatterned films whereas the value for the unpatterned film at same time point was nearly one third; 0.66 ± 0.35 MPa. Support for this is found in the literature where it was previously shown that aligned MC3T3 cells produce aligned collagen type I as ECM (Wang et al., 2003). Similar results were reported when smooth muscle cell-seeded collagen scaffolds were mechanically stimulated using cyclic distension (Isenberg et al., 2003). In the first 2 weeks of their incubation, the authors observed no effect of cell presence or cyclic distension but after 5 weeks the UTS had increased by 1.6 fold to around 0.4 MPa (still not high enough for vascular tissue engineering applications). The UTS values of cell free, pristine or cell seeded unpatterned films in the present study are lower than the average UTS of the straight portion of an artery (around 1.3 MPa) (Yamada, 1970). Thus, aligning the cells on nanopatterned films raised the mechanical strength almost to the level of the UTS of fresh carotid arteries (1.76 MPa to 2.64 MPa, Kurane et al., 2007).

There was no significant difference between the Young's Modulus' of different groups; all the test groups had values around 4 MPa (Table 3.3) and with time a slight increase was observed in all the sample types indicating some stiffening. The value of 4 MPa is somewhat higher than that of the veins (3.11 ± 0.65 MPa) and is significantly higher than that of the arteries (1.54 ± 0.33 MPa) (Pukacki et al., 2000).

Similar to our case, Grenier and coworkers showed mechanical stimuli applied by static stretching aligned fibroblasts and this resulted in about 7 fold improved mechanical properties of cell sheets compared to unoriented cell sheets (Grenier et al., 2005). A recent study comparing orientation of VSMCs by mechanical stimuli and by topographical cues showed that cells tend to orient themselves in the direction of the topographical cues (microgrooves) rather than in the direction of the mechanical stimulus (Houtchens et al., 2008). Orientation with mechanical stimuli was enhanced in the presence of similar direction topographical cues which implies that microtopographical cues modulate the orientation response of VSMCs to mechanical stimuli. Wang et al. (2005) also observed the same with fibroblasts. Although the present study uses nanochannels instead of microchannels, effectiveness of topographical cues in cell orientation, and in improving collagen film strength is evident.

3.5.3. VSMCs on Tubular Scaffolds

3.5.3.1. Optimization of VSMC Seeding on Tubular Scaffolds

VSMCs (passage: 4) were seeded on the exterior of the tubular constructs as described in Section 2.2.3.2.5, in different densities in order to establish the optimum seeding density for the tubes. To this end, 3 different seeding densities were tried; 5×10^4 cells, 1×10^5 cells and 2×10^5 cells in 2mL of their standard medium. During cell seeding and throughout the culture duration tubular scaffolds were placed in the wells in an inclined fashion (leaning against the wall of the well) in order to prevent any contact with the well and thus to allow the VSMCs

to grow evenly around the whole tube. Cell attachment and cell proliferation were determined by Alamar Blue assay and microscopical analysis were performed.

3.5.3.1.1. Cell Attachment and Proliferation

On Days 1, 7, 14 and 21 Alamar Blue assay was performed to examine the VSMC attachment and proliferation on the outside of the tubular scaffolds (Figure 3.41).

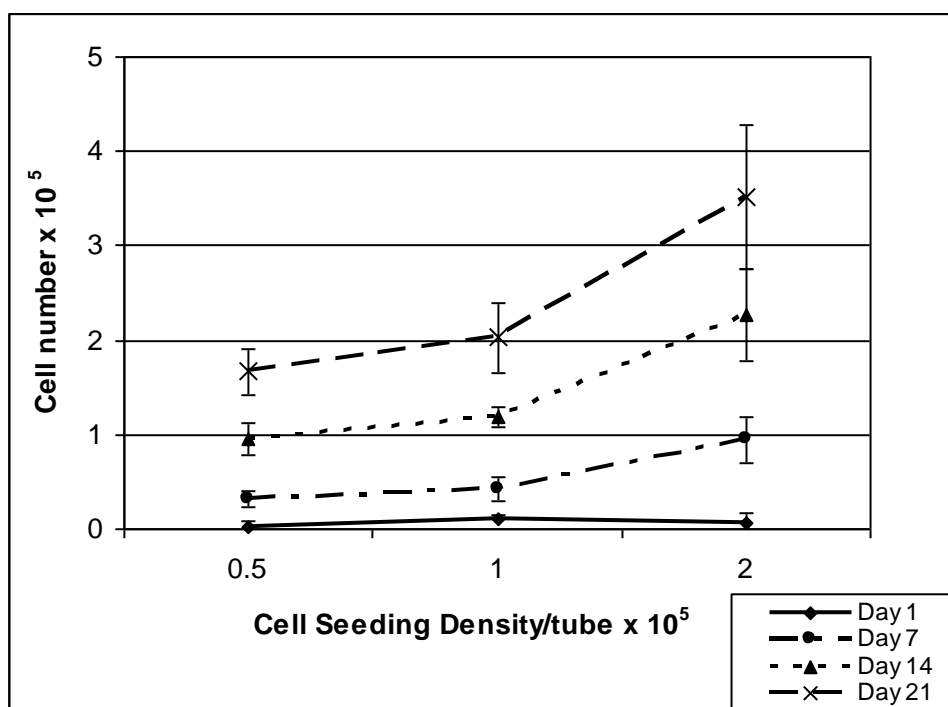


Figure 3.41. VSMC proliferation seeded at different densities on tubular scaffolds as determined with Alamar Blue assay.

Alamar Blue results showed that cells attached and proliferated properly with all three seeding densities. 2×10^5 cells/tube seeding density was chosen for use in the co-culture of VSMCs and endothelial cells. This seeding density (2×10^5 VSMC/tube) was also used to study the cell proliferation (for 21 Days) on patterned (650 nm) and unpatterned tubular scaffolds and the cell numbers were found to be

very similar as expected from the results of VSMC proliferation on the films (compare Figure 3.42 with Figure 3.28).

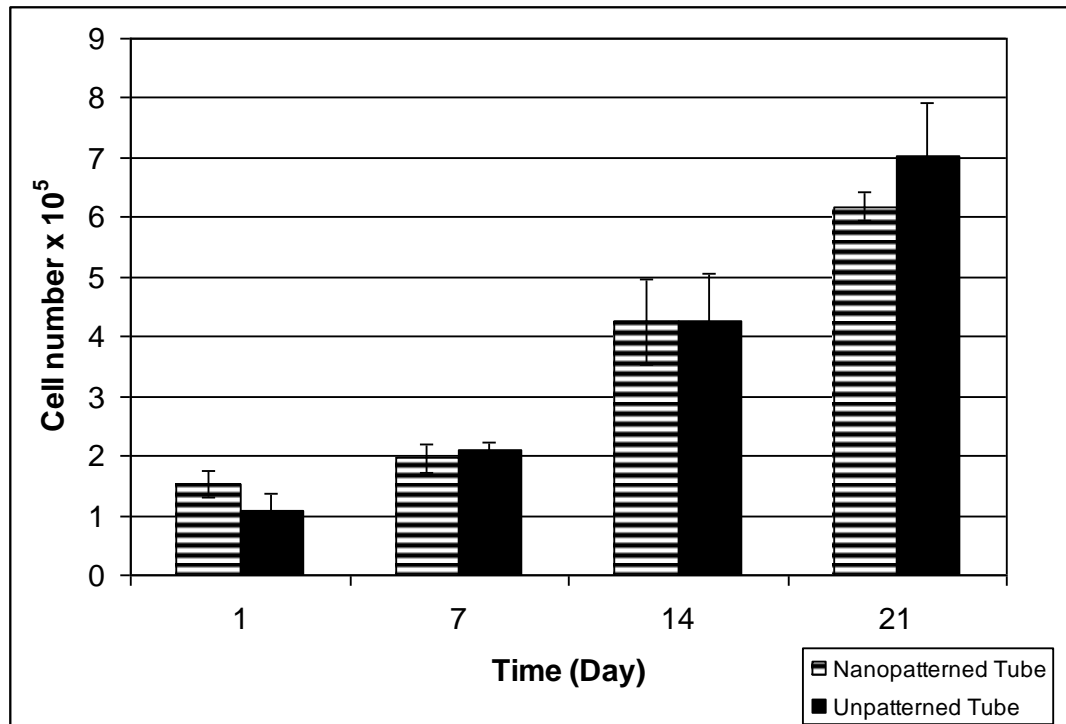


Figure 3.42. VSMC proliferation on nanopatterned (650 nm) and unpatterned tubular scaffolds as determined with Alamar Blue assay (2×10^5 cells/tube seeding density).

3.5.3.1.2. Microscopy (SEM, Fluorescence)

On day 21, VSMCs seeded with different initial seeding densities on unpatterned tubular scaffolds were stained with DAPI and α -smooth muscle actin and examined with fluorescence microscopy (Figure 3.43). Fluorescence microscopy supported the Alamar Blue assay results in terms of cell proliferation and also confirmed the maintenance of VSMC phenotype on the tubular scaffolds.

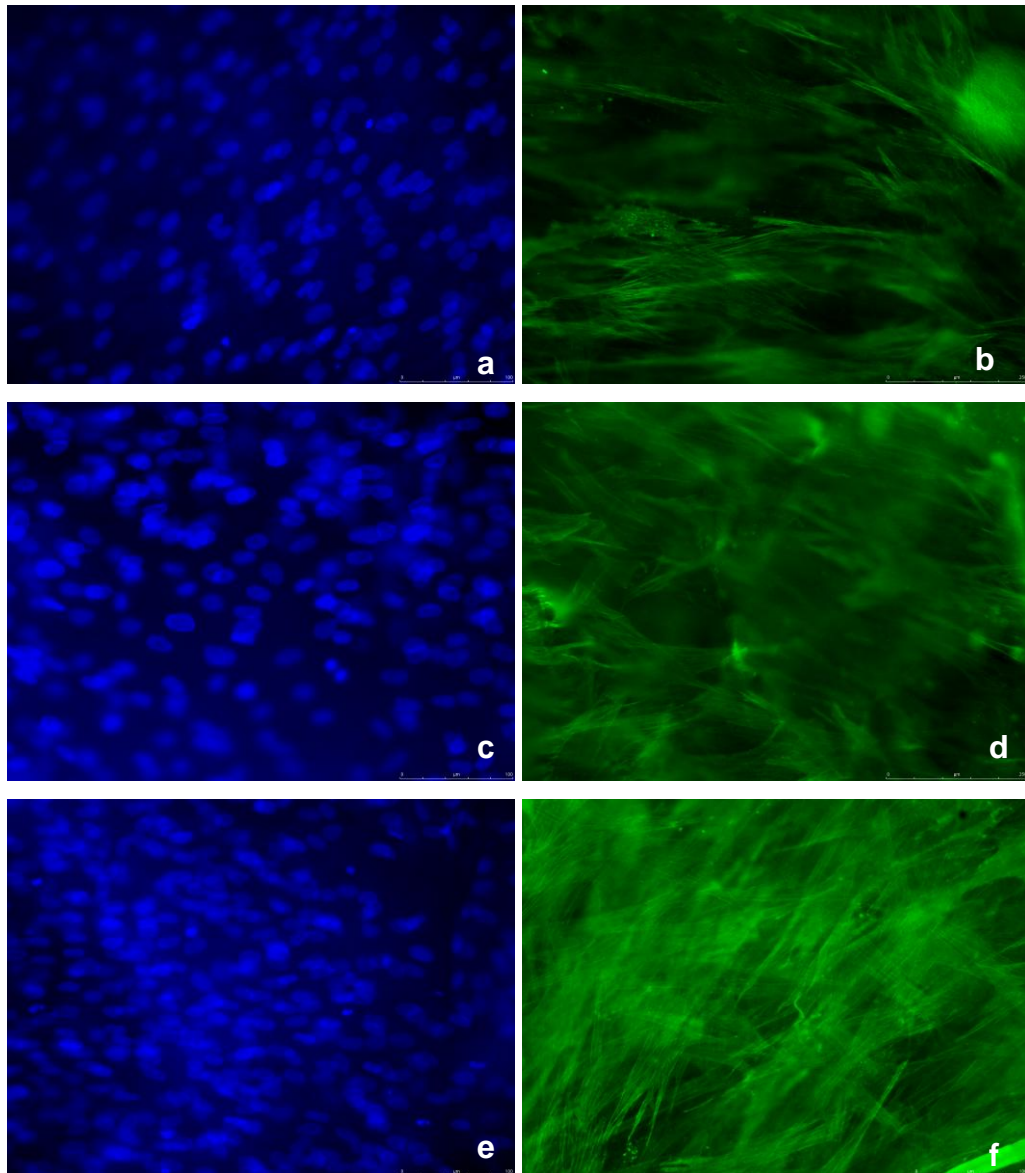


Figure 3.43. Fluorescence micrographs of VSMCs on collagen tubes stained with DAPI for cell nuclei and with anti- α -smooth muscle actin. a) 5×10^4 cells/tube initial seeding density, DAPI staining, b) 5×10^4 cells/tube initial seeding density, stained for α -smooth muscle actin, c) 1×10^5 cells/tube initial seeding density, DAPI staining, d) 1×10^5 cells/tube initial seeding density, stained for α -smooth muscle actin e) 2×10^5 cells/tube initial seeding density, DAPI staining, f) 2×10^5 cells/tube initial seeding density, stained for α -smooth muscle actin (x 200).

On Day 21, VSMCs seeded with 2×10^5 cells/tube initial seeding density on outside of the both side nanopatterned tubular scaffolds were examined with SEM. Figure 3.44 shows the SEM image of the inside of the tubular scaffold. There

are no cells since the Teflon madrel was left in the tube and no cell seeding on the inside of the tube was done in this step. The nanopatterns in the inside of the tube were in high fidelity even after 21 days of incubation under cell culture conditions indicating that they would help enhance the endothelial cell retention under flow shear conditions in the co-culture experiments, too.

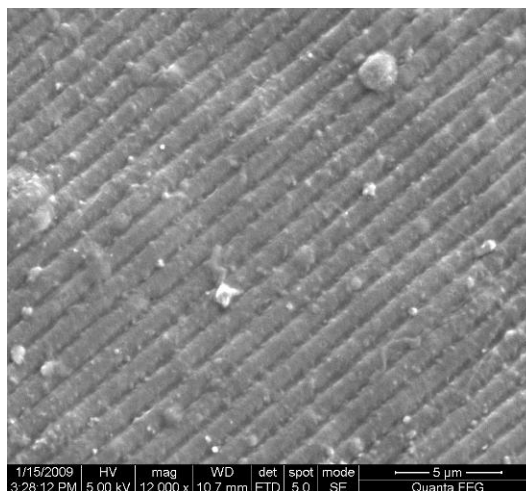


Figure 3.44. SEM of the inside (unseeded side) of the VSMC seeded tubular scaffold. Day 21 (x 12,000).

SEM images of the outside of the VSMC seeded tubular scaffold on Day 21 shows that the VSMCs were highly increased in number along the patterns and covered the whole surface of the tubular scaffold forming a cell sheet (Figure 3.45 a to e). The region at the edge of the cell sheets show the nanopatterns confirming the direction of cell alignment (Figure 3.45 f).

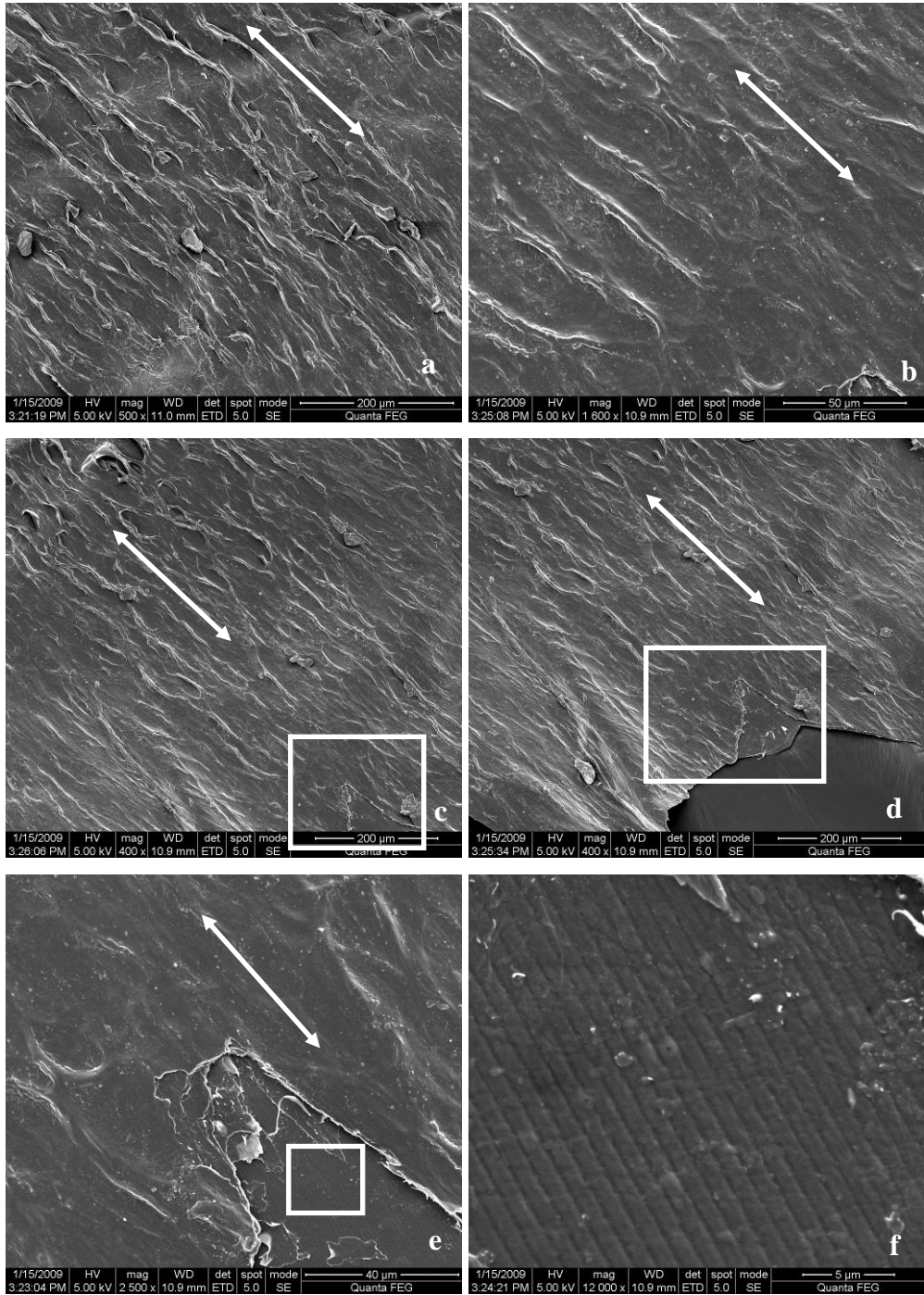


Figure 3.45. SEM images of the outside of the VSMC seeded tubular scaffold. a to c) VSMC sheets on different regions, d) region labeled with white rectangle in part c showing the cell sheet-film interface, e) magnification of white rectangle in part d, f) magnification of white rectangle in part e.

3.6. Tubular Scaffolds with 2 cell types: Co-culture of VSMCs and HITAECs on Tubular Scaffolds

3.6.1. Characterization of HITAECs

HITAECs were used in the co-culture studies because they were commercially available while the HMECs were not. For characterization, HITAECs were seeded on TCPS on their second passage and stained with anti-PECAM, an endothelial cell marker in order to confirm the endothelial cell phenotype of the cells (Figure 3.46). Cell nuclei were stained with DAPI.

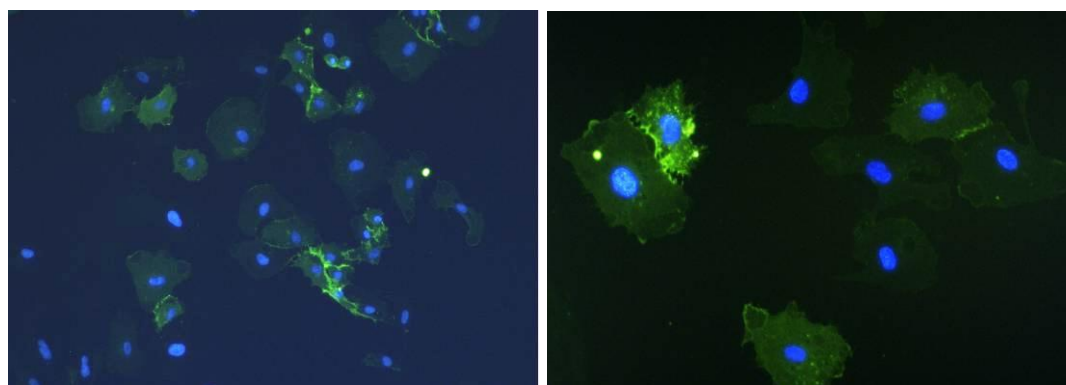


Figure 3.46. Fluorescence micrographs of anti-PECAM and DAPI staining of HITAECs at x 100 (left) and x 200 (right) magnifications.

3.6.2. Cell proliferation

In the co-culture proliferation of the cells on the both-side nanopatterned collagen tubes were determined by Alamar Blue assay. During the first two weeks there was only the VSMCs on the tubes. The % reduction values obtained in the assay were converted into cell numbers by using the calibration curve constructed earlier for VSMCs. Figure 3.47 shows that VSMCs proliferated steadily on the tubes prior to HITAEC seeding.

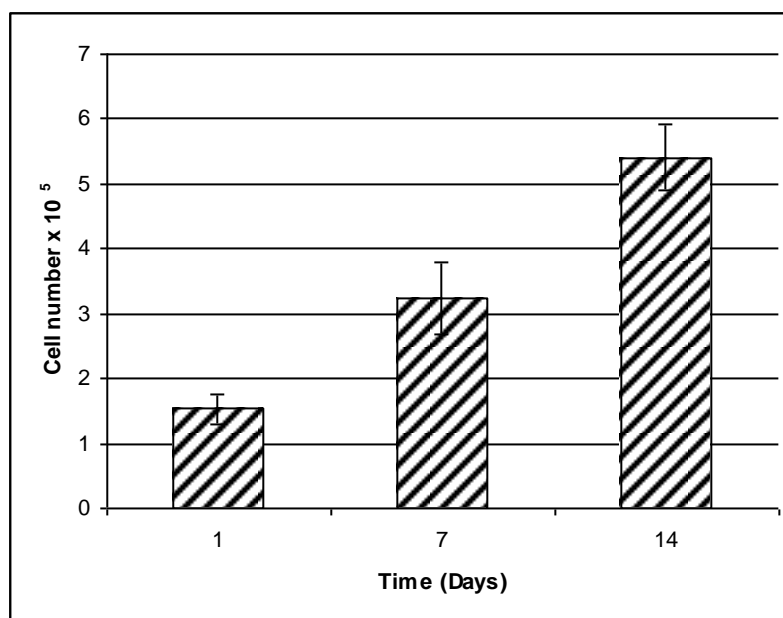


Figure 3.47. VSMC growth on nanopatterned tubular scaffold before endothelial cell seeding on Day 14.

Proliferation was also studied with Alamar Blue test after seeding the inside of the tubes with HITAECs on Day 14. This time, the values are presented as percent reduction and not as cell numbers since this co-culture had two cell types with probably two different proliferation rates and no way to differentiate. The steady increase in the percent reduction values show that the cells continued to proliferate after the co-culture was initiated on Day 14 (Figure 3.48). On Day 21, the reduction of the Alamar Blue dye for the co-culture was 31.61 %, where as it was 28.39 % for the only-VSMC seeded tubes (Figure 3.42). This 10 % increase in the reduction values is consistent with the 10 % difference between the numbers of 2 cell types at the moment of endothelial cell seeding (500,000 VSMC vs 50,000 HITAEC), assuming the cells did not affect each other's metabolic and growth rates in the co-culture, thus providing a quantitative proof of healthy and viable cell presence in the co-culture. This was further supported with microscopical examinations.

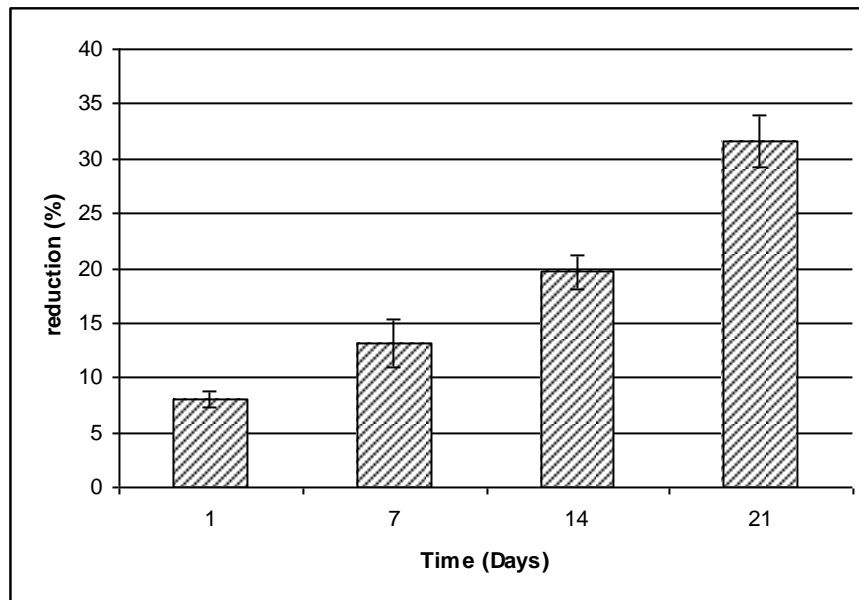


Figure 3.48. Cell proliferation in VSMC and HITAEC co-culture for 21 Days.

3.6.3. Microscopy (SEM, Fluorescence)

Nanopatterned tubular scaffolds were examined microscopically on Days 1, 7, 14 and 21 of co-culture.

On Days 1, 7 and 14 the tubes were stained only with anti- α -smooth muscle actin and on Day 21 both with anti- α -smooth muscle actin (for the VSMCs) and with anti-CD31 (PECAM) (for HITAECs). Figure 3.49 a to d shows the cells stained with anti- α -smooth muscle actin, and therefore, confirms the VSMC phenotype of the cells on the outside of the tube. Since anti- α -smooth muscle actin stains the cytoskeletal elements, the alignment of the cytoskeleton could also be seen in these micrographs. The inside of the tube was stained positive for the endothelial cell marker CD31 confirming the presence and phenotype of the endothelial cells on the inner surface of the tubes (Figure 3.49 e and f). These micrographs also show that the endothelial cells were as a continuous layer since CD31 is a surface receptor and the staining shows the cell membranes.

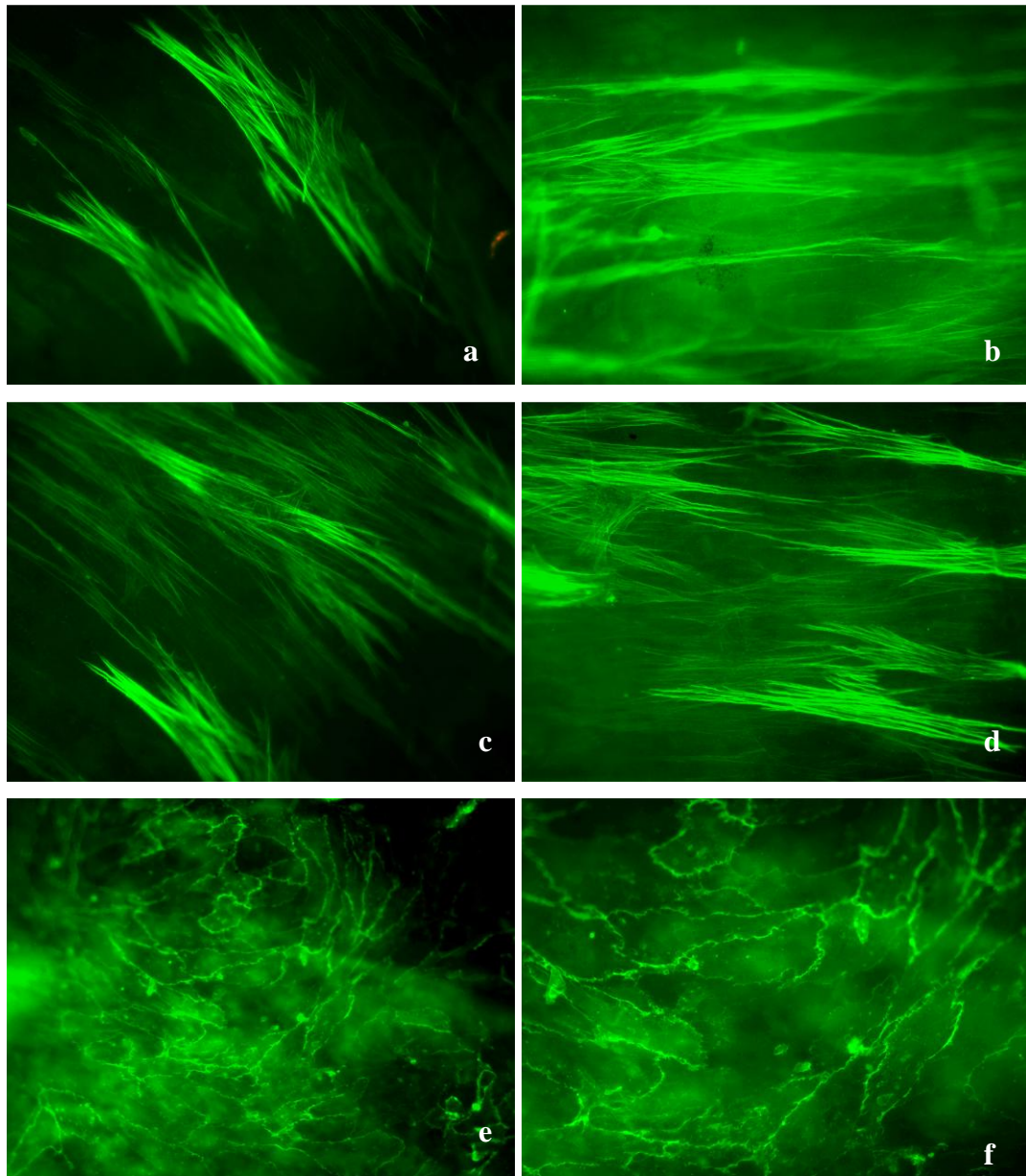


Figure 3.49. Fluorescence micrographs of immunostained VSMCs and HITAECs on nanopatterned tubular scaffolds. Anti- α -smooth muscle actin staining on a) Day 1 (x 200), b) Day 7 (x 200), c) Day 14 (x 200) and d) Day 21. Anti-CD31 staining on e) Day 21 (x 100) and f) Day 21 (x 200).

At the same time points, VSMCs seeded on the tubes were examined with SEM (Figure 3.50). Increase in cell number and the alignment of the cells could be observed as the duration of the incubation period increased. In Figure 3.50 (b), the patterns on the surface of the tubes can be seen to be in the direction of cell alignment. At later time points, the patterns could not be observed since the entire

surface was covered with the cells. On Day 21, multilayer formation by the VSMCs could be seen and this was also confirmed with the histology examinations (Figure 3.50 g and h). Figure 3.51 (a) to (d) shows that HITAECs covered the inner surface of the tubes as a continuous layer.

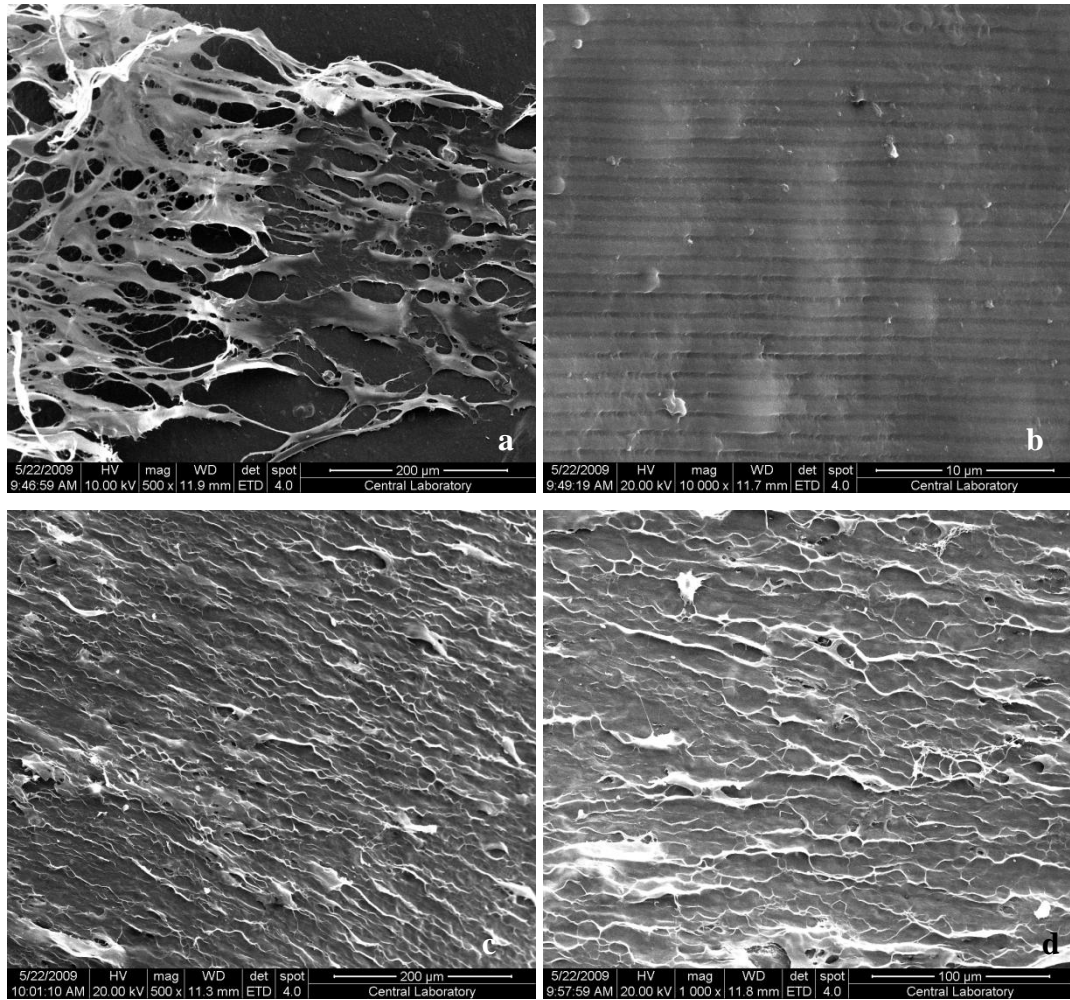


Figure 3.50. SEM images of the outside of the nanopatterned tubular scaffold, seeded with VSMCs. a) Day 1 (x 500), b) nanopatterns on the surface near the VSMCs on Day 1 (x 1000), c) Day 7 (x 500), d) Day 7 (x 1000), e) Day 14 (x 500), f) Day 14 (x 1000), g) on Day 21 (x 500), h) Day 21 (x 1000).

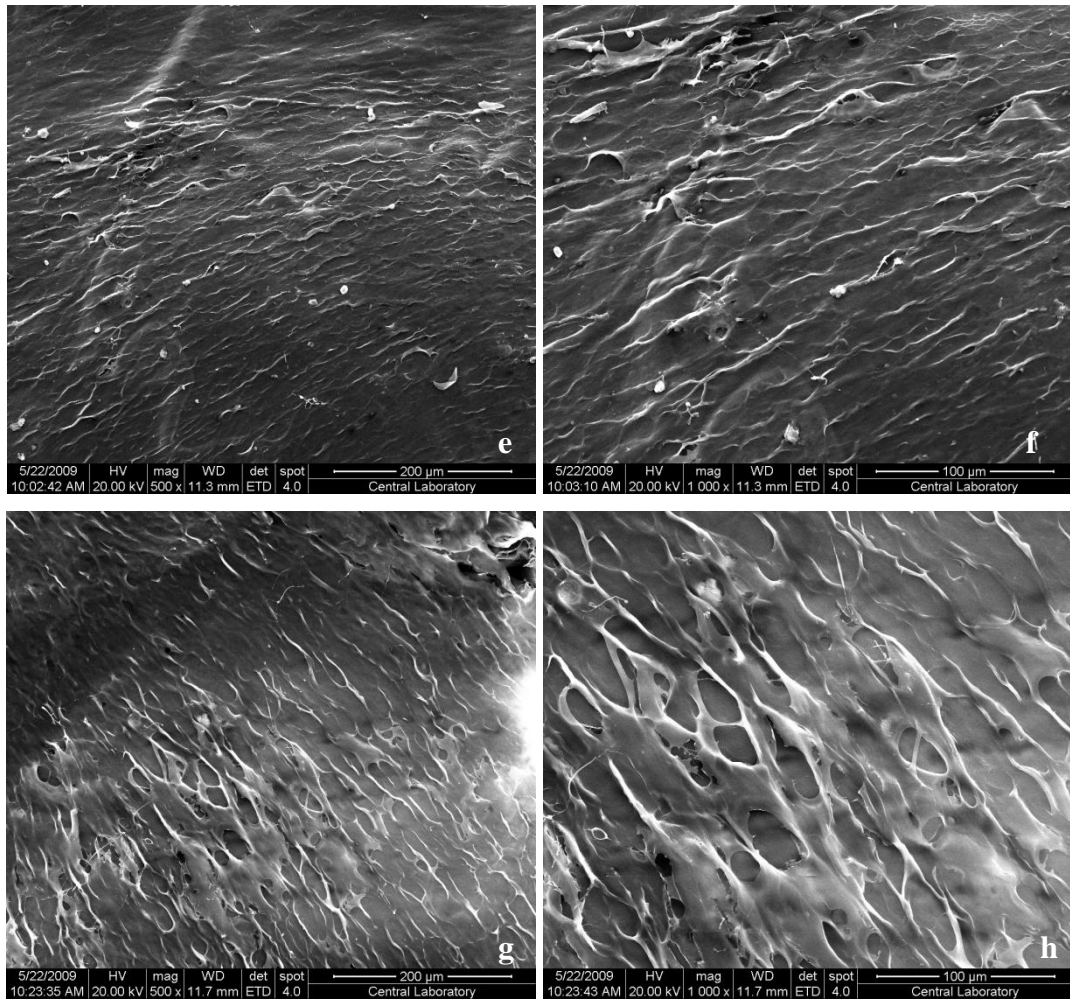


Figure 3.50. (Continued)

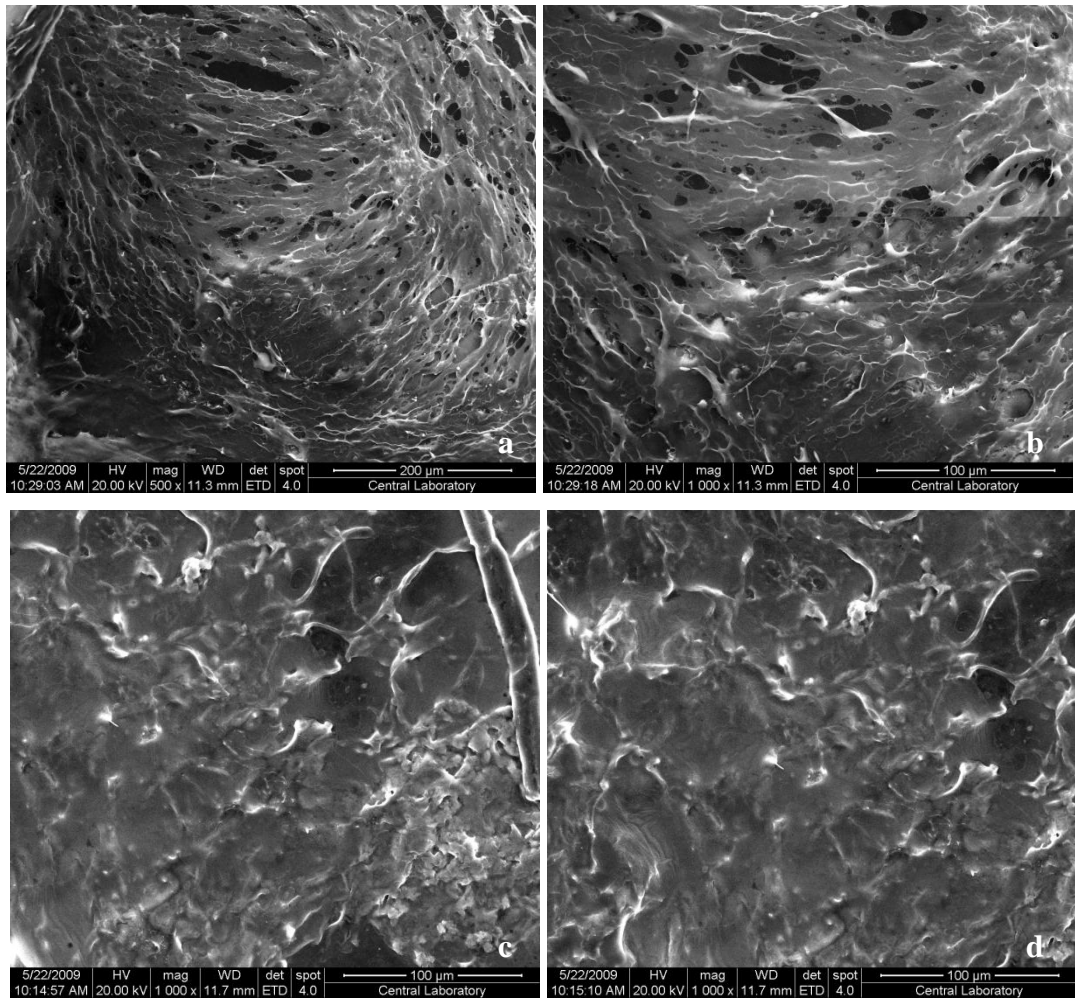


Figure 3.51. SEM images of the inside of the nanopatterned tubular scaffolds seeded HITAECS. Day 21. a) x 500, b) x 1000, c) another region x 1000, d) another region x 1000.

3.6.4. Histology

On day 21, cell seeded tubes and unseeded tubes were histologically examined after taking 5 μm thick sections using a microtome. The unseeded tube served as a control and also showed the cross-section of the tubular scaffold (Figure 3.52)

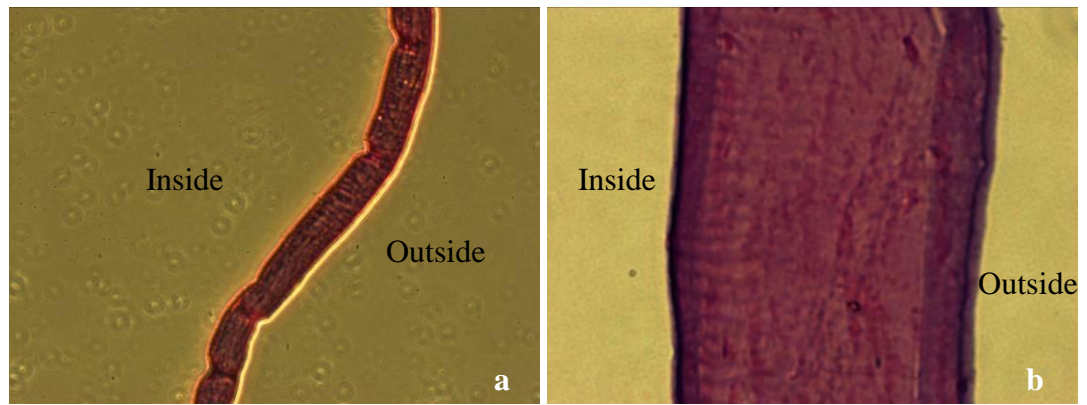


Figure 3. 52. Histological examination of unseeded tubular scaffolds on Day 21. a) x 100 and b) x 400.

The sections from Day 21 co-culture showed the HITAECS as a monolayer on the inside of the tube and the VSMCs on the exterior as multilayer sheets as in the natural vessel (Figure 3.53). Especially Figure 3.53 (d) clearly shows the multilayer formation by VSMCs.

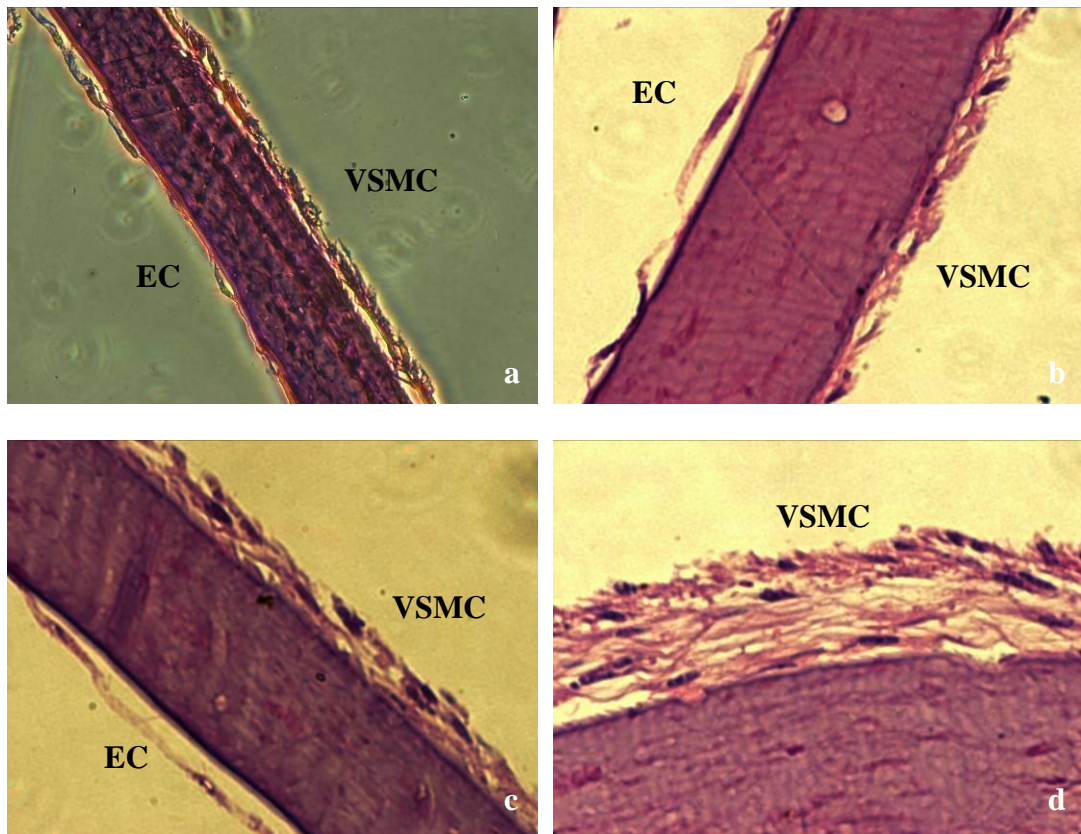


Figure 3.53. Histological examination of VSMC and HITAEC seeded tubular scaffolds on Day 21. a) x100, b and c) x200, d) x 400.

CHAPTER 4

CONCLUSION

A functional tissue engineered vessel could be the optimum solution for vascular reconstruction. In this study, natural ECM was mimicked using a nanopatterned tubular collagen scaffold seeded with vascular smooth muscle cells and endothelial cells. It was observed that the nanopatterned collagen films could support and align human VSMC isolated from human saphenous vein biopsy samples. This indicates that saphenous vein could serve as the cell source for vascular tissue engineering applications. Nanopatterns could be successfully transferred onto collagen films and maintained after crosslinking and they could guide the VSMC along the pattern axis. This guidance is especially important since natural VSMC in vessels are all oriented in one direction and alignment of cells improved the construct strength. Although the presence of nanopatterns did not affect endothelial cell proliferation and had a minimal effect on cell alignment, they significantly enhanced cell retention under shear. Films proved to have high diffusion coefficients for microsolute.

As a conclusion, it is possible to obtain a viable 3D vascular graft through tissue engineering using nanopatterns and co-culture of at least 2 types of vascular cells

Future Plans:

Although the *in vitro* results are very promising, *in vivo* characterization of the tissue engineered vessel in this study should be performed in order to examine the behavior of the cells and the scaffold under *in vivo* conditions.

REFERENCES

Badami A.S., Kreke M.R., Thompson M.S., Riffle J.S., Goldstein A.S. Effect of fiber diameter on spreading, proliferation, and differentiation of osteoblastic cells on electrospun poly(lactic acid) substrates. *Biomaterials* 2006; 27 (4): 596-606 15.

Basmanav F.B., Kose G.T., Hasirci V. Sequential growth factor delivery from complexed microspheres for bone tissue engineering. *Biomaterials* 2008; 29: 4195-204

Benditt E.P. and Schwartz S.M. Blood vessels, In: *Pathology*, Rubbin E, Faber JL (Eds.). JP, Lippincott Publishers, Philadelphia, 452-495 (1988)

Berglund J.D., Mohseni M.M., Nerem R.M. Sambanis A. A biological hybrid model for collagen-based tissue engineered vascular constructs. *Biomaterials* 2003; 24 (7): 1241-54

Bibb R., Freeman P., Brown R., Sugar A., Evans P., Bocca A. An investigation of three-dimensional scanning of human body surfaces and its use in the design and manufacture of prostheses. *Proc Inst Mech Eng H* 2000; 214 (6): 589-94

Boccafoschi F., Habermehl J., Vesentini S., Mantovani D. Biological performances of collagen-based scaffolds for vascular tissue engineering. *Biomaterials* 2005; 26 (35): 7410-17

Boccafoschi F., Rajan N., Habermehl J., Mantovani D. Preparation and characterization of a scaffold for vascular tissue engineering by direct assembling of collagen and cells in a cylindrical geometry. *Macromol Biosci* 2007; 25: 719-26

Bondar B., Fuchs S., Motta A., Migliaresi C., Kirkpatrick CJ. Functionality of endothelial cells on silk fibroin nets: Comparative study of micro- and nanometric fibre size. *Biomaterials* 2008; 29 (5): 561-72

Borne C.H., Roon A.J., Moore W.S. Maintenance of viable arterial allografts by cryopreservation. *Surgery* 1977; 83: 382-91

Bosman F.T. and Stamenkovic I. Functional structure and composition of the extracellular matrix. *J Pathol* 2003; 200 (4): 423-8

Branden C. and Tooze J. *Introduction to Protein Structure*, 2nd Edition, Garland Publishing, New York (2006)

Brems J., Castaneda M., Garvin P.J. A five-year experience with the bovine heterograft for the vascular access. *Arch Surg* 1986; 121: 941-99

Buma P., Ramrattan N.N., van Tienen T.G., Veth R.P. Tissue engineering of the meniscus. *Biomaterials* 2004; 25 (9): 1523-32

Callow A.D. Arterial homografts. *Eur J Vasc Endovasc Surg* 1996; 12: 272-81

Chakfe N., Kretz J.G., Petit H. Albumin impregnated polyester vascular prosthesis for abdominal aortic surgery: an improvement? *Eur J Vasc Endovasc Surg* 1996; 12: 346-53

Choi D.G., Jeong J.H., Sim Y.S., Lee E.S., Kim W.S., Bae B.S. Fluorinated organic-inorganic hybrid mold as a new stamp for nanoimprint and soft lithography. *Langmuir* 2005; 21 (21): 9390-2

Chong M.S.K., Lee C.N., Teoh S.H. Characterization of smooth muscle cells on poly(ϵ -caprolactone) films. *Mat Sci Eng C* 2007; 27: 309–12

Craighead H.G., James C.D., Turner A.M.P. Chemical and topographical patterning for directed cell attachment. *Curr Opin Solid St M* 2001; 5 (2-3): 177-84

Curtis AS. Cell-cell recognition: positioning and patterning systems. *Symp Soc Exp Biol.* 1978; 32: 51-82

Dalby M.J., Riehle M.O., Johnstone H., Affrossman S., Curtis A.S.G. In vitro reaction of endothelial cells to polymer demixed nanotopography. *Biomaterials* 2002; 23 (14): 2945-54

Dalton B.A., Evans M.D.M., McFarland G.A., Steele J.G. Modulation of corneal epithelial stratification by polymer surface topography. *J Biomed Mater Res* 1999; 45 (4): 384-94

Dardik H., Miller N., Darchk A. A decade of experiance with the glutaraldehyde-tanned human umbilical vein graft for revascularization of the lower limb. *J Vasc Surg* 1988; 7: 336-46

Diehl K.A., Foley J.D., Nealey P.F., Murphy C.J. Nanoscale topography modulates corneal epithelial cell migration. *J Biomed Mater Res A* 2005; 75 (3): 603-11

Duncan A.C., Rouais F., Lazare S., Bordenave L., Baquey C. Effect of laser modified surface microtopochemistry on endothelial cell growth. *Colloid Surface B* 2007; 54: 150-9

Eiselt P., Kim B.S., Chacko B., Isenberg B., Peters M.C., Greene K.G., Roland W.D., Loeb sack A.B., Burg K.J., Culberson C., Halberstadt C.R., Holder W.D., Mooney D.J. Development of technologies aiding large-tissue engineering. *Biotechnol Prog.* 1998;14 (1): 134-40

Elliott J.T., Woodward J.T., Langenbach K.J., Tona A., Jones P.L., Plant A.L., Vascular smooth muscle cell response on thin films of collagen. *Matrix Biol* 2005; 24: 489-502

Engel E., Michiardi A., Navarro M., Lacroix D., Planell J.A. Nanotechnology in regenerative medicine: the materials side. *Trends Biotechnol* 2008; 26: 39-47

Faraj KA, van Kuppevelt TH, Daamen WF. Construction of Collagen Scaffolds That Mimic the Three-Dimensional Architecture of Specific Tissues. *Tissue Eng* 2007; 13 (10): 2387-94

Farsak B., Tokmakoglu H., Kandemir O., Gunaydin S., Aydin H., Yorgancioglu C., Suzer K., Zorlutuna Y. Angiographic assessment of sequential and individual coronary artery bypass grafting. *J Card Surg* 2003; 18 (6): 524-31

Feng Z., Yamato M., Akutsu T., Nakamura T., Okano T., Umezu M. Investigation on the mechanical properties of contracted collagen gels as a scaffold for tissue engineering. *Artif Organs* 2003; 27: 84-91

Ferrari E.R. and von Segesser L.K. Arterial grafting for myocardial revascularization: how better is it? *Curr Opin Cardiol* 2006; 21(6): 584-8

Freyman T.M., Yannas I.V., Gibson L.J. Cellular materials as porous scaffolds for tissue engineering. *Prog in Mater Sci* 2001; 46: 273-82

Greenwald S.E. and Berry C.L. Improving vascular grafts: the importance of mechanical and haemodynamic properties. *J Pathol*, 2000; 190, 292-9

Geeracrt A.J. and Callaghan J.C. Experimental study of selected small calibre arterial grafts. *J Cardiovasc Surg* 1977; 18: 155

Gildner C.D., Lerner A.L., Hocking D.C. Fibronectin matrix polymerization increases tensile strength of model tissue. *Am J Physiol Heart Circ Physiol* 2004; 287: 46-53

Grenier G., Remy-Zolghadri M., Guignard R., Bergeron F., Labbe R., Auger F.A., Germain L. Isolation and culture of the three vascular cell types from a small vein biopsy sample. *In Vitro Cell Dev Biol-Animal* 2003; 39: 131-9

Grenier G., Rémy-Zolghadri M., Larouche D., Gauvin R., Baker K., Bergeron F., Dupuis D., Langelier E., Rancourt D., Auger F.A., Germain L. Tissue reorganization in response to mechanical load increases functionality. *Tissue Eng* 2005; 11: 90-100

Grenier S., Sandig M., Holdsworth D.W., Mequanint K. Interactions of coronary artery smooth muscle cells with 3D porous polyurethane scaffolds. *J Biomed Mater Res A* 2009; 89 (2): 293-303

Harkness R.D. Biological function of collagen *Biol. Rev.* 1961; 36: 399-463

Hasirci V., Vrana E., Zorlutuna P., Ndreu A., Yilgor P., Basmanav F.B., Aydin E. Nanobiomaterials: a review of the existing science and technology, and new approaches. *J Biomater Sci Polym Ed.* 2006; 17 (11): 1241-68

Hellener G., Cohn D., Marom G. Elastic response of filament wound arterial prostheses under internal pressure. *Biomaterials* 1994; 15 (14): 1115-21

Henze U., Kaufmann M., Klein B., Handt S., Klosterhalfen B. Endothelium and biomaterials: morpho-functional assessments. *Biomed Pharmacother* 1996; 50 (8): 388

Heyderman L.J., Solak H.H., David C., Atkinson D., Cowburn R.P., Nolting F. Arrays of nanoscale magnetic dots: Fabrication by x-ray interference lithography and characterization. *Appl Phys Lett* 2004; 85 (21): 4989-91

Hile D.D., Amirpour M.L., Akgerman A., Pishko M.V. Active growth factor delivery from poly(D,L-lactide-co-glycolide) foams prepared in supercritical CO₂. *J Control Release*. 2000; 66 (2-3): 177-85

Houtchens G.R., Foster M.D., Desai T.A., Morgan E.F., Wong J.Y. Combined effects of microtopography and cyclic strain on vascular smooth muscle cell orientation. *J Biomech* 2008; 41: 762-9

Hu S., Eberhard L., Chen J., Love J.C., Butler J.P., Fredberg J.J., Whitesides G.M., Wang N. Mechanical anisotropy of adherent cells probed by a three-dimensional magnetic twisting device. *Am J Physiol Cell Physiol* 2004; 287: 1184-91

Huang L., Apkarian R.P., Chaikof E.L. High-resolution analysis of engineered type I collagen nanofibers by electron microscopy. *Scanning* 2001; 23 (6): 372-5

Huang L., Nagapudi K., Apkarian R.P., Chaikof E.L. Engineered collagen-PEO nanofibers and fabrics. *J Biomater Sci Polym Ed* 2001; 12 (9): 979-93

Isenberg B.C. and Tranquillo R.T. Long-term cyclic distention enhances the mechanical properties of collagen-based media-equivalents. *Ann Biomed Eng* 2003; 31: 937-49

Jackman R.J., Brittain S.T., Adams A., Prentiss M.G., Whitesides G.M. Design and fabrication of topologically complex, three-dimensional microstructures *Science*. 1998; 280 (5372): 2089-91

Kader K.N. and Yoder C.M. Endothelial cell death on biomaterials: Theoretical and practical aspects of investigation. *Mater Sci Eng C* 2008; 28: 387-91

Karuri N.W., Liliensiek S., Teixeira A.I., Abrams G., Campbell S., Nealey P.F., Murphy C.J. Biological length scale topography enhances cell-substratum adhesion of human corneal epithelial cells. *J Cell Sci* 2004 ;117 (15): 3153–64

Kane R.S., Takayama S., Ostuni E., Ingber D.E., Whitesides G.M. Patterning proteins and cells using soft lithography. *Biomaterials* 1999; 20 (23-24): 2363-76

Kannan R.Y., Salacinski H.J., Butler P.E., Hamilton G., Seifalian A.M. Current status of prosthetic bypass grafts: a review. *J Biomed Mater Res B Appl Biomater* 2005; 74 (1): 570-81

Kelley C., D'Amore P., Hechtman H.B., Shepro D. Microvascular Pericyte Contractility In Vitro: Comparison with Other Cells of the Vascular Wall. *The J Cell Biol* 1987; 104: 483-90

Kenar H., Kose G.T., Hasirci V. Tissue engineering of bone on micropatterned biodegradable polyester films. *Biomaterials* 2006; 27 (6): 885-95

Kenawy el R., Layman J.M., Watkins J.R., Bowlin G.L., Matthews J.A., Simpson D.G., Wnek G.E. Electrospinning of poly(ethylene-co-vinyl alcohol) fibers. *Biomaterials* 2003;24 (6): 907-13

Kim S.W. and Jacobs H. Design of nonthrombogenic polymer surfaces for blood-contacting medical devices. *Blood Purif* 1996; 14 (5): 357-72

Kose G.T., Kenar H., Hasirci N., Hasirci V. Macroporous poly(3 hydroxybutyrate-co-3-hydroxyvalerate) matrices for bone tissue engineering. *Biomaterials* 2003; 24: 1949-58

Kurane A., Simionescu D.T., Vyavahare N.R. In vivo cellular repopulation of tubular elastin scaffolds mediated by basic fibroblast growth factor. *Biomaterials* 2007; 28: 2830–38

Kwon K., Kidoaki S., Matsuda T. Electrospun nano- to microfiber fabrics made of biodegradable copolyesters: structural characteristics, mechanical properties and cell adhesion potential. *Biomaterials* 2005; 26: 3929–39

Landers R, Hübner U, Schmelzeisen R, Mülhaupt R. Rapid prototyping of scaffolds derived from thermoreversible hydrogels and tailored for applications in tissue engineering *Biomaterials* 2002; 23 (23): 4437-47

Langer R. and Vacanti J. P. *Tissue engineering Science* 1993; 260: 920-26

Lee C.H., Singla A., Lee Y. Biomedical applications of collagen *Int J Pharm* 2001; 221 (1-2): 1-22

Leyh R.G., Wilhelmi M., Rebe P., Fischer S., Kofidis T., Haverich A., Mertsching H. In vivo repopulation of xenogeneic and allogeneic acellular valve matrix conduits in the pulmonary circulation. *Ann Thorac Surg* 2003; 75 (5): 1457-63

L'Heureux N., Paquet S., Lacoë R., Germain L., Auger F.A. A completely biological tissue-engineered human blood vessel. *FASEB J* 1998; 12: 47–56

Li Y.J., Haga J.H., Chien S. Molecular basis of the effects of shear stress on vascular endothelial cells. *J Biomech* 2005; 38: 1949–71

Lu J., Rao M.P., MacDonald N.C., Khang D., Webster T.J. Improved endothelial cell adhesion and proliferation on patterned titanium surfaces with rationally designed, micrometer to nanometer features. *Acta Biomater* 2008; 4: 192–201

Marois Y., Guidoin R., Roy R., Vidovsky T., Jakubiec B., Sigot-Luizard M.F., Braybrook J., Mehri Y., Laroche G., King M. Selecting valid in vitro biocompatibility tests that predict the in vivo healing response of synthetic vascular prostheses. *Biomaterials* 1996; 17 (19): 1835-42

McNeil S.E. Nanotechnology for the biologist. *J Leukoc Biol* 2005; 78 (3): 585-94

Marois Y., Paris E., Zhang Z., Doillon C.J., King M.W., Guidoin R.G. Vascugraft microporous polyesterurethane arterial prosthesis as a thoraco-abdominal bypass in dogs. *Biomaterials* 1996; 17: 1289-300

Matthews J.A., Wnek G.E., Simpson D.G., Bowlin G.L. Electrospinning of collagen nanofibers. *Biomacromolecules*. 2002; 3 (2): 232-8

Miller D.C., Thapa A., Haberstroh K.M., Webster T.J. Endothelial and vascular smooth muscle cell function on poly(lactic-co-glycolic acid) with nano-structured surface features. *Biomaterials* 2004; 25 (1): 53-61

Mironov V., Boland T., Trusk T., Forgacs G., Markwald R.R. Organ printing: computer-aided jet-based 3D tissue engineering. *Trends Biotechnol.* 2003; 21 (4): 157-61

Mitchell S.L. and Niklason L.E. Requirements for growing tissue-engineered vascular grafts. *Cardiovasc Pathol* 2003; 12 (2): 59-64

Morawski A.M., Winter P.M., Yu X., Fuhrhop R.W., Scott M.J., Hockett F., Robertson J.D., Gaffney P.J., Lanza G.M., Wickline S.A. Quantitative "magnetic resonance immunohistochemistry" with ligand-targeted (19)F nanoparticles. *Magn Reson Med* 2004; 52 (6): 1255-62

National Center for Chronic Disease Prevention and Health Promotion, Chronic Disease Overview, United States Government, http://www.cdc.gov/nccdphp/overview_text.htm, last access date: 10.06.2009

Ndreu A., Nikkola L., Ylikauppilar H., Ashammakhi N., Hasirci V. Electrospun biodegradable nanofibrous mats for tissue engineering. *Nanomedicine* 2008; 3: 45-60

Nerem R.M., Alexander R.W., Chappell D.C., Medford R.M., Varner S.E., Taylor R.W. The study of the influence of flow on vascular endothelial biology. *Am J Med Sci* 1998; 316: 169–75

Niemeyer P., Seckinger A., Simank H.G., Kasten P., Sudkamp N., Krause U. Allogenic transplantation of human mesenchymal stem cells for tissue engineering purposes: an in vitro study. *Orthopade* 2004; 33 (12): 1346-53

Nishida K., Yamato M., Hayashida Y., Watanabe K., Yamamoto K., Adachi E., Nagai S., Kikuchi A., Maeda N., Watanabe H., Okano T., Tano Y. Corneal reconstruction with tissue-engineered cell sheets composed of autologous oral mucosal epithelium. *N Engl J Med* 2004; 351 (12): 1187-96

Nitschke M., Schmack G., Janke A., Simon F., Pleul D., Werner C. Low pressure plasma treatment of poly(3-hydroxybutyrate): toward tailored polymer surfaces for tissue engineering scaffolds. *J Biomed Mater Res.* 2002; 59 (4): 632-8

Nunn D.B., Freeman M.N., Hudgkins P.C. Post-operative alterations in the size of Dacron grafts: an ultrasonic evaluation. *Ann Surg* 1979; 189: 741

Ozcan C., Zorlutuna P., Hasirci V., Hasirci N., Influence of Oxygen Plasma Modification on Surface Free Energy of PMMA Films and Cell Attachment. *Macromol. Symp* 2008; 269: 128–37

Perets A., Baruch Y., Weisbuch F., Shoshany G., Neufeld G., Cohen S. Enhancing the vascularization of three-dimensional porous alginate scaffolds by incorporating controlled release basic fibroblast growth factor microspheres. *J Biomed Mater Res A* 2003;65 (4): 489-97

Pins G.D., Toner M., Morgan J.D. Microfabrication of an analog of the basal lamina: biocompatible membranes with complex topographies. *FABES J* 2000; 14: 593-602

Pukacki F., Jankowski T., Gabriel M., Oszkinis G., Krasinski Z., Zapalski S. The Mechanical Properties of Fresh and Cryopreserved Arterial Homografts. *Eur J Vasc Endovasc Surg* 2000; 20: 21–4

Punshon G., Vara D.S., Sales K.M., Kidane A.G., Salacinski H.J., Seifalian A.M. Interactions between endothelial cells and a poly(carbonate-silsesquioxane-bridge-urea)urethane. *Biomaterials* 2005; 26: 6271–9

Ratcliffe A. Tissue engineering of vascular grafts. *Matrix Biol* 2000; 19: 353-7

Rhee R.Y., Glovieszki P., Camria R.A., Miller V.M. Experimental evaluation of bleeding complications, thrombogenicity and intimal characteristics of prosthetic patch materials used for carotid angioplasty. *Cardiovasc Surg* 1996; 4: 746-52

Robinson A.P.G., Palmer R.E., Tada T., Kanayama T., Allen M.T., Preece J.A., Harris K.D.M. 10 nm scale electron beam lithography using a triphenylene derivative as a negative/positive tone resist. *J Phys D Appl Phys* 1999; 32 (16): 75-8

Sandusky G.E., Lantz G.C., Badylak S.F. Healing comparison of small intestine submucosa and ePTFE grafts in the canine carotid artery. *J Sur Res* 1995; 58 (4): 415-20

Rong Z., Rashid S., Vadgama P. A Bipartite Expression for Transient amperometric current at a membrane covered planar electrode to characterize solute diffusion through the membrane. *Electroanal* 2006; 17: 1703-9

Rong Z., Cheema U., Vadgama P. Needle enzyme electrode based glucose diffusive transport measurement in a collagen gel and validation of a simulation model. *Analyst* 2006; 131: 816–21

Salacinski H. J., Goldner S., Giudiceandrea A., Hamilton G., Seifalian A.M.J. The mechanical behavior of vascular grafts: a review. *Biomater. Appl* 2001; 15: 241–76

Santerre J.P., Labow R.S., Duguay D.G., Erfle D., Adams G.A. Biodegradation evaluation of polyether and polyester-urethanes with oxidative and hydrolytic enzymes. *J Biomed Mater Res* 1994; 28: 1187-99

Sarkar S.J., Sales K.M., Hamilton G., Seifalian A.M. Addressing thrombogenicity in vascular graft construction. *Biomed Mater Res B Appl Biomater* 2007; 82 (1): 100-8

Schift H., Heyderman L.J., Padeste C., Gobrecht J. Chemical nano-patterning using hot embossing lithography. *Microelectron Eng* 2002; (61-62): 423-28

Schmalenberg K.E., Buettner H.M., Uhrich K.E. Microcontact printing of proteins on oxygen plasma-activated poly(methyl methacrylate). *Biomaterials* 2004; 25: 1851-57

Shen J.Y., Chan-Park M.B., He B., Zhu A.P., Zhu X., Beuerman R.W., Yang E.B., Chen W., Chan V. Three-dimensional microchannels in biodegradable polymeric films for control orientation and phenotype of vascular smooth muscle cells. *Tissue Eng* 2006, 12 (8): 2229-40

Shen J.Y., Chan-Park M.B., Feng Z.Q., Chan V., Feng Z.W. UV-embossed microchannel in biocompatible polymeric film: application to control of cell shape and orientation of muscle cells. *J Biomed Mater Res B* 2006; 77: 423-30

Shi C., Zhu Y., Ran X., Wang M., Su Y., Cheng T. Therapeutic potential of chitosan and its derivatives in regenerative medicine. *J Surg Res* 2006; 133 (2):185-92

Shum-Tim D., Stock U., Hrkach J., Shinoka T., Lien J., Moses M.A., Stamp A., Taylor G., Moran A.M., Landis W., Langer R., Vacanti J.P., Mayer J.E. Jr. Tissue engineering of autologous aorta using a new biodegradable polymer. *Ann Thorac Surg* 1999; 68 (6): 2298-304

Staros J.V., Wright R.W., Swingle D.M. Enhancement by N-hydroxysulfosuccinimide of water-soluble carbodiimide-mediated coupling reactions. *Anal Biochem* 1986; 156: 220-2

Sun J.S., Wu S.Y.H., Lin F.H. The role of muscle-derived stem cells in bone tissue engineering. *Biomaterials* 2005; 26: 3953-60

Tajima S, Chu JS, Li S, Komvopoulos K. Differential regulation of endothelial cell adhesion, spreading, and cytoskeleton on low-density polyethylene by nanotopography and surface chemistry modification induced by argon plasma treatment. *J Biomed Mater Res A* 2008; 84 (3): 828-36

Takayama S., McDonald J.C., Ostuni E., Liang M.N., Kenis P.J., Ismagilov R.F., Whitesides G.M. Patterning cells and their environments using multiple laminar fluid flows in capillary networks. *Proc Natl Acad Sci U S A*. 1999; 96 (10): 5545-8

Takei T., Yamaguchi S., Sakai S., Ijima H., Kawakami K. Novel Technique for Fabricating Double-Layered Tubular Constructs Consisting of Two Vascular Cell Types in Collagen Gels Used as Templates for Three-Dimensional Tissues. *J Biosci Bioeng* 2007; 104 (5): 435-8

Tang Q., Shi S.Q., Zhou L. Nanofabrication with atomic force microscopy. *J Nanosci Nanotechnol* 2004; 4 (8): 948-63

Tanzi M.C., Fare S., Petrini P. In vitro stability of polyether and polycarbonate urethanes. *J Biomater Appl* 2000; 14 :325-48

Teebken O.E., Bader A., Steinhoff G., Haverich A. Tissue engineering of vascular grafts: human cell seeding of decellularised porcine matrix. *Eur J Vasc Endovasc Surg* 2000; 19 (4): 381-6

Thomas A.C., Campbell G.R., Campbell J.H. Advances in vascular tissue engineering. *Cardiovasc Pathol* 2003; 12: 271–6

Thomas V., Zhang X., Catledge S.A., Vohra Y.K. Functionally graded electrospun scaffolds with tunable mechanical properties for vascular tissue regeneration. *Biomed Mater* 2007; 2: 224–32

Thompson M.M., Budd J.S., Bell P.R.F. Use of freshly isolated capillary endothelial cells for the immediate establishment of a monolayer on a vascular graft at surgery. *Surgery* 1994;100: 392-9

Tranquillo R.T., Girton T.S., Bromberek B.A., Triebes T.G., Mooradian D.L. Magnetically-oriented tissue equivalent tubes: application to a circumferentially orientated media-equivalent. *Biomaterials* 1996; 17: 349–53

Tu J.V., Pashos C.L., Naylor C.D. Use of cardiac procedures and outcomes in elderly patients with myocardial infarction in the united States and Canada. *N Engl J Med* 1997; 366: 1500-5

Turkish Society of Cardiology, National Heart Health Policy, Part 2, p: 23-62, http://www.tkd-online.org/UKSP/UKSP_Bolum02.pdf, last access date: 10.06.2009

van Delft F.C.M.J.M., van den Heuvel F.C., Loesberg W.A., te Riet J., Schön P., Figdor C.G., Speller S., van Loon J.J.W.A., Walboomers X.F., Jansen J.A. Manufacturing substrate nano grooves for studying cell alignment and adhesion. *Microelectron Eng* 2008; 85 (5-6): 1362-6

van Wachem P.B., Schakenraad J.M., Feijen J., Beugeling T., van Aken W.G., Blaauw E.H., Nieuwenhuis P., Molenaar I. Adhesion and spreading of cultured endothelial cells on modified and unmodified poly(ethylene terephthalate): a morphological study. *Biomaterials* 1989; 10 (8): 532-9

Vartanian K.B., Kirkpatrick S.J., Hanson S.R., Hinds M.T. Endothelial cell cytoskeletal alignment independent of fluid shear stress on micropatterned surfaces. *Biochem Bioph Res Co* 2008; 371 (4): 787-92

Vernon RB., Gooden M.D., Lara S.L., Wight T.N. Microgrooved fibrillar collagen membranes as scaffolds for cell support and alignment. *Biomaterials* 2005; 26: 3131-40

Vleggeert-Lankamp C.L., Pego A.P, Lakke E.A., Deenen M., Marani E., Thomeer R.T. Adhesion and proliferation of human Schwann cells on adhesive coatings. *Biomaterials* 2004; 25 (14): 2741-51

Vozzi G., Flaim C, Ahluwalia A., Bhatia S. Fabrication of PLGA scaffolds using soft lithography and microsyringe deposition. *Biomaterials* 2003; 24 (14): 2533-40

Vrana N.E., Elsheikh A., Builles N., Damour O., Hasirci V. Effect of human corneal keratocytes and retinal pigment epithelial cells on the mechanical properties of micropatterned collagen films. *Biomaterial* 2007; 28 (29): 4303-10

Xu C.Y., Inai R., Kotaki M., Ramakrishna S. Aligned biodegradable nanofibrous structure: a potential scaffold for blood vessel engineering. *Biomaterials* 2004, 25: 877-86

Yamada H. *Strength of Biological Materials*. p. 114-130. Williams & Wilkins, Baltimore (1970)

Yang W., Barth R.F., Wu G., Bandyopadhyaya A.K., Thirumamagal B.T., Tjarks W. Binns P.J., Riley K., Patel H., Coderre J.A., Ciesielski M.J., Fenstermaker R.A. Boronated epidermal growth factor as a delivery agent for neutron capture therapy of EGF receptor-positive gliomas. *Appl Radiat Isot* 2004; 61: 981-5

Yang J., Motlagh D., Webb A.R., Ameer G.A. Novel Biphasic Elastomeric Scaffold for Small-Diameter Blood Vessel Tissue Engineering. *Tissue Eng* 2005; 11 (11-12): 1876-86

Yang M., Zheng Z., Liu Y., Zhang B. Kinetics of atomic force microscope-based scanned probe oxidation on an octadecylated silicon (111) surface. *J Phys Chem B Condens Matter Mater Surf Interfaces Biophys* 2006; 110 (21): 10365-73

Yilgor P., Sousa R.A., Reis R.L., Hasirci N., Hasirci V. 3D plotted PCL scaffolds for stem cell based bone tissue engineering. *Macromol Symp* 2008; 269: 92-9

Yilgor P., Tuzlakoglu K., Reis R.L., Hasirci N., Hasirci V. Incorporation of a Sequential BMP-2/BMP-7 Delivery System into Chitosan-Based Scaffolds for Bone Tissue Engineering. *Biomaterials* doi:10.1016/j.biomaterials.2009.03.024, 2009

Walboomers X.F. and Jansen J.A. Cell and tissue behavior on micro-grooved surfaces. *Odontology* 2001; 89: 2-11

Wang J.H.C., Jia F., Gilbert T.W., Woo S.L.Y. Cell orientation determines the alignment of cell-produced collagenous matrix. *J of Biomech* 2003; 36: 97-102

Wang J.H., Yang G., Li Z. Controlling cell responses to cyclic mechanical stretching. *Ann Biomed Eng* 2005; 33: 337-42

Wilson D.L., Martin R., Hong S., Cronin-Golomb M., Mirkin C.A., Kaplan D.L. Surface organization and nanopatterning of collagen by dip-pen nanolithography. *Proc Natl Acad Sci USA* 2001; 98 (24): 13660-4

Williams S.F., Martin D.P., Horowitz D.M. and Peoples O.P. PHA applications: addressing the price performance issue: I. Tissue engineering. *Int J Biol Macromol* 1999; 25: 111-21

Wu C.C., Li Y., Haga J.H., Kaunas R., Chiu J., Su F., Usami S., Chien S. Directional shear flow and Rho activation prevent the endothelial cell apoptosis induced by micropatterned anisotropic geometry. *PNAS* 2007; 104 (4): 1254–9

Zdrahala R.J. Small caliber vascular grafts. Part I: state of the art. *J Biomater Appl* 1996; 10 (4): 309-29

Zein I., Hutmacher D.W., Tan K.C., Teoh S.H. Fused deposition modeling of novel scaffold architectures for tissue engineering applications. *Biomaterials* 2002; 23 (4): 1169-85

Zhang Z., Marois Y., Guidoin R.G., Bull P., Marois M., How T., Laroche G., King M.W. Vascugraft polyurethane arterial prosthesis as femoro-popliteal and femoro-peroneal bypasses in humans: pathological, structural and chemical analyses of four excised grafts. *Biomaterials* 1997; 18: 113-24

Zhang Y., Ouyang H., Lim C.T., Ramakrishna S., Huang Z.M. Electrospinning of gelatin fibers and gelatin/PCL composite fibrous scaffolds. *J Biomed Mater Res B* 2005; 72 (1): 156-65

Zhang X., Baughman C.B., Kaplan D.L. In vitro evaluation of electrospun silk fibroin scaffolds for vascular cell growth. *Biomaterials* 2008; 29: 2217-27

Zhang X., Wang X., Keshav V., Wang X., Johanas J.T., Leisk G.G., Kaplan D.L. Dynamic culture conditions to generate silk-based tissue-engineered vascular grafts. *Biomaterials* 2009, Article in Press

Zisch A.H., Lutolf M.P., Hubbell J.A. Biopolymeric delivery matrices for angiogenic growth factors. *Cardiovasc Pathol* 2003; 12 (6): 295-310

Zorlutuna P., Tezcaner A., Kiyat I., Aydinli A., Hasirci V. Cornea engineering on polyester carriers. *J Biomed Mater Res A* 2006; 79 (1): 104-13

Zorlutuna P., Builles N., Damour O., Elsheikh A., Hasirci V. Influence of keratocytes and retinal pigment epithelial cells on the mechanical properties of polyester-based tissue engineering micropatterned films. *Biomaterials* 2007; 28 (24): 3489-96

Zorlutuna P., Hasirci N., Hasirci V. Nanopatterned collagen tubes for vascular tissue engineering. *J Tissue Eng Regen Med* 2008; 2 (6): 373-7

APPENDIX A

ETHICAL COMMITTEE APPROVAL

 Ankara, 27.12.2007
Sayı : BH/THD-272/07

Sayın Prof. Dr. Vasif HASIRCI
ODTÜ Fen Fakültesi
Biyolojik Bilimler Bölümü
ANKARA

Konu : Proje değerlendirme sonucu.

Sayın Prof. Dr. Hasirci,

Yürütücüsü olduğunuz "Nanodesenli Hücre İskeleleri Üretimi ve Doku Mühendisliği Yöntemiyle Yapay Damar Yapımında Kullanımı" başlıklı projeniz Tıbbi Etik ve Deontoloji Kurulu'muz tarafından değerlendirilerek etik açıdan uygun bulunmuştur.

Saygılarımla,


Doç. Dr. Yaman ZORLUTUNA
Bayındır Hastaneleri
Tıbbi Direktör
Tıbbi Etik ve Deontoloji Kurulu Başkanı

 BAYEK TEDAVİ SAĞLIK HİZMETLERİ VE İŞLETMECİLİĞİ A.Ş.
Bağcıbaşı / Kızılay Mah. 53. Cad. No: 17 / Söğütözü 06520 ANKARA
Tel : 0312 287 90 50 • Faks : 0312 285 07 33 • Çim : 0312 715 0 911
e-mail: bayek@bayekhizmetleri.com.tr • www.bayekhizmetleri.com.tr

Kavaklıdere / Katolik Bulvarı No: 201 / Kavaklıdere 06580 ANKARA
Tel : 0312 428 08 08 • Faks : 0312 428 08 20 • Çim : 0312 715 0 911
e-mail: bayek@bayekhizmetleri.com.tr • www.bayekhizmetleri.com.tr

Bayındır Hastaneleri DA TÜRKiYE SAKNASTI Kuruluşudur.

Figure A.1. Ethical committee approval

APPENDIX B

EQUATIONS FOR ALAMAR BLUE CALCULATIONS

$$\text{Reduction} = \frac{(\varepsilon_{ox})\lambda_2 \cdot A_{\lambda_1} - (\varepsilon_{ox})\lambda_1 \cdot A_{\lambda_2}}{(\varepsilon_{red})\lambda_1 \cdot A'_{\lambda_2} - (\varepsilon_{red})\lambda_2 \cdot A'_{\lambda_1}}$$

$$(\varepsilon_{ox})\lambda_1 = 80.586$$

$$(\varepsilon_{red})\lambda_1 = 155.677$$

$$(\varepsilon_{ox})\lambda_2 = 177.216$$

$$(\varepsilon_{red})\lambda_2 = 14.652$$

$$\lambda_1 = 570 \text{ nm}$$

$$\lambda_2 = 595 \text{ nm}$$

A_{λ_1} = Observed absorbance reading for test well at 570 nm

A_{λ_2} = Observed absorbance reading for test well at 595 nm

A'_{λ_1} = Observed absorbance reading for negative control well at 570 nm

A'_{λ_2} = Observed absorbance reading for negative control well at 595 nm

APPENDIX C

CALIBRATION CURVES FOR CELL NUMBER DETERMINATION

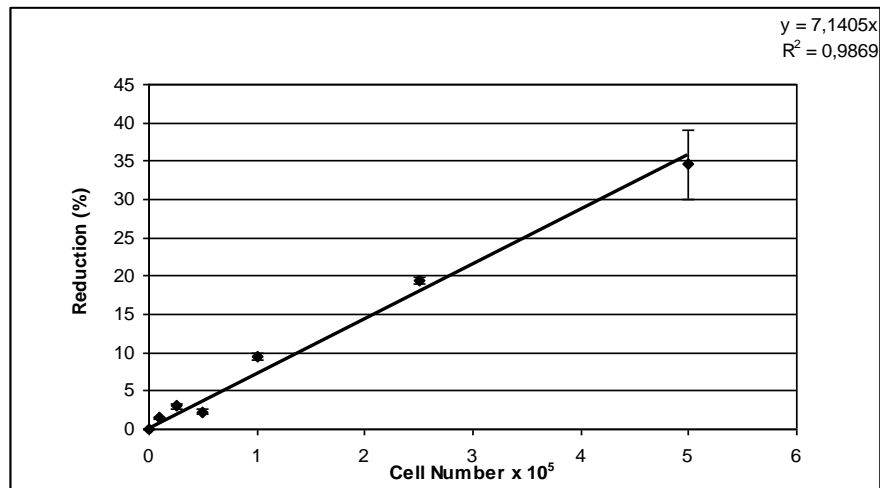


Figure C.1. Calibration curve of VSMCs for Alamar Blue Assay.

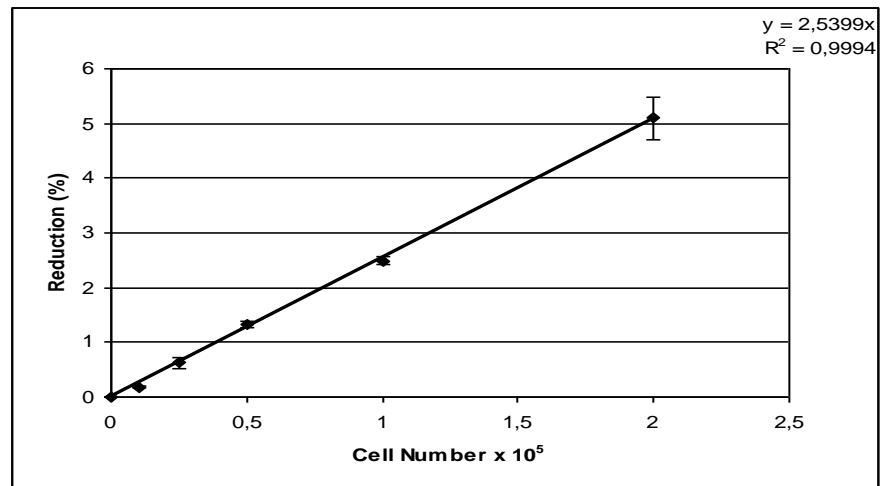


Figure C.2. Calibration curve of VSMCs for Alamar Blue Assay.

CURRICULUM VITAE

PERSONAL INFORMATION

Surname, Name: Zorlutuna, Pinar

Nationality: Turkish (T.C.)

Date and Place of Birth: 9 June 1981, Ankara, Turkey

Marital Status: Single

Phone: +90 312 210 51 68

Fax: +90 312 210 15 42

E-mail: pinarzorlutuna@yahoo.com, pinarzorlutuna@hotmail.com

EDUCATION

Degree	Institution	Year of Graduation
MS	METU, Dept. of Biotechnology	2005
BS	Ankara University, Biology Dept.	2002
High School	METU High School	1998

ACADEMIC EXPERIENCE

Year	Place	Enrollment
2004-2007	METU, Biotechnology Research Unit	Full time Researcher
November 2004 August 2005	Universite Louis Pasteur, INSERM Unite 595	Visiting Researcher
April-May 2008	QM, University of London, Interdisciplinary Research Centre in Biomedical Materials	Visiting Researcher

FOREIGN LANGUAGES: Advanced English, Basic French

PUBLICATIONS

1. P. Zorlutuna, Z. Rong, P. Vadgama and V. Hasirci, Influence of Nanopatterns on Endothelial Cell Adhesion: Enhanced Cell Retention under Shear Stress, *Acta Biomaterialia*, 2009, *in press*.
2. P.Zorlutuna, P.Yılgör, F.B.Başmanav, V.Hasirci, Biomaterials and tissue engineering research in Turkey: The METU Biomat Center experience, *Biotechnology Journal*, 2009, DOI 10.1002/biot.200800335.
3. P. Zorlutuna, A. Elsheikh and V. Hasirci, Nanopatterning of Collagen Scaffolds Improve the Mechanical Properties of Tissue Engineered Vascular Grafts, *Biomacromolecules*, 10 (4): 814–821, 2009.
4. P. Zorlutuna, N. Hasirci, V. Hasirci, Nanopatterned collagen tubes for vascular tissue engineering, *J Tissue Eng Regen Med*. 2(6): 373-377, 2008.
5. C. Ozcan, P. Zorlutuna, V. Hasirci, N. Hasirci, Influence of Oxygen Plasma Modification on Surface Free Energy of PMMA Films and Cell Attachment, *Macromol. Symp.* 269: 128–137, 2008.
6. P. Zorlutuna, A.Tezcaner, V. Hasirci, A Novel Construct as a Cell Carrier for Tissue Engineering, *J Biomater Sci Polym Ed.*19(3): 399-410, 2008.
7. V Hasirci, N.E. Vrana, P. Zorlutuna, Polyester and collagen scaffolds for cornea tissue engineering, *Tissue Engineering*, 13 (7): 1743-1743, Meeting Abstract, 2007.
8. P. Zorlutuna, N. Builles, O. Damour, A. Elsheikh and V. Hasirci, Influence of keratocytes and retinal pigment epithelial cells on the mechanical properties of polyester-based tissue engineering micropatterned films *Biomaterials* 28 (24):3489-3496, 2007.
9. V. Hasirci, E. Vrana, P. Zorlutuna, A. Ndreu, P. Yilgor, B. Basmanav, E. Aydin, Nanobiomaterials; A review of the existing science and technology, and new approaches, *J Biomater Sci Polym Ed.* 17(11):1241-68, 2006.
10. P. Zorlutuna, A.Tezcaner, I. Kiyat, A. Aydinli, V. Hasirci, Cornea engineering on polyester carriers. *J Biomed Mater Res A.* 79(1):104-13, 2006.